Aus dem Medizinischen Zentrum für Innere Medizin,

Schwerpunkt Gastroenterologie und Stoffwechsel

Geschäftsführender Direktor: Prof. Dr. med. T. M. Gress

des Fachbereichs Medizin der Philipps-Universität Marburg

Functional roles of the candidate genes COA4 and POLr3K in Pancreatic Ductal Adenocarcinoma

Inaugural-Dissertation

zur Erlangung des Doktorgrades der Naturwissenschaften (Dr. rer. nat.)

dem Fachbereich Medizin der Philipps-Universität Marburg

vorgelegt von

Yajing Yang

aus Wuhan, China

Marburg, 2022

Angenommen vom Fachbereich Medizin der Philipps-Universität Marburg am:

28-April-2022

Gedruckt mit Genehmigung des Fachbereichs Medizin.

Dekan: Frau Prof. Dr. D. Hilfiker-Kleiner

Referent: Herr Prof. Dr. M. Buchholz

Korreferent: Herr. Prof. Dr. J.W. Bartsch

Table of contents

Table of contents I
Catalogue of Figures V
Catalogue of Tables VI
Abbreviations 1
1. Introduction 4
1.1 Background of Pancreatic Ductal Adenocarcinoma (PDAC) 4
1.1.1 Epidemiology 4
1.1.2 Etiology and Tumor Development 5
1.1.3 Diagnosis and Treatment 6
1.2 Cellular and Molecular Aspects of Pancreatic Cancer 8
1.3 COA4 - Cytochrome C Oxidase (COX) Assembly Factor 4 Homolog 10
1.4 POLr3K - RNA Polymerase III Subunit K 13
1.5 Role of microRNA in Pancreatic Cancer 15
1.6 Objective of My Work 17
2. Materials and Methods 18
2.1 Materials 18
2.1.1 Cell Lines 18
2.1.2 Instruments 18
2.1.3 Lab Materials 19
2.1.4 Chemicals 20
2.1.5 Buffers & Solutions 21
2.1.6 Molecular Biology Kits 23
2.1.7 Antibodies 23
2.1.8 Software 24
2.1.9 Primers 24
2.1.10 siRNAs 26

2.1.11 Plasmid 27
2.2 Methods 28
2.2.1 Cell Culture 28
2.2.1.1 Cell Line Cultivation 28
2.2.1.2 Cell Number Determination and Calculation 28
2.2.2 Transfection 28
2.2.2.1 Lipofectamine™ RNAiMAX-Transfection 28
2.2.2.2 PEI-Transfection 29
2.2.3 Plasmid Stably Transfected Cell Selection by Geneticin (G418) 30
2.2.4 RNA Isolation 30
2.2.5 cDNA Synthesis 30
2.2.6 qPCR 31
2.2.7 Cell Protein Extraction 32
2.2.8 Determination of Protein Concentration by Bradford Method 33
2.2.9 Western Blot 33
2.2.9.1 SDS Polyacrylamide Gel-Electrophoresis 34
2.2.9.2 Blotting 35
2.2.9.3 Blocking and Antibody Incubation 35
2.2.9.4 Chemiluminiscence Detection 36
2.2.10 MTT Assay 36
2.2.11 BrdU Assay 37
2.2.12 Anchorage-Independent Growth and CellTiter-Glo Assay 38
2.2.13 Time-Lapse Microscopy Assay 38
2.2.14 Flow Cytometry 39
2.2.14.1 Cell Cycle Analysis 39
2.2.14.2 Cell Apoptosis and Necrosis 40
2.2.15 mRNA-Seq and Statistical Analysis 41
2.2.16 PLAU-pIRES2-EGFP Plasmid Purification 41
2.2.16.1 Isolating Bacteria on LB Agar Plate 41

2.2.16.2 Inoculating a Liquid Bacterial Culture 41
2.2.16.3 Midi-Prep for Recovering and Purification of Plasmid DNA 42
2.2.17 TaqMan® MicroRNA Assay 42
2.2.17.1 microRNA Isolation by mirVana Kit 43
2.2.17.2 microRNA Reverse Transcription 44
2.2.17.3 cDNA Preamplification 45
2.2.17.4 TaqMan Human microRNA Array Real-Time PCR 46
2.2.18 Validation of microRNA of Interest 47
2.2.18.1 Candidate microRNA Selection 47
2.2.18.2 Stem-Loop Primer Design for miR real-time PCR 47
2.2.18.3 cDNA Synthesis 48
2.2.19 Tissue Microarray Analysis of Patients Specimens 49
2.2.19.1 Ethics Statement 49
2.2.19.2 Immunohistochemistry 50
2.2.19.3 Kaplan–Meier Survival Analysis 50
2.2.20 Statistic Analysis 50
3. Results 51
3.1 COA4 and POLr3K were highly expressed in human PDAC tissues 51
3.2 Loss function of COA4 impaired cell proliferation 55
3.3 Effects of COA4 inhibition on cell cycle progression 57
3.4 COA4 knockdown reduced cell anoikis resistance, and COA4 also affected cell migration 60
3.5 Data analysis of RNA- Seq - Differentially expressed genes (DEGs) between control groups and COA4 siRNAs treatment groups 61
3.6 Verification of DEGs by qRT-PCR - PLAU was downregulated following loss function of COA4 64
3.7 COA4 regulated cell migration and cell growth (3D cell culture) by targeting PLAU 65
3.8 COA4 expression did not correlate with patient survival 69

3.9 Suppression of POLr3K induced cell growth reduction and necrosis. 71
3.10 POLr3K had no impact on cell cycle progression 74
3.11 POLr3K regulated cell anchorage independent growth but not cell migration 76
3.12 POLr3K silencing led to miR-30d-5p repression 77
3.13 Verification of miRNA candidates on S2-007 cell line by real-time PCR 78
3.14 POLr3K regulated 3D cell growth via miR-30d-5p 79
3.14.1 miR-30d-5p did not affect POLr3K mediated cell growth in 2D cell culture conditions 79
3.14.2 POLr3K regulated cell growth in 3D cell culture via miR-30d-5p 80
3.15 POLr3K expression was not correlated with patient survival 81
4. Discussion 83
4.1 COA4 promotes PDAC cell proliferation 83
4.2 RNA Seq and DEGs validation - The capacity of COA4 to regulate cell migration by targeting PLAU 84
4.3 POLr3K regulated cell growth and cell cycle, and may exist as protein complex or protein isoforms 86
4.4 miR-30d-5p mediated POLr3K-stimulated cell growth 88
4.5 Difference of tumor cell culture between 2D and 3D conditions 89
4.6 Localization of COA4 and POLr3K in primary PDAC tissues 90
4.7 Conclusion and perspective 91
5. Summary 93
6. Zusammenfassung 95
7. References 97
8. Appendix 113
8.1 Supplementary Table 113
8.2 Verzeichnis der akademischen Lehrer 116
8.3 Acknowledgement 117

Catalogue of Figures

Figure 1. Primer test of candidate genes by qRT-PCR..... 53
Figure 2. COA4 and POLr3K were differentially overexpressed among human PDAC specimens. 54
Figure 3. qRT-PCR demonstrated strong expression of COA4 (A) and POLr3K (B) in pancreatic cancer cell lines. 55
Figure 4. Independent COA4-specific siRNAs led to significant knockdown on mRNA and protein level in 3 pancreatic cancer cell lines. 56
Figure 5. COA4 mediated reduction in cell proliferation rather than apoptosis in PDAC. 57
Figure 6. COA4 regulated cell cycle progression.. 59
Figure 7. Impaired COA4 influenced cell anchorage independent growth and cell migration. 61
Figure 8. Workflow of RNA-Seq data analysis to find functional effector genes upon COA4 knockdown. 64
Figure 9. Expression of PLAU was attenuated following COA4 inhibition. 48h after COA4 siRNA transfection, real-time PCR analysis of PLAU expression was performed. 65
Figure 10. PLAU expression levels in stably transfected cell clones were analyzed by qRT-PCR. 66
Figure 11. Cell viability and Cell-anchorage-independent growth assessed by A) MTT assay, B) CellTiter-Glo assay in COA4 siRNA transfected parental S2-007 cells (left panels) and PLAU DNA stable expressed clones respectively (right panels) 72 h after transfection. 68
Figure 12. Induction of cell migration reduction through loss-of COA4 could be rescued in PLAU overexpressed cells. 68
Figure 13. Representative images of TMA based IHC analysis of COA4 expression in pancreatic cancer and normal pancreatic tissues..... 70
Figure 14. Knockdown of POLr3K mRNA on pancreatic cancer cell lines. 72
Figure 15. Inhibition of POLr3K attenuated cell proliferation and elevated cell necrosis. 74
Figure 16. POLr3K inhibition had no overt effect on cell cycle. 76
Figure 17. Reduction of POLr3K expression reduced cell anchorage dependent growth but not cell migration. 77
Figure 18. microRNAs of interest were verified by real-time PCR. 79
Figure 19. Overexpression of miR30d did not rescue POLr3K inhibition-induced attenuation of cell growth under 2D cell culture conditions..... 80
Figure 20. miR30d could prevent POLr3K impacted cell growth change in 3D cell culture. 81
Figure 21. Representative images of tissue microarray based IHC analysis of POLr3K expression in normal pancreas and pancreatic cancer tissues..... 82

Catalogue of Tables

Table 1. Cell lines 18
Table 2. Instruments 18
Table 3. Lab materials 19
Table 4. Chemicals 20
Table 5. Buffers and solutions 21
Table 6. Molecular biology kits 23
Table 7. Antibodies 23
Table 8. Software 24
Table 9. Primers were used in the PCR and real time-PCR 25
Table 10. siRNA list 27
Table 11. MasterMix of cDNA synthesis for real-time PCR 31
Table 12. MasterMix of one 96-Well PCR reaction plate 32
Table 13. Buffer of SDS polyacrylamide gel 34
Table 14. MasterMix of microRNA reverse transcription 44
Table 15. Program setting for microRNA reversed transcription 44
Table 16. microRNA to cDNA preamplification MasterMix 45
Table 17. microRNA to cDNA preamplification program setting 45
Table 18. MasterMix of TaqMan Human microRNA Array Real-Time PCR 46
Table 19. Program setting of TaqMan Human microRNA Array Real-Time PCR 46
Table 20. MaterMix of cDNA synthesis with microRNA stem-loop primer pool .. 48
Table 21. Program setting of cDNA synthesis with microRNA stem-loop primers pool 49
Table 22. List of candidate genes. 52
Table 23. Analyzed data of Candidate microRNAs 78
Table 24. List of genes with significant expression alteration upon COA4 knockdown. 113

Abbreviations

APS	Ammonium Persulfate
ASR	Age-Standardized-Rate
BrdU	5-bromo-2’-deoxyuridine
BSA	Bovine serum albumin
CA19-9	Carbohydrate antigen 19-9
cDNA	complementary DNA
CEA	Carcinoembryonic antigen
COA4	Cytochrome C Oxidase Assembly Factor 4
Complex I	ubiquinone oxidoreductase
Complex III	cytochrome c oxidoreductase
Complex IV	COX Cytochrome C Oxidase
CT	computed tomography
DMEM	Dulbecco's Modified Eagle Medium
DNA	deoxyribonucleic acid
dNTP	Deoxynucleotide
DPBS	Dulbecco's phosphate-buffered saline
DTT	Dithiothreitol
dTTP	Deoxythymidine triphosphate
ECL	enhanced chemiluminescence
EDTA	Ethylenediaminetetraacetic acid
EGFR	epidermal growth factor
ERCP	Endoscopic retrograde cholangiopancreatography
EUS	Endoscopic ultrasonography
FAMMM	familial atypical multiple mole melanoma
FCS	Fetal Calf Serum
FITC	Fluorescein isothiocyanate

GFP	Green fluorescent protein
GSEA	gene set enrichment analysis
G418	Geneiticin
HCL	hydrogen chloride
HEPES	4-(2-hydroxyethyl)-1-piperazineethanesulfonic acid
HRP	horseradish peroxidase
IHC	Immunohistochemistry
IMM	inner mitochondrial
IMS	inter-membrane space
LB	Lysogeny broth - nutritionally rich medium for bacteria growth
MDCT	Multidetector CT scanning
MMP1	Matrix Metalloproteinase 1
mRNA	messenger RNA
mtDNA	mitochondrial DNA
MTT	3-(4,5)-dimethylthiahiazo(-z-y1)-3,5-di-phenytetrazoliumromide
PanIN	Pancreatic intraepithelial neoplasia
PARP	Poly (ADP-ribose) polymerase
PDAC	Pancreatic Ductal Adenocarcinoma
PEI	Polyethyleneimine
PI	Propidium iodide
POLr3K	RNA Polymerase III subunit K
Poly-HEMA	Polyhydroxyethylmethacrylate
Pol I	RNA polymerases I
Pol II	RNA polymerases II
Pol III	RNA polymerases III
PPI	Protein-Protein-Interaction
PS	Phosphatidyleserine
P21	cyclin-dependent kinase inhibitor 1
qPCR	quantitative polymerase chain reaction

RNA	ribonucleic acid
RPMI	Roswell Park Memorial Institute - growth medium of cell culture
SDS	Sodium dodecyl sulfate
SDS-PAGE	sodium dodecyl sulfate polyacrylamide gel electrophoresis
siRNA	small interfering RNA
st-primer	Stem-Loop primer
TBS	Tris Buffered Saline
TBST	Tris Buffered Saline with TWEEN20
TEMED	N′-Tetramethyl ethylenediamine
THBS1	Thrombospondin 1
TMA	Tissue Microarray
VHL	Von Hippel-Lindau syndrome

1. Introduction

1.1 Background of Pancreatic Ductal Adenocarcinoma (PDAC)

Pancreatic cancer arises from the exocrine or endocrine portions of the pancreas, but 93% of them develop from the exocrine portion (=PDAC), including the ductal epithelium, acinar cells, connective tissue, and lymphatic tissue [113]. Of all types of pancreatic cancers, approximately 75% occur within the head or neck of the pancreas, 15-20% occur in the body of the pancreas, and 5-10% occur in the tail [43]. Pancreatic cancer is a tragically lethal disease, because at the time of diagnosis, approximately half of patients are at terminal stage with distant metastases. The asymptomatic or unclear signs and symptoms at early stages make early detection difficult or impossible. Therefore, the chance for tumor resection after definite diagnosis is shrinking, and the 5-year survival rate is only 10% [100]. Current standard treatment of pancreatic cancer is surgery plus chemotherapy and radiotherapy, as well as some targeted agents [74]. Unfortunately, even complete resection rarely cures the patient, since many may still die of complications or recurrent diseases after 5-year survival point [102]. Crucially, it is imperative to understand the underlying biology and develop molecular diagnosis of pancreatic cancer, since next-generation-sequencing results and other molecular data increasingly point to complex interdependencies and strong intratumoural heterogeneity of pancreatic malignancies [98].

1.1.1 Epidemiology

Pancreatic cancer worldwidely ranks 11th in cancer incidence and 7th as a cause of cancer death [35]. In Western Europe, the age-standardized rate (ASR) incidence is 8.3 per 100,000 population, and it is distributed a little bit more in men. Meanwhile, as for individuals younger than 50 years old, the incidence of pancreatic cancer is increasing in Germany [52]. Thus, if there is no upgraded

intervention, the occurrence of pancreatic cancer would be expected to increase also among the younger population. As for continuing high mortality in Western Europe, in Germany, the absolute number of new cases and deaths has risen continuously over the years for both sexes, as demonstrated by data from the Robert Koch Institute [50].

1.1.2 Etiology and Tumor Development

A number of lifestyle and risk factors associated with incidence and metastasis of pancreatic cancer have been identified [52]. Among these, smoking and excessive alcohol consumption are most strongly related to the etiology of pancreatic cancer. A series of abnormal signs such as high cholesterol, hyperglycemia and hypertension which could cause high BMI are commonly seen among patients.

Long-standing chronic pancreatitis is also a substantial risk factor to progress to malignancy. In a study by Lowenfels et al., following up more than 2000 patients with chronic pancreatitis, a 26-fold increase in the risk of developing pancreatic cancer was found [67]. Additionally, molecular analyses indicate that about 5%-10% patients have genetic predispositions [38]. Analyzing the PDAC biological landscape of sporadic PDAC by next generation sequencing revealed that the KRAS (Kirsten rat sarcoma) gene is activated in > 90% PDAC patients. In more than 50% of cases, TP53 and CDKN2A mutations, and in about 40% cases SMAD4 mutations are detected [118]. Moreover, some inherited disorders increase the risk of pancreatic cancer, for example, hereditary pancreatitis, multiple endocrine neoplasia, Von Hippel-Lindau syndrome (VHL) and familial atypical multiple mole melanoma (FAMMM) syndrome which is associated with germline mutations in the BRCA1 and BRCA2 genes [69] [68] [7].

It is thought that PDAC most commonly evolves through precursor lesions termed pancreatic intraepithelial neoplasia (PanIN). PanINs are stratified into

different stages according to their levels of atypia. Epithelial lesions with papillary features are defined as PanIN 1B, otherwise flat epithelial lesions are classified as PanIN 1A. When lesions progress with some nuclear abnormalities and detectable mitoses (even if rare), it is called PanIN 2. Papillary or micropapillary lesions with disorganized cell structure as well as nuclear irregularities with prominent nucleoli are characteristic of PanIN3 [30]. Some work on serial autopsies indicate that KRAS, p16/CDKN2A, GNAS, or BRAF may already be mutated in low-grade PanIN [57], and at late stage, SMAD4/DPC4 and TP53 genes could be deregulated in high-grade PanIN [131].

1.1.3 Diagnosis and Treatment

Nonspecific and subtle symptoms at onset are distinct manifestations of pancreatic cancer [24]. Laboratory tests tend to yield nonspecific results, sometimes, pancreatic cancer patients at terminal stage may only have general laboratory evidence of malnutrition and elevation of serum amylase and/or lipase levels [49]. Some tumor markers are applied to assist diagnosis. Carcinoembryonic antigen (CEA) is commonly found in fetal tissues, but it elevated in some types of carcinomas. However, the rate of abnormal findings among patients with pancreatic carcinoma is only 40% [61]. Moreover, benign and malignant conditions other than pancreatic cancer can also induce elevation of CEA [13]. Thus, CEA is not a suitably sensitive and specific marker for pancreatic cancer diagnosis. Carbohydrate antigen 19-9 (CA19-9) is commonly found in circulating mucins of patients suffering from different forms of cancer. A CA19-9 value of greater than 100 U/mL is highly suspicious for pancreatic malignancy if patients are without biliary obstruction, pancreatitis or other benign diseases, with specificity of detection of up to 75-85% [32]. However, sensitivity is low especially at early tumor stages [115], so that CA19-9 is generally not considered to be a gold standard for diagnosis of pancreatic cancer, but it could be an adjunct diagnostic method and used as a prognostic

value of preoperative patients [53].

Imaging techniques, such as computed tomography (CT), Endoscopic ultrasonography (EUS) and Endoscopic retrograde cholangiopancreatography (ERCP) are important tools in the clinical diagnosis of pancreatic cancer [105]. However, imaging largely depends on the local availability and expertise with the procedure, as well as local cancer protocols. Multidetector CT scanning (MDCT) is recommended by National Comprehensive Cancer Network to detect pancreas tumor, because it could be used to accurately estimate tumor condition and its resectability by involvement of angiography. However, even such advanced techniques have a significant risk of missing small tumors [117].

As to treatment considerations, it is consensus that pancreatectomy is the potential curative treatment for pancreatic cancer. Unfortunately, the difficulty of early diagnosis often leads to a situation where local invasion or metastasis decrease the possibility to receive surgery [27]. Application of adjuvant therapy brings a significant survival benefit after tumor resection or when metastases are present [114]. Gemcitabine is now accepted as standard therapy for surgically resected pancreatic cancer or unresectable cases [120]. A modified FOLFIRINOX (mFOLFIRINOX) protocol offers better performance as demonstrated by superior survival, but it is also associated with significantly enhanced adverse effects [108] [90]. Targeted therapy using Erlotinib, which inhibits the intracellular phosphorylation of epidermal growth factor (EGFR) tyrosine kinase, is approved by the US Food and Drug Administration (FDA) to apply to metastatic and unresectable patients in combination with Gemcitabine, but this regimen is also associated with additional toxicity [78].

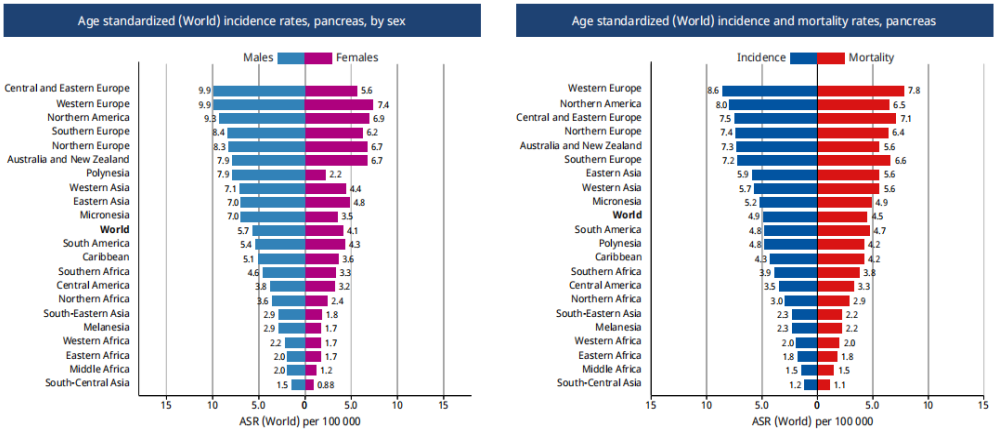

Diagram of pancreatic cancer incidence of both gender throughout the world in 2020. Data originated from “The Global Cancer Observatory - Globocan 2020.12”.

1.2 Cellular and Molecular Aspects of Pancreatic Cancer

A number of genetically engineered mouse models (GEMMs) for PDAC research have been created to functionally study genetic alterations commonly observed in pancreatic cancer patients. As mentioned before, 90% of pancreatic cancer patients carry activating KRAS mutations. The GTPase activity of the KRAS protein is impaired upon KRAS mutation, which leads to blocking of GTPase-activating proteins (GAPs) which can no longer hydrolyze GTP. Therefore, KRAS remains activated and stimulates downstream pathways to influence cell growth, cell invasion and metastasis [34]. In 75% of PDAC cases, the tumor suppressor p53 is inactivated [5]. Moreover, activation of KRAS could inactivate p53, and together both alterations promote the progression from precancerous pancreatic tissue to aggressive tumors [48]. The tumor suppressor SMAD4 is an intracellular transcriptional mediator of the TGFβ signaling pathway encoded by the SMAD4 gene. SMAD4 is commonly seen at terminal stages of pancreatic cancer [23]. Intragenic mutation or homozygous deletion leads to downregulation of SMAD4, it is related to the degree of differentiation, tumor size, and lymph node metastasis. In addition, SMAD4 is a prognostic marker of pancreatic cancer, Oshima’s work showed decreased overall survival rates in SMAD4 mutated cases (18.3 months versus 30.1 months for preserved SMAD4; $p < 0.001$) [85]. Treatment of

patients with loss of SMAD4 with Gemcitabine-based regimens showed no association with overall survival (HR 1.008; $p = 0.656$) but extended progression free survival (HR 1.565, $p = 0.038$) [84]. Abnormally glycosylated MUC1 is upregulated in more than half of PDAC cases, and mostly in high-grade PanINs [106]. A majority of KRAS mutations are recurrent "hot spot" driver mutations that most occur at codons 12, with KRASG12D being the most common KRAS mutation in human gastrointestinal cancers, and this mutation is usually associated with high expression of MUC1 [106]. Tinder et al. established a KRASG12D mouse model to overexpress MUC1 at levels similarly to those in human pancreatic cancer. They observed that tumor weight, metastatic lesions and cell proliferation were greater in the double mutant mice, suggesting that MUC1 in the context of KRasG12D is associated with tumor progression. They also found increased epithelial-mesenchymal transition (EMT) resulting in increased cell invasion and metastasis. MUC1 thus connects the cellular microenvironment to metabolism and may be a valuable therapeutic target of pancreatic cancer.

Although EGFR mutations are found in less than 3% of PDAC cases, it is still crucial for pancreatic cancer progression. EGFR is absent from normal pancreas, and it is significantly stained in precancerous PanINs [99] and PDAC [81]. Navas et al. observed overexpression of wild-type EGFR on a KRAS-mutant background led to PDAC. Moreover, their results suggested that EGFR function is independent of p53 in pancreatic cancer.

Urokinase plasminogen activator (PLAU or uPA) and its specific membrane receptor uPA receptor (uPAR) serve as prognostic factors in pancreatic cancer [14]. Cantero et al. demonstrated strong staining on cancer lesions with signs of invasion among 30 human pancreatic cancer cases. Patients with overexpression of PLAU and uPAR had a shorter post-operative survival than patients only with PLAU or uPAR overexpression, or non-expression of both factors. A second study confirmed that PLAU overexpression predicted negative prognosis of pancreatic cancer [70]. Moreover, administration of

anti-uPAR monoclonal antibodies to tumor-bearing mice resulted in tumor growth reduction and inhibition of retroperitoneal invasion [107].

Advanced technologies like DNA or RNA sequencing generated a growing list of potential genes and signaling pathways driving initiation and progression of pancreatic cancer [98] [73]. Therefore, more biofunctions and mechanisms of action of these genes should be investigated to provide novel biomarker of diagnosis and personalized targets of drug development of pancreatic cancer. Our previous high-throughput analysis of whole genome oligonucleotide microarrays experimentally screened out a list of genes which were associated with progress of PDAC [12]. Among those candidate genes, cytochrome C oxidase (COX) assembly factor 4 homolog (COA4) and RNA polymerase III subunit K (POLr3K) were differentially overexpressed in human PDAC tissues.

1.3 COA4 - Cytochrome C Oxidase (COX) Assembly Factor 4 Homolog

COA4 which is predicted to localize in mitochondrial intermembrane space is a protein coding gene with small molecular weight of 10 kDa [37]. As an assembly factor of COX, the function of COA4 is closely linked with COX. COX is the unique terminal oxidase of the mitochondrial respiratory chain (as following picture showed) in eukaryotes which produces ATP. Most of the ATP is synthesized at the inner membrane of mitochondria where a series of enzymes that perform electron transfer and proton translocation from the internal mitochondrial matrix (IMM) space to the inter-membrane space (IMS) through the inner mitochondrial, so that a proton gradient is generated [8]. The electrochemical gradient is regulated by ubiquinone oxidoreductase (Complex I), cytochrome c oxidoreductase (Complex III) and Cytochrome C Oxidase (Complex IV, COX). COX is a large transmembrane protein complex on mitochondria that acts as a proton pump, receiving electrons and pumping H+ from the matrix to the membrane gap, then oxygen is converted to water, thus a proton electrochemical potential energy difference is created across the

membrane which allows production of ATP through adenosine triphosphate synthase [36] [91]. The three complexes mentioned above are comprised of subunits of dual genetic origin and embedded into the inner mitochondrial membrane. The subunits with catalytic activity of the complexes are encoded by the mitochondrial genome [48]. The subunits of COX are encoded by three mitochondrial genes, COX1, COX2 and COX3 which require additional messenger and subunit factors to start biogenesis of synthesis, membrane insertion, maturation and assembly of the complex [36] [91]. In this context, the role of COA4 in respiratory chain is not entirely clear. While COX is highly conserved between yeast and mammalian systems [101], transcription and translation factors seem to be poorly conserved at the primary sequence level among mammalian genomes [84]. Nonetheless, some studies provided insights into the COX assembly process and its association with human disorders. Leigh syndrome (subacute necrotizing encephalomyelopathy) is a typical disease of COX deficiency which may also have an association with COA4. Gene mutations are a primary pathogenic factor of Leigh syndrome. Among the described gene alterations, mitochondrial DNA (mtDNA) is affected 20% of the time [77]. MT-ATP6, which guides synthesis of the ATP synthase protein complex, is commonly affected by mtDNA mutation and contributes to block downstream ATP production. Other mtDNA mutations in Leigh syndrome block generation of mitochondrial proteins by decreasing the activity of other processes at the last step of electron transfer [79]. On the other hand, mutations of the nuclear-encoded gene SURF1, which assists to assemble COX protein complex, generates an abnormal SURF1 protein that leads to reduced COX complex formation and indirectly diminishes mitochondria energy production [62]. SURF1 thus shows several similarities with COA4, although a direct involvement of COA4 in Leigh syndrome pathogenesis is not clearly described yet.

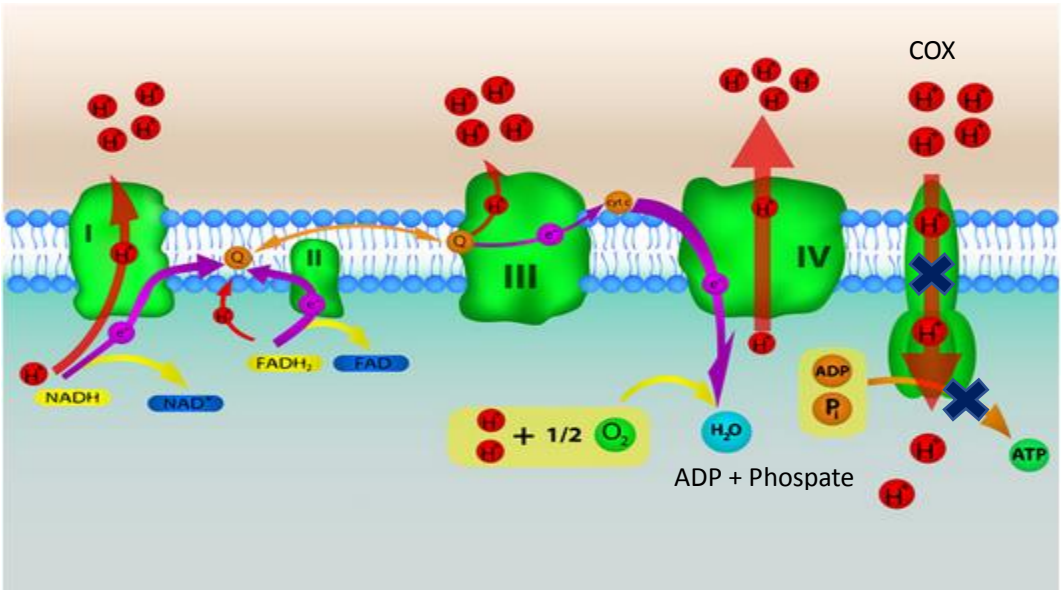

Oxidative phosphorylation and the electron transport chain. Source: https://www.shutterstock.com, ID: 174872780

COX drives cancer progression of many cancer types. An example is breast cancer, where elevated receptor tyrosine kinase signaling is a key pathway to enable tumor growth. Stimulation of epidermal growth factor (EGF) was shown to induce EGFR translocation to mitochondria where it phosphorylates COX subunit II and directly binds COX [9]. Furthermore, studies on glioblastoma showed that there was high activity of COX in primary glioma tissues, and COX could be a marker of poor outcome. Inhibition of COX via its inhibitor gene ADDA5 could reverse the chemoresistance to temozolomide. The expression level of COX is low in tumor tissues, because of endogenous respiration consumption, so 7%-22% COX activity reduction could sufficiently alter energy homeostasis in malignant cells [83]. In gastrointestinal cancers, KRAS was shown to activate COX and mitochondrial respiration via COX Vb which is a regulatory subunit of COX [75] [104]. Regarding COX assembly factors, it has been shown in colorectal cancer that COA1 could promote cell proliferation and reduce apoptosis rates by PI3K/AKT signaling pathway activation [119] [125]. To date there are no reports on a role of COA4 in cancer cells. Research on a putative COA4 ortholog in yeasts could be taken to indicate that inhibition of COA4 would generate excess hydrogen peroxide and

then cause COX defect, which would be expected to lead to reduce cell proliferation [8]. It remains unclear, though, if these results are indeed transferable to mammalian cells and if transformed cells would be affected differently.

As mentioned before, COA4 as a new target of functional study was screened out by whole-genome oligonucleotide microarrays on different types of microdissected pancreatic tissues [12]. COA4 is highly expressed on precursor lesions of pancreatic intraepithelial neoplasia (PanIN) and PDAC tissues compared to low grade of PanINs and normal pancreas. Therefore, COA4 may have an important role of COX accurately functionating in the respiratory chain, and it may be related to diseases progression in various ways.

1.4 POLr3K - RNA Polymerase III Subunit K

POLr3K encodes a subunit of RNA polymerase III, which is responsible for RNA transcription processing and mostly localizes to the nucleus. There are three distinct DNA-dependent RNA polymerases (Pol I, Pol II and Pol III) that transcribe gene information into mobile RNA entities [93]. The basal mechanism of Pol III transcription includes the enzyme itself and transcription factors that guide Pol III to different promoters [116].

Pol III related gene transcription processes are different between Pol III promoter structures. Type 1 and 2 promoters are gene-internal, type 3 promoters located in the 5′ flanking region. For type1 promoters, Pol III is guided to a DNA-bound complex composed of TFIIIA, TFIIIC, and BRF1-TFIIIB (consisting of BDP1, BRF1, and TBP [TATA binding protein]). TFIIIA which specifically regulates 5S RNA transcription through site-specific binding to the 5S gene promoter is not involved in type 2 promoter binding. In type 3 promoters, Pol III involvement is mediated by snRNA-activating protein complex and BRF2–TFIIIB [95]. TFIIIC is a six-subunit complex that recognizes the promoter elements of all Pol III transcription units [97]. The transcription

cycle of Pol III is started with binding to Nab2 and terminates at oligo (U) rich region [112]. From yeast to humans, RNA Polymerase III is highly conserved and contains 17 subunits, 5 of them are mutually shared among Pol I, Pol II and Pol III, 2 of them are shared among Pol I and Pol III, and ten are specific to Pol III. Difference in the specific composition of these subunits result in formation of distinct enzymes (Pol IIIA and Pol IIIB) which have been identified in mouse myeloma cells [96] [3].

Pol III has previously been reported to be involved in tumor development. An enlarged nucleus is typical in cancer cells, and this feature is tightly related to rRNA synthesis and Pol III expression [59]. Overexpression of Pol III has been demonstrated in a number of cancer cell types, including breast and lung cancer [21]. Concerning the aforementioned transcription factors, in normal cells, TFIIIB is at a depressed state, which is regulated by RB and TP53. However, RB and TP53 are decreased when cells undergo malignant transformation, leading to increased TFIIIB expression, which together with other oncogenic proteins such as Erk promotes TFIIIC overexpression [121]. While it has been shown that TFIIIC as Pol III specific factor is involved in tumor growth–control, the exact mechanisms remain unclear.

Mutations of genes which code for certain Pol III transcription factors, like mutations of BRF1 and BRF2, result in impaired activity of Pol III. BRF1 is associated with kidney and colorectal cancers and found to be upregulated in gastric and lung cancers. Impaired Pol III activity because of mutations of Pol III subunits is a cause of leukodystrophy [130] [88] [31]. POLr3K is the most frequently affected subunit as shown by whole-exome sequencing. Study by Yee et al. [128] [129] indicates that Pol III activity is required for exocrine pancreatic epithelial proliferation during morphogenesis in zebrafish. In human pancreatic cancer cells, inhibition of histone deacetylases (HDACs) and Pol III cooperatively suppressed exocrine pancreatic growth. Combined treatment with the HDAC inhibitor suberoylanilide hydroxamic acid (SAHA) and inhibitor of POLr3-mediated transcription ML-60218 resulted in efficient inhibition of cell

growth as well as cell cycle arrested by p21 activation. Furthermore, ML-60218 repressed SAHA-stimulated expression of tRNAs.

POLr3K was identified as a potential target gene in PDAC in large-scale expression profiling analyses which were conducted by Prof. Malte Buchholz [12]. Comparing to normal tissue and different grades of PanINs, POLr3K was differentially overexpressed in PDAC. qRT-PCR analyses confirmed that POLr3K is significantly overexpressed among malignant tissues compared to normal pancreas tissue and chronic pancreatitis.

1.5 Role of microRNA in Pancreatic Cancer

microRNA is a kind of noncoding single stranded RNA which is composed of 21 ~ 23 nucleotides. So far, there are thousands of human miRNAs which have been described [72]. Except for the earliest found Lin-4 and let-7, microRNAs are represented by miR - #-# where miR represents microRNA, the first # represents serial number, and the second # represents different transcripts that could be transcribed from one microRNA gene. During biosynthesis of microRNA in the nucleus, through the action of RNA transcriptase, a pri-micro RNA is produced as original transcript, and then the pri-micro RNA is cleaved to form the miRNA precursor (pre-microRNA) through the action of RNA polymerase III. Finally, the mature microRNA is produced through further cleavage of the pre-miRNA and is then ready to evoke downstream biological activities. Mature microRNA forms an RNA-induced silencing complex (miRISC) and acts on target mRNA to regulate gene expression by shearing or inhibiting the mRNA translation process [45]. However, the mechanism of activity between microRNA and target mRNA is still not completely understood. Studies indicate that mature microRNAs form a 15S ribonucleoprotein complex (RISC) with Gemin3, Gemin4, and EIF-C2 [80]. miRISC is not only acting on the 3′ untranslated region (3′-UTR) of mRNA of specific genes through the classic microRNA pathway, inhibiting the translation

of mRNA without affecting the stability of mRNA, but also degrading RNA in cases where it is completely complementary to the target sequence. Recent reports demonstrate that microRNA may also act on the 5'-UTR region, but the exact mechanisms, especially in cases where the sequence of microRNA is not completely complementary to the 5'-UTR remain unclear [82].

Aberrant microRNAs expression is associated with carcinogenesis of pancreatic cancer which includes tumor suppressor avoidance, cell death modulation, tumor invasion, angiogenesis, and metastasis [133]. Some reports demonstrate functions of microRNA in cell proliferation and cell cycle regulation of pancreatic cancer. miR-424-5p enhances cell proliferation and migration through downregulating suppressor of cytokine signaling 6 (SOCS6) which leads to elevated activity of the ERK pathway. Downregulation of miR-203 promotes cell proliferation by inducing cell progression to the G1 phase [44]. Others like oncogene KRAS expression could be altered by miR-143, let-7-d, and miR-126, which is correlated with abnormal cellular proliferation [44] [51] [54]. Several oncogenic microRNAs negatively affect tumor-suppressor genes that impact cell cycle progression. Inhibition of microRNA-21 by transfection of antisense oligonucleotides results in upregulation of tumor-suppressor PTEN (phosphatase and tensin homologue), which controls the frequency of cell division, thus inducing antiproliferative effects [86]. Moreover, upregulated miR-192 in pancreatic cancer facilitates progression from G0/G1 to S phase by suppression of SIP1 and elevation of collagen I [135].

Abnormal expression of miR-30d-5p (miR30d) was found in several cancer types. For instance, overexpressed miR30d accelerates invasion and migration of breast cancer by targeting KLF-11 and pSTAT3 [46]. In non-small cell lung cancer, miR30d inhibits cell proliferation and motility via CCNE2 [18]. However, miR30d is downregulated in colon cancer, where cell proliferation and invasion activities are stimulated by targeting LRH-1 [126]. miR30d regulates beclin-1 to impact the sensitivity of anaplastic thyroid carcinoma cells

to cisplatin [134]. In pancreatic cancer, miR30d was reported to be downregulated compared to noncancerous tissue [123]. Based on data from the TCGA database, Kaplan-Meier analysis indicates miR30d could be a prognostic marker of pancreatic cancer. In addition, miR30d is observed to regulate cell growth and invasion by targeting SOX4 and suppressing the SOX4/PI3K-AKT signaling pathway. Therefore, better understanding of the complex mechanisms of microRNA and regulation of associated genes may bring new approaches in pancreatic cancer diagnosis and therapy.

1.6 Objective of My Work

COA4 and POLr3K were potential candidate molecules to mediate progression of PDAC which were identified from large scale profiling analyses. To investigate how COA4 and POLr3K may impact pancreatic cancer progression, knockdown of the candidate genes in pancreatic cancer cell lines with specific siRNAs was to be applied and effects on cell growth, cell cycle progression and cell migration were observed. Potential downstream effectors of COA4 were to be identified by RNA-Seq, followed by functional analyses of these effectors. As Pol III is described to drive transcription of microRNA [10], TaqMan human microRNA arrays were to be employed to detect microRNAs that could be regulated by POLr3K and disclosing biomechanisms linking of POLr3K and functional microRNAs. Therefore, following points were to be addressed in this thesis:

1. Expression level of COA4 and POLr3K on human normal pancreas, chronic pancreatitis and pancreatic cancer specimens.
2. Function of COA4 and POLr3K on cell proliferation, cell cycle and cell migration *in vitro* studies.
3. Role of COA4 and POLr3K on overall survival of PDAC.
4. Identity and role of potential mRNA or miRNA downstream mediators of the candidate genes in pancreatic cancer.

2. Materials and Methods

2.1 Materials

2.1.1 Cell Lines

Table 1. Cell lines

Name	Description	Origin	Maintained Medium
HEK-293	Embryonic kidney cells; Human[3]	American Type Culture Collection	DMEM-5 % FCS
Klon2.2	Pancreatic Stellate Cells; Human	-	RPMI + 10% FCS
LON556	Primary Pancreatic ductal adenocarcinoma; Human	Established by Prof. Dr. C. Heeschen, Queen-Mary-University, London	RPMI + 10% FCS
Panc-1	Pancreatic ductal adenocarcinoma; Human[2]	American Type Culture Collection	DMEM-5 % FCS
S2-007	Pancreatic ductal adenocarcinoma; Human Derived from metastatic in the liver[1]	T Iwamura (medical school, Miyazaki, Japan)	DMEM-5 % FCS

Information Reference:

1. Iwamura T, Caffrey TC, Kitamura N, Yamanari H, Setoguchi T, Hollingsworth MA. P-selectin expression in a metastatic pancreatic tumor cell line (SUIT-2). Cancer Res 1997;57:1206–12.

2. Lieber M, Mazzetta J, Nelson-Rees W, Kaplan M, Todaro G. Establishment of a continuous tumor-cell line (panc-1) from a human carcinoma of the exocrine pancreas. Int J Cancer 1975;15:741–7.

3. Zur HH. Induction of specific chromosomal aberrations by adenovirus type 12 in human embryonic kidney cells. J Virol 1967;1:1174–85.

2.1.2 Instruments

Table 2. Instruments

Instruments	Manufacture
Autoclave 3850 El	Tuttnauer Europe B.V. (Breda, Netherland)
Agilent Bioanalyzer	Agilent Technologies (Santa Clara, USA)
Bio-Rad T100 Thermal Cycler	Applied Biosystems (Waltham, USA)
BD FACSCanto Ⅱ	BD Biosciences (Allschwil, Swizerland)
Cell Culture Bench: Msc-Advantage 1.2	Thermo Fisher Scientific, Life Technologies (Dreieich, Germany)
Chemo Cam Imager	INTAS Imaging Sciences (Goettingen, Germanyd)

Centro LB 960 Microplate Luminometer	Berthhold (Bad Wildbad, Germany)
Electrophoresis Power Supply Ev261	Biotec Fischer GmbH (Reiskirchen, Germany)
Fluorescence Microscope Axiovert 200m (XI-3 474)	Carl Zeiss (Cologne, Germany)
Freezer Mediline Lkexv 3910 (4°C, -20°C)	LIEBHERR (Bulle, Switzerland)
Hera Freeze Hfu T Series (-80°C)	Thermo Fisher Scientific, Life Technologies (Dreieich, Germany)
Heraceus Pico 17 Centrifuge	Thermo Fisher Scientific, Life Technologies (Dreieich, Germany)
Heracell CO_2 Incubator	Thermo Fisher Scientific, Life Technologies (Dreieich, Germany)
Incubator	Memmert GmbH (Buchenbach, Germany)
Leica Dmil Led Inverse Microscope	Leica Mikrosysteme (Wetzlar, Germany)
Multiscan Fc (MTT, Bradford)	Thermo Fisher Scientific, Life Technologies (Dreieich, Germany)
Multifuge 3SR+ Centrifuge	Thermo Fisher Scientific, Life Technologies (Dreieich, Germany)
Mini Rocker Shaker PMR-30	Grant-bio (Chelmsford, the United Kingdom)
NanoDrop 1000	Peqlab Biotechnologies GmbH (Erlangen, Germany)
Neubauer Chamber	Plan Optik AG (Elsoff, Germany)
Orbital Shaker KS250	IKA - Werk GmbH & Co. KG (Staufen, Germany)
Peqpower E300 Power Supply	Peqlab Biotechnologies GmbH (Erlangen, Germany)
PerfectBlue Semi-Dry, Elektroblotter Sedec	Peqlab (Darmstadt, Germany)
QuantStudio 7 Flex Real-Time PCR System	Applied Biosystems (Waltham, USA)
Shaking Device (Ks 250 Basic)	IKA Labortechnik (Staufen, Germany)
Special Accuracy Weighing Machine Bp 110 S	Sartorius AG (Guxhagen, Germany)
Thermomixer 5436	Eppendorf AG (Hamburg, Germany)
Vortexer Reax 2000	Heidolph Instruments (Schwabach, Germany)
ZEISS Axiovert 200M Microscopy	Carl Zeiss MicroImaging (Frankfurt, Germany)
ZEISS Axio Scope A1	Carl Zeiss MicroImaging (Frankfurt, Germany)
7500 Fast Realtime-PCR System	Applied Biosystems (Waltham, USA)

2.1.3 Lab Materials

Table 3. Lab materials

Lab Materials	Manufacture
Amersham Protran Nitrocellulose Membran, 0,2 µm	GE Healthcare Europe GmbH (Freiburg, Germany)
Cell Scraper	Greiner Bio-One (Frickenhausen, Germany)
Combitips Advanced	Eppendorf AG (Hamburg, Germany)
Cover glass, Menzel Gläser	Thermo Fisher Scientific (Waltham, USA)
Filter paper MN 218B, sponges	Biozym Scientific GmbH (Oldendorf, Germany)
Glass Beaker	Duran Group GmbH (Wertheim/Main, Germany)
Micro Tubes	Sarstedt AG & Co. (Nuembrecht, Germany)
MicroAmp Fast 96-well reaction plate	Applied Biosystems by Life Technologies (Waltham, USA)
Multipipette Plus	Eppendorf AG (Hamburg, Germany)

MicroAmp Optical Adhesive Film	Applied Biosystems by Life Technologies (Waltham, USA)
Object Slide, Menzel-Gläser	Thermo Fisher Scientific (Waltham, USA)
PARA Film	BEMIS (Terre Haute, US)
Pipetboy	INTEGRA Biosciences AG (Zizers, Switzerland)
Pipettes	Sarstedt AG & Co. (Nuembrecht, Germany)
Pipette Tips	Sarstedt AG & Co. (Nuembrecht, Germany)
PVDF	Bio-Rad Laboratories Inc. (United States)
RNA Nano Chips	Agilent Technologies (Waldbronn, Germany)
SDS-Page/ Blotting Device	Peqlab Biotechnologies GmbH (Erlangen, Germany)
TC flasks T75 Standard	Sarstedt AG & Co. (Nuembrecht, Germany)
TC flasks T25 Standard	Sarstedt AG & Co. (Nuembrecht, Germany)
Tissue culture dish (10 cm)	Becton Dickinson (Heidelberg, Germany)
Transfection Tubes	Sarstedt AG & Co. (Nuembrecht, Germany)
TaqMan Array Human MicroRNA A+B Cards Set 3.0	Thermo Fisher Scientific (Waltham, USA)
Variable Volume Pipette Series	HTL Lab Solution (Warsaw, Poland)
15 ml Falcons	Sarstedt AG & Co. (Nuembrecht, Germany)
50 ml Falcons	Greiner Bio-One (Frickenhausen, Germany)
6-well &12-well cell culture plate	Greiner Bio-One
96-well microplate	PerkinElmer Cellular Technologies (Hamburg, Germany)
75 x 12 mm PS tube	Sarstedt AG & Co. (Nuembrecht, Germany)

2.1.4 Chemicals

Table 4. Chemicals

Chemicals	Manufacture
Aqua dest	B. Braun (Melsungen, Germany)
Ampuwa Plastipur for Washing	Fresenius Kabi France
Acrylamid: Rotiphorese Gel 30	Carl Roth GmbH (Karlsruhe, Germany)
Annexin V Alexa Flour 488 Conjugate	Thermo Fisher Scientific (Waltham, USA)
APS	Merck KGaA (Darmstadt, Germany)
Bromphenol blue	Sigma-Aldrich Chemie GmbH (Steinheim, Germany)
BSA	Sigma-Aldrich Chemie GmbH (Steinheim, Germany)
Collagen	Sigma-Aldrich GmbH (St. Louis, USA)
CellTiter-Glo	Promega Corporation (Madison, USA)
Dako antibody diluent	Agilent Technologies (Carpinteria, USA)
Dimethyl sulfoxide	Carl Roth GmbH (Karlsruhe, Germany
DMEM	Gibco, Life Technologies (Darmstadt, Germany)
DTT	Serva Electrophoresis (Heidelberg, Germany)
DPBS	Gibco, Life Technologies (Darmstadt, Germany)
ECL	Bio-Rad Laboratories GmbH (Munich, Germany)
ECL-Ultra	Bio-Rad Laboratories GmbH (Munich, Germany)
Ethanol absolute 100%	Sigma-Aldrich Chemie GmbH (Steinheim, Germany)
Ethylene Glycol Tetraacetic Acid	Sigma-Aldrich Chemie GmbH (Steinheim, Germany)
FBS	Gibco, Life Technologies (Darmstadt, Germany)
Glycerin	Sigma-Aldrich Chemie GmbH (Steinheim, Germany)
Glycerol (87 %)	Arcos Organics (New Jersey, USA)
Glycin	Carl Roth GmbH (Karlsruhe, Germany)
HCL 37 % (fuming)	Carl Roth GmbH (Karlsruhe, Germany)

Hemalum solution acid according to Mayer	Carl Roth GmbH (Karlsruhe, Germany)
HEPES	Sigma-Aldrich Chemie GmbH (Steinheim, Germany)
Hydrochlorid acid (1 M)	Fisher Scientific (Loughborough, United Kingdom)
Hydrogen Peoxide 30%	Carl Roth GmbH (Karlsruhe, Germany)
iTaq Universal SYBR Green Supermix	Bio-Rad Laboratories GmbH (Munich, Germany)
ImPRESS Reagent Kit Peroxidase Anti-Rabbit Ig	Vector Laboratories (Burlingane, USA)
Isopropanol	Arcos Organics (New Jersey, USA)
Lipofectamine RNAiMAX Transfection	Thermo Fisher Scientific (Waltham, USA)
Megaplex PreAmp Primers	Life Technologies Corporation (Pleasanton, USA)
Methanol ≥99.8 %	Sigma-Aldrich Chemie GmbH (Steinheim, Germany)
Milk Powder	Carl Roth GmbH (Karlsruhe, France)
NaF	Sigma-Aldrich Chemie GmbH (Steinheim, Germany)
$Na_4P_2O_7$	Sigma-Aldrich Chemie GmbH (Steinheim, Germany)
Nocodazole	AdipoGen Corporation (San Diego, USA)
PageRulerTM prestained protein ladder	Thermo Fisher Scientific (Dreieich, France)
Polyhydroxyethylmethacrylate	Sigma-Aldrich GmbH (St. Louis, USA)
Polyethylenimine, Linear, MW 25.000 (PEI 25000)	Polysciences, Inc. (Warrington, USA)
PreAmp MasterMix	Life Technologies Corporation (Pleasanton, USA)
Protease Arrest	G-Biosciences (Maryland Heights, USA)
Propidium Iodide	Sigma-Aldrich
RNase A	Thermo Fisher Scientific (Waltham, USA)
RPMI	Gibco, Life Technologies (Darmstadt, Germany)
SDS	Carl Roth GmbH (Karlsruhe, Germany)
Sodium Chloride	Sigma-Aldrich Chemie GmbH (Steinheim, Germany)
Sodium Citrate Trisbasic Dihydrate	Sigma-Aldrich GmbH (St. Louis, USA)
TEMED	Merck KGaA (Darmstadt, Germany)
Thiazolyl blue	Carl Roth GmbH (Karlsruhe, Germany)
Tris	Arcos Organics (New Jersey, USA)
TritonX-100	Carl Roth GmbH (Karlsruhe, Germany)
Trypsin-EDTA (0.5 %)	Gibco, Life Technologies (Darmstadt, Germany)
Tween-20	Sigma-Aldrich GmbH (St. Louis, USA)
5 x Annexin V Binding Buffer	Thermo Fisher Scientific (Waltham, USA)

2.1.5 Buffers & Solutions

Table 5. Buffers and solutions

Buffer/Solution	Composition		pH-Value
10 % APS	1.0 g	Ammoniumpersulfat	-
	10.0 ml	ddH_2O	
10x Blotting Buffer	250 nM	Tris Base Glycin	pH 8.3
	1.92 M		
	ad 1 L	A. dest	
1x Blotting Buffer	10 %	10x Blotting Buffer	pH 8.3
	20 %	Methanol Absolute	
	ad 1 L	ddH_2O	

10 % BSASolution	0,1 g ad 1 ml	BSA ddH_2O	-
Citrate Buffer	2.1g ad 1L	Citrate Monohydrate ddH_2O	PH 6.0
70 % Ethanol	70 ml 30 ml	Ethanol absolute (100 %) ddH_2O	-
Gel Running Buffer	1,5 M 0,4 % ad 100 ml	Tris Base SDS ddH_2O	pH 8.8
Gel Stacking Buffer	0,5 M 0,4 % ad 100 ml	Tris Base SDS ddH_2O	pH 6.8
Gel Separating Buffer	1,5 M 0,4 %	Tris Base SDS	pH 8.8
10x Loading Buffer	250 nM 1,92 M 1 % ad 1 l	Tris Base Glycin SDS ddH_2O	pH 8.3
1x Loading Buffer	10 % ad 1 l	10x Loading Buffer ddH_2O	pH 8.3
1xLysis Buffer	50 mM 150 mM 1 mM 10 % 1 % 100 mM 10 mM	HEPES (1 M; pH 7.5) NaCl EGTA Glycerin Triton-X-100 NaF $Na_4P_2O_7$	-
MTT-Solubilization solution	8 ml 1 ml 1 ml	Isopropanol Triton-X-100 HCl (1 M)	-
MTT-Solution	5 mg 1 ml	Thiazolyl blue DPBS	-
5 % Milk Powder Solution	2 g 40 ml	Milk Powder TBST	-
20mg/ml Poly-HEMA	0.1 g ad 5 ml	Poly-HEMA 96% Ehtanol	-
4x SDS Loading Buffer	253 nM 0,05 % 40 % 2 % ad 50 ml	Tris HCl Bromphenol blue Glycerol SDS ddH_2O	pH 6.8
10x TBS	24,2 g 80 g 15 ml ad 1 l	Tris Base NaCl HCL (37 %) ddH_2O	pH 7.6

1x TBST	10 % 0,1% ad 1l	10x TBS Tween 20 ddH_2Ot	pH 7.6
10 x TBS for immunohistochemistry	60.57g 87.33g ad 500 ml	Tris NaCl ddH_2O	pH 7.6

2.1.6 Molecular Biology Kits

Table 6. Molecular biology kits

Kit	Manufacture	Application
AgilentRNA 6000 Nano Kit	Agilent Technologies (Santa Clara, USA)	RNA integrity measurement
Clarity Western ECL Substrate	BioRad Laboratories GmbH (Munich, Germany)	Detection of bundled Ab of Western Analysis
Cell Proliferation Elisa Kit (BrdU)	Roche Diagnositics GmbH (Mannheim, Germany)	Cell proliferation assay
ImmPACT DAB Peroxidase Substrate Kit	Vector Laboratories (Burlingane, USA)	Immunohistochemistry
MirVanamiRNA Isolation Kit	Thermo Fisher Scientific ((Waltham, USA)	microRNA extraction
PeqGold Total RNA Kit	VWR (Leuven, Belgium)	cDNA-Synthesis
PeqGold Total RNA Kit	Peqlab Biotechnologies GmbH (Erlangen, Germany)	cDNA-Synthesis
Pierce Coomassie Plus (Bradford) Assay Kit	Thermo Fisher Scientific (Dreieich, Germany)	Protein concentration measurement
Qiagen Plasmid Midi Kit	Qiagen (Hilden, Germany)	Purification of plasmid DNA
Taqman MicroRNA Reversed Transcription Kit	Life Technologies Corporation, (Pleasanton, USA)	For microRNA analysis with preamplification
VECTASTAIN ABC Kit	Vector Laboratories (Burlingane, USA)	Immunohistochemistry

2.1.7 Antibodies

Table 7. Antibodies

Antibody	Binding Point	Host Species	Instruction
Anti-COA4 polyclonal abcam ab105678	Internal sequence amino acids 37-86 of human COA4	Rabbit	1:500 in 5% non-fat milk with TBST
Anti-COA4 polyclonal Sigma Aldrich HPA040126 (For IHC)	Primary antibody for immunochemistry	Rabbit	1:200-1:500 in Dako antibody diluent
Anti-rabbit-IgG, HRP linked, Cell Signaling 7074S	Secondary antibody	Rabbit	1:10,000 in 5% non-fat milk with TBST
Anti-β actin, HRP-monoclonal,	β actin, N-terminales piptide	Mouse	1:10,000 in 5% non-fat

Sigma-Aldrich, A3854			milk with TBST
Anti-POLr3K polyclonal abcam ab121238	Amino acids 6-108 of human POLr3K	Rabbit	1:500 in 5% non-fat milk with TBST
Anti-Cyclin D1 monoclonal Abcam ab16663	detects endogenous levels of cyclin D1	Rabbit	1:500 in 5% non-fat milk with TBST
Anti-P21 Cell Signaling 2947	Detects endogenous levels of total p21 protein	Rabbit	1:1000 in 5% BSA with TBST
Anti-PARP Cell Signaling 9542	caspase cleavage site in PARP	Rabbit	1:1000 in 5% non-fat milk with TBST

2.1.8 Software

Table 8. Software

Program	Version	Manufacture
Axiovision	4.8	Carl Zeiss Microimaging GmbH
Axiovision SE64	4.8	Carl Zeiss Microimaging GmbH
ChemoStar Image	-	Intas Science Imaging Instruments GmbH
ClusterProfiler	4.2.0	Maintainer: Guangchuang Yu Available at: https://bioconductor.org/
Cytoscape	3.8.2	for maintenance is funded by NIGMS
Flowjo	V10	FlowJo LLC of Becton Dickinson
GraphPad	Prism7	GraphPad Software
ImageJ	1.46r	National Institutes of Health
Microsoft Office	2013	Microsoft Corporation
Mikro2000	4.36	Mikrotek Laborsysteme GmbH
Modfit LT	3.0	Verity Software House
NanoDrop	V3.7.1	Thermo Scientific
Oligo 7	7.6	Molecular Biology Insights, Inc.
Primer Express	3.0	Applied Biosystems
SnapGene Viewer	5.2.4	GSL Biotech
TimeLapseAnalyser	V01_34	http://www.informatik.uni-ulm.de/ni/staff/HKestler/tla/
2100 Expert Bionalyzer Software	-	Agilent Technologies, Inc.
7500 Fast System Software	1.4	Applied Biosystems

2.1.9 Primers

All primers were constructed by Biomers.net (Ulm, Germany). The primer concentration was adjusted to 100 pmol /L with ddH_2O. The storage was kept at -20°C.

Table 9. Primers were used in the PCR and real time-PCR

	Primer	Sequence	
Primer for qPCR	**EXD2_for**	Sense:	5' -gctccagtgtcccagcatagtc- 3'
	EXD2_rev	Antisense:	5' -caaacacaatgatcagggagcat- 3'
	COA4_for	Sense:	5' -acccaacgggtgaagaaagac- 3'
	COA4_rev	Antisense:	5' -tgcactcctgcactgcaaag- 3'
	CNTLN_for	Sense:	5' -tcctgccatacccttttgg- 3'
	CNTLN_rev	Antisense:	5' -ttgagtgcagagtattctagaaagagaga- 3'
	MTMR6_for	Sense:	5' -aggcccatcagatgtaggtaataatg- 3'
	MTMR6_rev	Antisense:	5' -caagttggcaagggcacaa- 3'
	POLr3K_for	Sense:	5' -gtcccaaatgcgaacatcct- 3'
	POLr3K_rev	Antisense:	5' -cactgagcattgcagcacttg- 3'
	SLC35B2_for	Sense:	5' -ttccagttactcttcccacaagttc- 3'
	SLC35B2_rev	Antisense:	5' -agggtaagaaatgcaggtatttgc- 3'
	SQLE_for	Sense:	5' -gatgcccaggttgtaaatggtt- 3'
	SQLE_rev	Antisense:	5' -ccactctgcacttgattgttttct- 3'
	BCAR3_for	Sense:	5' -acaacgaccccaaggtcatc- 3'
	BCAR3_rev	Antisense:	5' -gagctcacccccatgttcct- 3'
	DRP2_for	Sense:	5' -tgggtatctggatagatggttgag- 3'
	DRP2_rev	Antisense:	5' -gccctccgtcccacattc- 3'
	THBS1_for	Sense:	5' -attagggaatcagaatcaaaccagt- 3'
	THBS1_rev	Antisense:	5' -gtaaccataaaaatataagcacggc- 3'
	PLAU_for	Sense:	5' -gagtgtcagcagccccactac- 3'
	PLAU_rev	Antisense:	5' -ctgagtctccctggcaggaa- 3'
	PLAU_for (out of PRF)	Sense:	5' -catttgtgaggcccatggtt- 3'
	PLAU_rev (out of PRF)	Antisense:	5' -accgctgctcccacattg- 3'
	MMP1_for	Sense:	5' -tcacacctctgacattcaccaag- 3'
	MMP1_rev	Antisense:	5' -aaaaggagagttgtcccgatga- 3'
	TP53_for	Sense:	5' -tcacacctctgacattcaccaag- 3'
	TP53_rev	Antisense:	5' -aaaaggagagttgtcccgatga- 3'
	RPLP0_for	Sense:	5' -agtttctccagagctgggttgt- 3'
	RPLP0_rev	Antisense:	5' -tgggcaagaacaccatgatg- 3'
	miR135a_5p_for	Sense	5' -cggctatggcttttattcctatg- 3'
	miR-30d-5p_for	Sense	5' -ctggtgtaaacatccccgactg- 3'

	miR-24-2-5p_for	Sense	5‘ -acgagcctactgagctgaaaca- 3’
	miR-1291_for	Sense	5‘ -tatggccctgactgaagac- 3’
	miR 191-5p_for	Sense	5‘ -gcaacggaatcccaaaagca- 3’
	miR-25-5p_for	Sense	5‘ -gctcaggcggagacttg- 3’
	miR-103a-3p_for	Sense	5‘ -ggcgagcagcattgtac- 3’
	U91	Sense: Antisense:	5‘ -gcggcggtggccgatgatgacg- 3’ 5‘ -atccagtgcagggtccgagg- 3’
	miR_rev Universal Generated from portion of Stem-Loop	Sense	5‘ -tcgtggagtcggcaa- 3’
Primer for PCR	**miR-1291 Stem Loop Primer**	Sense:	5‘ -gtcgtatccagtgcgtgtcgtggagtcggcaattgc actggatacgacactgctg- 3‘
	miR-24-2-5p Stem Loop Primer	Sense:	5‘ -gtcgtatccagtgcgtgtcgtggagtcggcaattgc actggatacgacctgtgt- 3‘
	miR135a_5p Stem Loop Primer	Sense:	5‘ -gtcgtatccagtgcgtgtcgtggagtcggcaattgc actggatacgactcacat- 3‘
	miR-30d-5p Stem Loop Primer	Sense:	5‘ -gtcgtatccagtgcgtgtcgtggagtcggcaattgc actggatacgaccttcca- 3‘
	miR 191-5p Stem Loop Primer	Sense:	5‘ -gtcgtatccagtgcgtgtcgtggagtcggcaattgc actggatacgaccagctgct- 3‘
	miR-25-5p Stem Loop Primer	Sense:	5‘ -gtcgtatccagtgcaattgccgactccacgacacg cactggatacgaccaattgc- 3‘
	miR-103a-3p Stem Loop Primer	Sense:	5‘ -gtcgtatccagtgcaattgccgactccacgacacg cactggatacgactcatagc- 3‘
	U91 Stem Loop Primer	Sense	5‘ -gtcgtatccagtgcgtgtcgtggagtcggcaattgc actggatacgaccggcct- 3‘
	Primer for PCR: Megaplex Primers Pool (Thermo Fisher Scientific-Dreieich, Germany**)**		

2.1.10 siRNAs

All siRNAs were constructed by Ambion Life Technologies (Darmstadt, Germany). The siRNAs were adjusted to 20 µM with nuclease-free

water, then stored at -20◦C. The siRNAs listed below were targeted ORF region of COA4 or POLr3K. A negative control “siControl” was produced by the AG Buchholz (ZTI, Department of Gastroenterology, Marburg).

Table 10. siRNA list

siRNA	Target Sequence	Sense and Antisense Strand	
COA4 siRNA1	5’-gattatagaggaagaaatcct- 3’	Sense:	5’ -cccagcaagauuauagaggtt-3‘
		Antisense:	5’ -ccucuauaaucuugcugggtg- 3‘
COA4 siRNA2	5’ -atgttcatggtcagatgtcat- 3’	Sense:	5‘-gcugucauauguucauggutt-3‘
		Antisense:	5‘ -accaugaacauaugacagctg- 3‘
COA4 siRNA3	5’-tgagtgaacagcaggcgaggc- 3’	Sense:	5’ -ggauugcaugagugaacagtt- 3‘
		Antisense:	5‘ -cuguucacucaugcaaucctt- 3’
POLr3K siRNA1	5’-ggtgaagagccaggggtcag- 3’	Sense:	5’ -ccuuuugaggugaagagcctt- 3‘
		Antisense:	5‘ -ggcucuucaccucaaaaggtt- 3’
POLr3K siRNA2	5’ -taaatatgctctgtgtaaagt- 3’	Sense:	5’ -cccauaacuaaauaugcuctt- 3‘
		Antisense:	5‘ -gagcauauuuaguuaugggtc- 3’
POLr3K siRNA3	5’ -tacaagtgctgcaatgctcag- 3’	Sense:	5’ -ccaccuucuacaagugcugtt- 3‘
		Antisense:	5‘ -cagcacuuguagaagguggtc- 3’

2.1.11 Plasmid

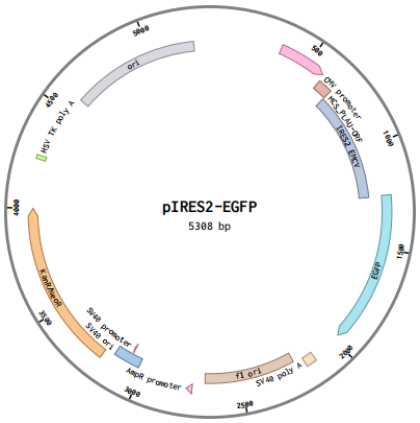

PLAU (NM_002658) Human cDNA/ORF Clone, in pIRES2-EGFP vector.

2.2 Methods

2.2.1 Cell Culture

2.2.1.1 Cell Line Cultivation

Cell lines were cultured in the respective media with 5%-10% fetal calf serum (FCS) (For more details refer to section 2.1.1) and cultivated at 37 °C, 5% CO_2 cell culture incubation. Cells were splitted when reached confluence of 80%-100%. Cells were washed with room temperature DPBS and incubated at 37 °C, 5% CO_2 for 5-15 min in Trypsin-EDTA. When cells were totally detached, trypsinization was stopped by adding respective cell culture medium. Depending on cell growth rate, appropriate amounts of detached cells were seeded on new T75 flask.

2.2.1.2 Cell Number Determination and Calculation

5-10 µL of a diluted cell suspension was transferred onto a Neubauer counting chamber (chamber factor 10^4 / mL) and all cells in the four quadrants were counted under the microscope. Finally, based on the formula: number of cells counted x 10^4 = number of cells / mL, the absolute number of cells in the original suspension was calculated.

2.2.2 Transfection

2.2.2.1 Lipofectamine™ RNAiMAX-Transfection

The Lipofectamine iMAX mediated siRNA or miRNA mimic transient transfection method was applied to transfect COA4 or POLr3K related siRNAs or miR-30d-5p mimics, respectively. The principle of this method is that negatively charged RNA is automatically binds to positively charged liposomes to form RNA-cationic liposome complexes. Then the captured RNA is

introduced into cells.

One day before the transfection, 50,000 cells / well of each cell line were seeded on 6-well plates. 2.0 µl single siRNA and 2.0 µl RNAiMax were respectively added in 150 µl DMEM without FCS to 2.0 ml low binding tubes, and incubated for 5 min at RT. Then siRNA and RNAiMAX were combined to get 300 µl volume, and incubated an additional 20 min at RT. Lastly, 300 µl compound were transfected into each well. Thus, a siRNA concentration of 17 nM was achieved.

Furthermore, siRNA plus miRNA mimic co-transfection was applied in some experiments. For this purpose, 2.0 µl single siRNA in combination with 5.0 µl miR30d mimic or negative control mimic as well as 3.5 µl RNAiMax were respectively added in 150 µl DMEM without FCS to 2.0 ml low binding tubes, also incubating for 5 min at RT. The remaining steps were as described above.

2.2.2.2 PEI-Transfection

This method was applied to transfection of plasmid constructs (PLAU-GFP plasmid) (plasmid construction sees 2.1.11). Polyethyleneimine (PEI) is a stable cationic polymer which can condense DNA into positively charged particles that bind to anionic cell surfaces. Then, the DNA-PEI complex is endocytosed by the cells and DNA released into the cytoplasm.

For the S2-007 cell line, 10 x 10^3 cells were sown on 10 cm dish at day one. After 24h, two 2.0 ml low binding tubes, numbered ① and ②, were prepared. 300 µl DMEM medium without FCS was pipetted into each low binding tube. Then, 12.0 µl PEI was added in tube ①, 3000 ng plasmid was added in tube ②, leaving for 5 min at RT. Subsequently, the content of both tubes was mixed and incubated for further 20 min at RT. During the time, the medium of the 10cm dish was replaced with 6 ml DMEM contained 5% FCS. Finally, 600 µl transfection mixture was added dropwise to the 10 cm dish (End volume was 6.6 ml).

2.2.3 Plasmid Stably Transfected Cell Selection by Geneticin (G418)

G418 is commonly used in gene selections to screen for resistant mammalian cells which expresses the neo gene which encodes an amino-glycoside 3'-phosphoransferase, and renders cells resistant to G418. 1.2mg/ml G418 was added to S2-007 cells which were transfected with 3000 ng PLAU-plasmid for 48h, changing medium once every other day until colony formation with stable Green fluorescent protein (GFP) signal was apparent. At this point, colonies could be transferred to a 6-well plate with G418 containing medium for cell growing, and finally transferred to cell culture flasks for routine maintenance.

2.2.4 RNA Isolation

RNA isolation was carried out by using peqGOLD Total RNA Kit (Peqlab Biotechnologies GmbH; Erlangen, Germany).
For 6-well plates, 350 µl lysis buffer was added to each well to dissolve, the lysate transferred to the DNA removing column and centrifuged (1 min, 12,000 x g). Then, an equal amount of 70% ethanol was added to the filtered solution. The mixture was added to a perfectBind RNA column and centrifuged for 1 min at 10,000 rpm. After centrifugation, 3 washing steps with initially 500 µl washing buffer 1 and then 2 times with 600 µl washing buffer 2 (15 sec each, 10,000 x g) were performed and the flow-through discarded. To dry the column, 2 min at 10,000 x g centrifugation was performed. At last, 30 µl RNase-free water was pipetted onto the columns and incubated for 3 min at RT. Centrifugation was performed for 1 min at 5,000 x g to elute RNA. RNA concentration was measured by NanoDrop 1000.

2.2.5 cDNA Synthesis

The Omniscript RT Kit (Qiagen; Hilden, Germany) was used for cDNA

synthesis. A MasterMix was created according to the number of samples (exact composition was set as below).

Table 11. MasterMix of cDNA synthesis for real-time PCR

MasterMix of One Sample
1.0 µl dH_2O
0,5 µl Reverse Transcriptase
2.0 µl dNTPs (5 mM)
2.0 µl 10× Buffer
0,4 µl Oligo dt Primer (20 µM)
End Volume = 5.9 µl

For each sample, 14.1 µl volume contained 500 ng RNA and dH_2O was prepared and combined with 5.9 µl MasterMix for a total volume of 20 µl. Then, the sample was incubated at 37 °C for 1h for synthesis. After the process, cDNA samples were frozen at -20 °C immediately.

2.2.6 qPCR

The quantitative polymerase chain reaction (qPCR) is an approach of detection and quantification of nucleic acids. It is based on monitoring fluorescence signal which is emitted from a reporter molecule, such as SYBR-Green, Taq-Man, or molecular beacons, etc. Accumulation of PCR products through each cycle of amplification is correlated to the initial amount of template. RPLP0 was selected as endogenous control. MasterMix was set up as following, all primers' concentration in this project was 10 µM.

Table 12. MasterMix of one 96-Well PCR reaction plate

MasterMix of One 96-Well PCR Reaction Plate
10.0 µl SYBR-Green
8.6 µl dH_2O
0.2 µl Primer *Forward*
0.2 µl Primer *Reverse*
End Volume = 19.0 µl

19.0 µl MasterMix were transferred to each well of 96-well PCR reaction plate, then adding 1.0 µl of the 1:10 diluted cDNA sample. Before initiating measurement, the plate was sealed with foil and briefly centrifuged. Finally, detection took place on the 7500 Fast Real-time PCR System, with parameter settings as following:

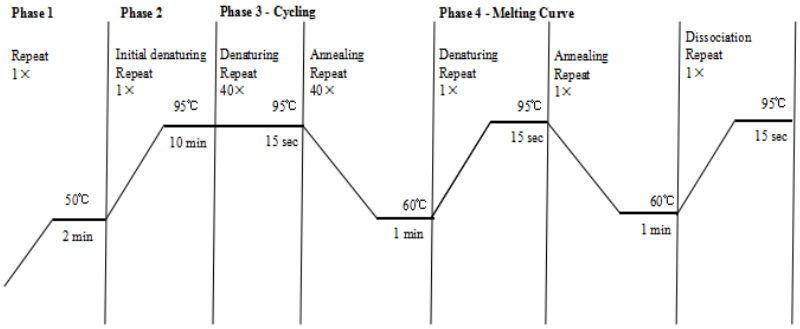

qPCR amplification melting curve of 7500 fast system

The amount of DNA was quantified by the ΔCt method. A duplication of the PCR product per cycle was assumed. The exact calculation formula was:

$$\Delta Ct = Ct_{\text{target gene}} - Ct_{\text{reference gene}}$$

$$\text{Relative Expression} = 2^{-\Delta Ct}$$

2.2.7 Cell Protein Extraction

For analysis of protein expression by Western Blot, cells on 6-well plates were detached by Trypsin-EDTA or cell scraper (based on cell line) and pelleted by centrifugation (3 min, 8,000 x g). Pellets were washed with 1.0 ml 1 x DPBS,

then centrifugation repeated.

Depending on the size of the pellet, the pellet was resuspended in 50-120 µl lysis buffer containing 1-fold concentration of protease arrest in the final solution. After 20 minutes lysing on ice, lysates were centrifuged at 13,300 x g for 1 min and the supernatant was transferred to a new Eppendorf tube. As preparation for ready-to-use samples for Western Blot, lysates were mixed with DTT and 4 × SDS (each sample contained: 50 µl protein sample + 7 µl DTT + 16 µl 4 × SDS) and stored at -20 °C.

2.2.8 Determination of Protein Concentration by Bradford Method

The Bradford protein assay involves addition of an acidic dye - Coomassie Brilliant G-250 to protein solutions. The dye binds to basic and aromatic amino acids which results in a shift of absorbance from 465 nm (brown) to 597 nm (blue). Based on comparison with a standard curve, the protein concentration is measured.

Bovine serum albumin (BSA) standard curves (1.0 – 6.0 µl BSA) were measured in duplicates. A 96 well plate was used for reagent loading. 200 µl of Coomassie solution was added to each well. Significantly, Coomassie solution should be mixed 1: 100 with lysis buffer in the wells for the standard curve samples, as this buffer has its own color. 2.0 µl protein samples were add to the Coomassie solution. After 10 minutes of incubation at RT, the plate was placed on the Multiscan FC at 597 nm. Using the values from the BSA standard series, a standard curve was created, thus, protein concentration determination was done.

2.2.9 Western Blot

This immunoblotting technique relies on the specificity of binding between a molecule of interest (protein) and a probe (a typical antibody raised against that target protein) to allow detection of the molecule of interest in a mixture of

many other similar molecules. Using gel electrophoresis to separate native or denatured proteins by the length of the polypeptide (denaturing condition) or by the 3-D structure of protein (native/non-denaturing condition), then proteins are transferred to a membrane (nitrocellulose or PVDF), where they can be probed by using specific antibodies.

2.2.9.1 SDS Polyacrylamide Gel-Electrophoresis

SDS-PAGE generally uses a discontinuous buffer system which provides higher resolution to separate proteins based on their molecular weight. Three types of gel were used: Stacking gel and separation gel were responsible for sample organization and separation, and stop gel was used for blocking bottom of glass when casting the gel (detailed below). It is important to note that APS and TEMED should be added last because they initiate polymerisation immediately. The stop gel was loaded first, followed by separation gel and stacking gel. A comb was inserted into the freshly cast stacking gel to form sample pockets. Around 1 hour later, the gel was ready to use, or stored it at 4 °C with plastic wrap.

Table 13. Buffer of SDS polyacrylamide gel

Buffer of SDS Polyacrylamide Gel (for 2 Gels)				
Stacking Gel	4 ml	Stacking gel buffer		
	10 µl	10 % APS		
	10 µl	TEMED		
Separation Gel	2.4 ml	dH_2O	5.2ml	dH_2O
	3 ml	Separating gel buffer	3.0 ml	Separating gel buffer
	6 ml	Acrylamide	3.2 ml	Acrylamide
	0,6 ml	Glycerol	0,6 ml	Glycerol
	20 µl	10 % APS	20 µl	10 % APS

	20 µl	TEMED	20 µl	TEMED
		15%		8%
Stopped Gel	500 µl	Separating gel buffer (without APS and TEMED)		
	5.0 µl	10 % APS		
	5.0 µl	TEMED		

Before loading samples, they were incubated with DTT and 4 x SDS at 95 °C for 5min. Then 15-20 µg sample were added to each gel pocket. Additionally, 7 µl PageRuler Prestained Marker was loaded into the left-side pocket. Finally, the gel was run at constant voltage of 120 V for 10 min, then changing to constant voltage to 140V until gel electrophoresis was complete, which usually took around 2h.

2.2.9.2 Blotting

After electrophoresis was done, proteins were transferred to membrane through wet or semi-dry blotting, depending on molecular weight.
For semi-dry blotting, nitrocellulose membrane and filter paper were prepared by immersing them in blotting buffer and stacking them in the following order: filter paper, polyacrylamide gel, NC membrane, and filter paper. A constant electric current of 60 mA per gel was applied for 45 min of blotting.
For wet blotting, the blotting buffer was same as for the semi-dry method, a stack of sponge, filter paper for wet blotting, polyacrylamide gel, PVDF membrane, filter paper and sponge were prepared, and all bubbles were removed. The stack was then fixed in a blotting tank and 300 mA of current was applied for 1 hour.

2.2.9.3 Blocking and Antibody Incubation

Before the primary antibody staining, blocking of the membrane in 5% skimmed milk with TBST solution was performed for 1 h at 4 °C to prevent unspecific binding of target antibody to the membrane. Then primary antibody

binding took place at 4 °C overnight. Washing 3 × 10 min with TBST at next day, the secondary antibody was subsequently incubated for 1h at RT. (for details on primary and secondary antibodies used, refer to Section 2.1.7). The membrane was then washed again by TBST 3 × 10 min. The membrane was then ready for chemiluminiscence detection.

2.2.9.4 Chemiluminiscence Detection

Detection and quantification of Western Blots was carried out using the Clarity Western ECL Substrate (Bio-Rad Laboratories GmbH; Munich, Germany). The ECL solution was made up 1: 1 of ECL substrate and Clarity substrate, then evenly dripped onto the membrane. After 3-4 min RT incubation, the amount of bound antibody on the membrane could be detected and quantified using a ChemoCam Imager. Subsequently, the same membrane was incubated with an anti- β-actin antibody as loading control. Band intensities were quantified using ImageJ freeware program and the intensities of the protein of interest were normalized to the structural protein (β-actin).

2.2.10 MTT Assay

Water soluble yellow 3-(4, 5)-dimethylthiahiazo (-z-y1)-3, 5-di-phenytetrazoliumromide (MTT) can be reduced to purple insoluble formazan by mitochondrial dehydrogenases. Formazan can then be solubilized by isopropanol solvent. This conversion can then be analyzed by spectrophotometric methods and serve as a measure for the number of viable, metabolically active cells.

For workflow, cells were seeded on a 6-well plate and pretreated according to the experiment. Normally, MTT measurement was carried out 72 hours after cell treatment (e.g. siRNA transfection). For the measurement, 90 µl MTT reagent was added to each well with culture medium. After 1h incubation at 37 °C, the medium was gently removed, 400 µl MTT dissolved solution was

added to each well, and the plate was transferred to a plate shaker for 5 min RT incubation. At last, 150 µl of each sample solution was transferred to a 96-well plate. The absorbance was measured at a wavelength of 570 nm on the Multiscan FC instrument.

2.2.11 BrdU Assay

The thymidine analog BrdU (5-bromo-2'-deoxyuridine) is readily incorporated into newly synthesized DNA within dividing cells and can subsequently be detected by an anti-BrdU antibody.

The cell proliferation ELISA, BrdU kit (Roche Diagnositics GmbH, Mannheim, Germany) was applied to this assay. 5,000 cells per well were seeded on 96-well Black ViewPlate, cells were treated with different siRNAs (refer to section 2.2.2.1), each independent siRNA treated sample was triplicated. In addition, a fourth well was arranged for measuring background. 48h after siRNA transfection, medium was aspirated with exception of the background control, each well was incubated with 100 µl 1:1000 BrdU solution which was diluted with corresponding cell line culture medium for 4h at 37 °C, 5% CO_2. Shortly before the end of 4h, the same BrdU solution was added to background control wells, and all liquid was aspirated after the end of the 4h incubation period. The plate was kept at 4 °C, or directly processed further. Firstly, 200 µl FixDenat solution was added to each well for cell fixation and DNA denaturing. After 30 min RT incubation, the solution was removed, and 100 µl anti-BrdU solution (1:100 diluted from the stock solution) was added to each well for 1h RT incubation. Then each well was washed 3 times x 5 min at RT with washing buffer (washing buffer 1:10 diluted in dH_2O). During washing time, the chromogenic substrate was prepared from one volume of substrate B and 100 volumes of substrate A and incubated on a rocker shaker for at least 15 min in the dark. Finally, 100 µl substrate mixture was added to each well and

incubated 3 min at RT in dark, and subsequently measured by microplate luminometer at 370 nm wavelength.

2.2.12 Anchorage-Independent Growth and CellTiter-Glo Assay

Anchorage-independent growth is a feature of anoikis resistance that it is related to tumor cell metastasis. The semisolid medium Polyhydroxyethylmethacrylate (Poly-HEMA) was used to create a 3D cell culture environment which replicated anchorage-independent growth. Cell viability under these conditions was monitored through measurement of ATP by employing CellTiter-Glo to test. For this purpose, CellTiter-Glo (Promega Corporation, Madison, USA) was applied. Before transferring cells, 20 mg/ml Poly-HEMA solution in 96% ethanol was prepared, dissolving Poly-HEMA by rotating at 40 °C. Then, 500 µl dissolved solution was pipetted per well in a new 12-well plate. The plate was dried under a laminar flow cell culture bench at RT for ethanol evaporation. Plates could then be kept at 4 °C or used directly. Before use, coated plates were washed twice with 1 x DPBS. After seeding of cells, the plates were incubated at 37 °C, 5% CO2 for 7 days. During incubation, cells would form tumor spheres. At measurement day, CellTiter-Glo solution was added to each well at amounts equal to the medium volume in each well, including one well only with culture medium for background control. After vigorous mixing and incubation on a rocker shaker for 25 min at RT, 200 µl of each sample were transferred to a 96-well black view plate and analyzed on a microplate luminometer at 370 nm wavelength.

2.2.13 Time-Lapse Microscopy Assay

In time-lapse microscopy, images of live cell cultures are taken at regular intervals and compiled into movies which enable direct observation of events such as cell movement, cell division etc.

To measure siRNAs impact on cell migration, cells in 6-well plate were treated like described in section 2.2.10. In this project, collagen coating of the wells provided a 3D cell culture environment and physical support for cells. 1.0 ml 10.0 µg/ml collagen was added to each well of new plate, then incubated for 3h at 37 °C, 5% CO2. Remaining collagen was aspirated after incubation, the plate was dried, and stored at 4 °C. Cells were re-seeded on collagen coated plates 48h after siRNA transfection. Time-lapse recording was started the following day using a ZEISS Axiovert 200M Microscope with temperature and CO_2 control. Images of defined regions of interest were taken at 10 min intervals. The average mean distance which mirrored cell migration activity was calculated by automated image analysis using the TimeLapseAnalyser software.

2.2.14 Flow Cytometry

2.2.14.1 Cell Cycle Analysis

Propidium iodide (PI) is a red-fluorescent nuclear and chromosome counterstain. As the duplication of DNA occurs during S-phase of cell cycle, PI binds to DNA by intercalating between the bases with little or no sequence preference. Thus, fluorescent intensity detection of stained cells at certain wavelengths is correlated with the amount of DNA. For flow cytometry analysis, cells in 6-well plate were treated as described in section 2.2.10. After 72h of siRNAs transfection, cells were left untreated or incubated with 0.1 µg/ml Nocodazole (AdipoGen Corporation, San Diego, USA) for 9h. Cells were collected to FACS tubes by cell scraper, centrifuged at 300 x g for 5min, washed twice with 1 ml 1 x DPBS per tube, centrifuged as before, and the supernatant was discarded. For cell fixation, 700 µl cold (-20 °C) 70% ethanol was added dropwise with gentle vortexing to make sure that cells were separately fixed, and samples were incubated at -20 °C for 5 min. Cells were centrifuged at 300 x g for 5 min, washed with 1 ml 1 x DPBS

per tube, and again centrifuged. During centrifugation, PI stain buffer was prepared by diluting PI solution and RNase A in 1 x DPBS at final concentration was 20 µg/ml PI and 50 µg/ml RNase A. After last centrifugation, 500 µl stain buffer was added to each tube, incubated for 30 min at RT in the dark, measured on a BD FACSCanto Ⅱ (BD Biosciences, Allschwil, Switzerland) and analyzed by Modfit LT software.

2.2.14.2 Cell Apoptosis and Necrosis

At onset of apoptosis, Phosphatidyleserine (PS) is translocated to the external membrane where it serves as a recognition signal for phagocytes. Annexin V binds exposed PS and can be used as an early indicator of apoptosis since it conjugates detectable fluorescence signal. Additionally, Propidium Iodide (PI) is used in combination with Annexin V-FITC, because PI is permeable to late apoptotic and necrotic cells, but not to viable and early apoptotic cells. Therefore, an Annexin V-FITC and PI dual stain allows for discrimination of viable, apoptotic and necrotic cells. For this purpose, cells in a 6-well plate were treated like described in section 2.2.10. Cells and culture medium were harvested to FACS tubes by Trypsin-EDTA and centrifugation at 300 x g, 10 min. Cells were resuspended in each tube with 2 ml cold 1 x DPBS, centrifuged at 300 x g, 10 min, the supernatant was discarded and the washing step was repeated. Then cells were resuspended in 100 µl 1 x Annexin V binding buffer by gently flicking tubes. After that, 5.0 µl Annexin V conjugate and 2.0 µl 100 µg/ml PI working solution were added to each 100 µl of cell suspension and incubated on ice for 15 min in dark. Negative control samples with untreated cells were stained with Annexin V conjugate or PI for compensation analysis.

2.2.15 mRNA-Seq and Statistical Analysis

Differential expression of genes upon inhibition of COA4 was analyzed by RNA-Seq. Total RNA was prepared as in section 2.2.4 and the quality was analyzed by RNA Nano Chips (Agilent Technologies, Waldbronn, Germany) on 2100 BioAnalyzer (Agilent Technologies). The library construction was implemented by the commercial vendor BGI, Hongkong. Parallel sequencing was performed on BGISEQ-500 platform with PE100 read length, and finally generating 50M paired-end reads per library.
Gene expression was normalized by FPKM (fragments per kilobase of exon model per million reads mapped). To detect differentially expressed genes, a two tailed t-Test was performed between samples with control siRNA and COA4-specific siRNAs. P-values <0.05 were regarded as significant. Genes with foldchange values equal or greater than 2, or equal or lower than 0.5, respectively, were regarded as potential downstream mediators of COA4.

2.2.16 PLAU-pIRES2-EGFP Plasmid Purification

2.2.16.1 Isolating Bacteria on LB Agar Plate

An E. coli bacteria stab culture carrying the construct was commercially obtained. Using a sterile loop, bacteria were transferred and gently spread over a section of an LB agar plate with Kanamycin ($C_{kanamycin}$ = 100 µg/ml), and incubated overnight at 37 °C. At the next day, single colonies should be visible.

2.2.16.2 Inoculating a Liquid Bacterial Culture

Liquid LB medium was added to a 15 ml Falcon tube and Kanamycin was added to the concentration of 100 µg/ml. A sterile pipette tip was used to select a single colony from the LB agar plate and transfer bacteria to the tube, the lid

attached only lightly to allow gas exchange, and the tube incubated overnight at 37°C on a shaking incubator.

2.2.16.3 Midi-Prep for Recovering and Purification of Plasmid DNA

The QIAGEN Plasmid Midi Kit was used to obtain large amount of purified plasmid. Firstly, 100 ml bacteria-saturated solution was centrifuged for 4440 rpm, 45 minutes at 4 ° C. The pellet was resuspended in 4 ml P1 buffer, inverted six times and incubated for 5 minutes to lyse cells. Then, 4 ml of P3 neutralization buffer were added, inverted six times and incubated on ice for 15 minutes. During this time, the Qiagen column was equilibrated with 4 ml of QBT buffer. The cell lysate supernatant was transferred to the column through a filter to separate cell debris. After the lysate completely passes through the silicagel column, 10 ml of QC buffer was applied to wash the column twice. For elution, 5 ml of QF buffer was added to the column and a new 15 ml of falcon was attached underneath. DNA contained in the eluate was precipitated by 3.5 ml isopropanol, then vortexed and centrifuged at 4440 rpm, 1h, at 4 °C. The supernatant was discarded, the pellet was resuspended in 400 µl TE buffer and transferred to a 1.5 ml low binding tube. For ethanol precipitation, 40 µl sodium acetate (3 M, pH 5.2) and 1.0 ml 100% ethanol were added with gentle mixing. After centrifugation at 17,000 x g for 10 minutes, the supernatant was removed, the pellet was dried at RT for approx. 30 min, until it appeared slightly glassy. At last, 100 µl sterile distilled water was added and the concentration was measured on a NanoDrop 1000.

2.2.17 TaqMan® MicroRNA Assay

The TaqMan® microRNA assay is an advanced technology which enables accurate quantification of the most common human mature miRNAs (Over 740 assays are available across the sets of TaqMan™ Array MicroRNA Card A and B). This product involves Megaplex™ Primer Pools for ligation-based universal

miRNA reverse transcription, as well as optional Megaplex™ PreAmp Primers which are applied for preamplification of limited samples prior to real-time PCR by TaqMan Array MicroRNA Card.

2.2.17.1 microRNA Isolation by mirVana Kit

The mirVana miRNA Isolation Kit (Thermo Fisher Scientific, Waltham, USA) was used for extraction and recovery of microRNAs from cell samples by using glass fiber filter (GFF) cartridges according to manufacturer's instructions.
In detail, cells were treated with anti-POLr3K siRNAs according to section 2.2.10 and harvested 24h after transfection. Before miRNA isolation, all solutions should be at RT. Firstly, cell pellet was resuspended in 300 µl Lysis/Binding solution, and 35 µl miRNA Homogenate Additive was added to prevent miRNA loss, then samples were kept on ice for 10 min. After incubation, 400 µl Acid-Phenol-Chloroform was pipetted to each sample, turning samples upside down 30 sec, centrifuging 10,000 x g, 5 min at RT for organic and aqueous phase separation. 250 µl supernatant of the aqueous phase was transferred to new Eppendorf tubes, discarding remaining liquid. Afterwards 85 µl 100 % ethanol was added, the mixture was loaded to a new filter catridge and centrifuged at 10,000 x g, 15 sec, keeping the flow-through. Now 2/3 volume (170 µl) 100 % ethanol was added for further RNA precipitation, the mixture was loaded to new filter cartridges and centrifuged at 10,000 x g, 15 sec, keeping columns and corresponding binding tubes. Secondly, filters were washed once with Wash Solution 1, adding 700 µl per sample, and twice with Wash Solution 2/3, adding 500 µl per sample, each round followed by centrifuging at 10,000 x g, 15 sec. Washing was further followed by a drying step by centrifuging 10,000 x g, 2 min. Finally, miRNA of each sample was eluted with 30 µl sterile distilled water, and centrifuging 10,000 x g, 30 sec. isolated miRNA sample could be stored at -80 °C.

2.2.17.2 microRNA Reverse Transcription

The TaqMan MicroRNA Reverse Transcription Kit (Life Technologies Corporation, Pleasanton, USA) was used to synthesize cDNA. A master mix was created according to the number of samples (see below for exact composition).

Table 14. MasterMix of microRNA reverse transcription

MasterMix of One Sample	
Megaplex RT Primer (10 x)	0.8 µl
dNTP or dTTP	0.2 µl
Multiscripe Reverse Transcriptase	1.5 µl
10 x RT Buffer	0.8 µl
$MgCl_2$ (25 mM)	0.9 µl
Rnase Inhibitor (20 U/µl)	0.1 µl
dH_2O	0.2 µl
End Volume	**4.5 µl**

4.5 µl of MasterMix was transferred to 0.2 ml Eppendorf tubes, then adding 3.0 µl of isolated miRNA, mixing them and putting on ice for 5 min incubation. Reverse transcription reaction was subsequently performed in a Bio-Rad T100 Thermal Cycler (Applied Biosystems Waltham, USA) with following setting:

Table 15. Program setting for microRNA reversed transcription

Stage	**Temp °C**	**Time**
	16	2 min
40 Cycles	42	1 min
	50	1 sec
Hold	85	5 min
Hold	4	∞

Samples could be stored at -20 °C for maximum 1 week.

2.2.17.3 cDNA Preamplification

For preamplification of miRNA targets from total RNA samples, PreAmp MasterMix and Megaplex PreAmp Primers (Life Technologies Corporation, Pleasanton, USA) were used. MasterMix composition was as following:

Table 16. microRNA to cDNA preamplification MasterMix

MasterMix of One Sample			
PreAmp MasterMix	(2 x)	12.5	µl
Megaplex PreAmp Primers	(10 x)	2.5	µl
ddH_2O		7.5	µl
End Volume		22.5	µl

22.5 µl of MasterMix were transferred to 0.2 ml Eppendorf tubes, then adding 2.5 µl cDNA from microRNA reverse transcription, mixing them and putting on ice for 5 min incubation. Preamplification was then performed in a Bio-Rad T100 Thermal Cycler (Applied Biosystems Waltham, USA) with following setting:

Table 17. microRNA to cDNA preamplification program setting

Step	**Stage**	**Temp °C**	**Time**	
Enzyme Activation	Hold	95	10	min
Anneal	Hold	55	2	min
Extend	Hold	72	2	min
Denature	12 Cycles	95	15	sec
Anneal/Extend		60	4	min
Enzyme Inactivation	Hold	99.9	10	min
Hold	Hold	4	∞	

The amplified cDNA was diluted by adding 75 µl 0.1 x TE (PH 8.0) buffer to

each sample. The cDNA was then ready to load on TaqMan array cards.

2.2.17.4 TaqMan Human microRNA Array Real-Time PCR

Upon pre-amplification, MasterMix and cDNA sample loading were set up as following,

Table 18. MasterMix of TaqMan Human microRNA Array Real-Time PCR

MasterMix for One Card with 8 Ports		
TaqMan Universal MasterMix (No AmpErase UNG 2 x)	450	µl
PreAmp Product	100	µl
dH_2O	350	µl
End Volume	900	µl

100 µl above MasterMix was loaded to each port. Before running real-time PCR, short centrifugation was performed, and array cards were sealed. Finally, detection took place on QuantStudio 7 Flex Real-Time PCR System (Applied Biosystems, Waltham, USA)). The program was set up as following, subsequently data were analyzed by the ΔC_t method, as explained in section 2.2.6.

Table 19. Program setting of TaqMan Human microRNA Array Real-Time PCR

Step	Temp °C	Time	Cycles
Enzyme Activation	95	10 min	1
Denature	95	15 sec	40
Anneal/Extend	60	60 sec	

2.2.18 Validation of microRNA of Interest

2.2.18.1 Candidate microRNA Selection

To identify microRNAs with altered expression upon POLr3K knockdown, relative expression of each microRNA on TaqMan human miR assay was calculated as explained in section 2.2.6. microRNA alteration upon POLr3K silencing with foldchange of siRNA2/siControl and siRNA3/siControl $>$ 2 or $<$ 0.5 was regarded as a potential mediator.

2.2.18.2 Stem-Loop Primer Design for miR real-time PCR

To validate microRNAs detected by TaqMan assay, Stem-Loop RT-PCR was performed. Therefore, Stem-Loop primers (st-primer) were designed that contained a constant region which formed a stem-loop and a variable six-nucleotide extension. The six nucleotides were the reverse complement of the last 6 nucleotides on the 3’ end of the targeted miRNAs. Thus, miRNA extension of length from -22 nt to more than 60 nt was achieved, providing higher specificity and allowing application of aforementioned real-time PCR in further steps. miRNA specific forward primers were designed as described in section 2.1.9, reverse primer was specific to a portion of stem-loop and therefore universal (schematic of stem-loop primers as following picture showed).

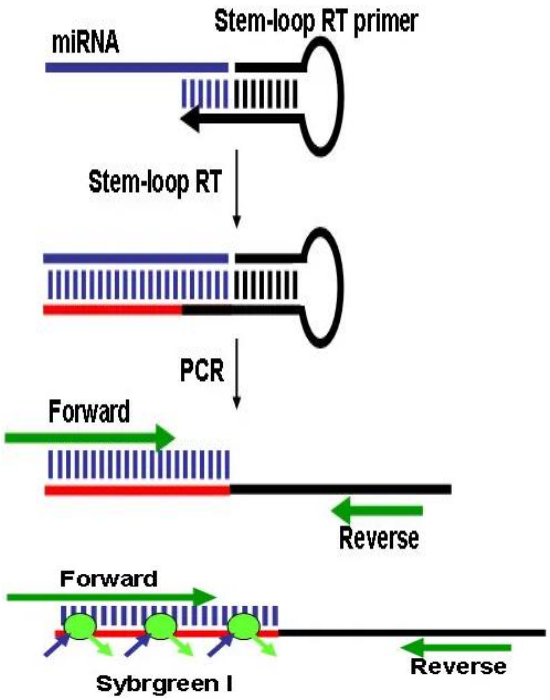

Schematic of stem-loop primers used in miRNA RT-PCR.
Erika Varkonyi-Gasic et al. 2017

2.2.18.3 cDNA Synthesis

After extraction of miRNA by mirVana kit, a MasterMix containing stem-loop primer pool was set up for reversed transcription.

Table 20. MaterMix of cDNA synthesis with microRNA stem-loop primer pool

MaterMix for One Sample		
microRNA	6.6	µl
Buffer (10 x)	4.0	µl
RNase Inhibitor (20 U/µl)	1.0	µl
$MgCl_2$ (25mM)	2.4	µl
Stem-Loop primers pool*	1.0	µl
Reversed Trancriptase	1.0	µl
dNTP (5 mM)	4.0	µl
End Volume	20.0	µl

* The Stem-Loop primer pool was constituted of 5 microRNA related stem-loop primers. Stock concentration of each primer was 10 μM; in the MasterMix, concentration of each primer was 0.1 μM.

cDNA was synthesized with following PCR program on Bio-Rad T100 Thermal Cycler to synthesize cDNA.

Table 21. Program setting of cDNA synthesis with microRNA stem-loop primers pool
Referring to: Mary Johnson (han at labome dot com)

Temp °C	Time	
25	5	min
42	60	min
70	15	min
4	∞	

Finally, qRT-PCR (same to section 2.2.6) was performed to analyze target miRNA expression upon POLr3K inhibition or co-transfected miRNA mimic and POLr3K siRNAs.

2.2.19 Tissue Microarray Analysis of Patients Specimens

2.2.19.1 Ethics Statement

Formalin-fixed, paraffin-embedded tumor tissue microarray came from 19 Intraductal Papillary Mucinous Neoplasia (IPMN) patients, 58 pancreatic cancer patients (9 of them were progressed from previously mentioned IPMN), and 61 adjacent normal pancreatic tissues. The Ethics Committee of the Philipps-University Marburg, Marburg, Germany approved the study protocol. Patient specimens and important medical records were acquired with informed consents. Medical records included tumor grade of histological abnormality, primary tumor (T), regional lymph node invaded (N), distant metastasis (M), as well as TNM stage which was defined using Union for International Cancer Control (UICC) standard. Invasion of lymphatic, vein and peripheral, resection margin of tumor, and survival situation upon follow-up time were also afforded.

2.2.19.2 Immunohistochemistry

Tissue microarray (TMA) preparation and immunohistochemistry staining was performed by the Pathology department of the University clinic of Giessen and Marburg. Staining for COA4 was performed using a 1:300 dilution of the anti-COA4 antibody with PH 6.0 Citrate buffer for antigen unmasking, and POLr3K-staining was performed with a 1:50 dilution of the anti-POLr3K antibody and Trilogy antigen unmasking.

2.2.19.3 Kaplan–Meier Survival Analysis

Kaplan–Meier survival analysis is a kind of univariate survival analysis method which can be used to estimate survival rates and analyze influence factors. The method is suitable to observe the change in survival time after a classified variable is given, for example, a certain treatment. Follow-up information of patients whose surgery resected tissues were applied to TMA analysis were obtained from the Department of Surgery, Philipps-University Marburg, Marburg, Germany. Kaplan-Meier survival analysis was performed using the GraphPad Prism7 program.

2.2.20 Statistic Analysis

The statistical analysis was carried out with the program GraphPad Prism 7. Data comparisons between groups were based on calculation of arithmetic mean and the standard deviation. Control group data was used for statistical normalization. Comparisons between experimental and control groups were analyzed by unpaired bilateral t-test. Significant differences between two groups were marked with an asterisk (*). A p-value<0.05 was regarded as significant.

3. Results

3.1 COA4 and POLr3K were highly expressed in human PDAC tissues

This project was based on previous work of large-scale expression profiling analyses of microdissected human pancreatic tissues which comprised normal pancreatic ducts, PanINs (Pancreatic Intraepithelia Neoplasia) of different grades and PDACs (M. Buchholz). 9 candidates were selected for further experimentation based on specific overexpression in PanIN3 lesions and invasive PDACs (**Table 22**). qRT-PCR analyses of cDNA preparations from cell lines BON-1, S2-007, Panc-1, LON556, LON560, LON707 suggested that expression of DRP2 was relatively low in PDAC cells (**Figure 1**), so that subsequent analyses were limited to the other 8 candidates. To verify whether selected genes were significantly overexpressed among human pancreatic cancer tissues, 8 human PDAC tissues, 10 chronic pancreatitis tissues and 5 normal pancreas tissues were obtained from Heidelberg University hospital. qRT-PCR analyses of prepared material of these tissues revealed varying expression patterns (**Figure 2**).For candidate genes COA4 and POLr3K, overexpression in tumor tissues, with high levels of overexpression in individual samples were recorded. Additionally, among a variety of different pancreatic cancer cell lines, S2-007, Panc-1 and LON556 cells showed high expression levels of COA4 and POLr3K (**Figure 3**) and were selected for following vitro research.

HUGO	Mean-Duct	Mean-1b	ttest 1b	Mean-2	ttest -2	Mean-3	ttest-3	Mean-PDAC	ttest-PDAC
SLC35B2	0.82	0.95	0.71	1.94	0.02	2.38	0.00	2.85	0.00
DRP2	0.28	0.70	0.07	0.75	0.01	0.89	0.00	0.93	0.00
BCAR3	0.77	0.99	0.30	2.90	0.01	2.94	0.01	2.03	0.01
MTMR6	1.06	1.34	0.34	2.11	0.01	4.06	0.03	2.52	0.02
POLR3K	0.85	1.19	0.17	2.58	0.00	2.62	0.00	2.02	0.00
COA4	0.15	0.28	0.24	0.62	0.02	0.49	0.01	0.85	0.00
SQLE	0.93	1.68	0.18	2.82	0.01	3.56	0.01	2.66	0.00
C14orf114	0.31	0.37	0.48	0.73	0.07	0.93	0.01	1.16	0.01
FLJ20276	1.16	1.89	0.11	5.00	0.03	3.15	0.00	4.08	0.00

Table 22. List of candidate genes. Original data generated from large-scale expression profiling analyses on microdissected tissues from normal pancreatic ducts, PanINs of different grades and PDACs (Duct=normal pancreatic duct; 1b, 2, 3=PanIN 1b, PanIN 2, PanIN 3). Values were original relative expression data (normalized to housekeeping gene RPLP0) and T-tests were performed for each stage in comparison to normal ducts, respectively.

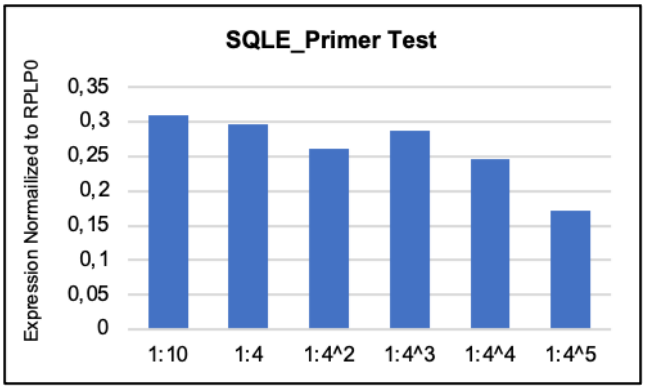

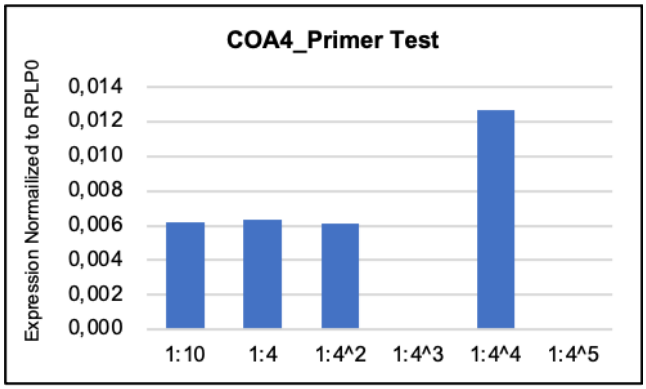

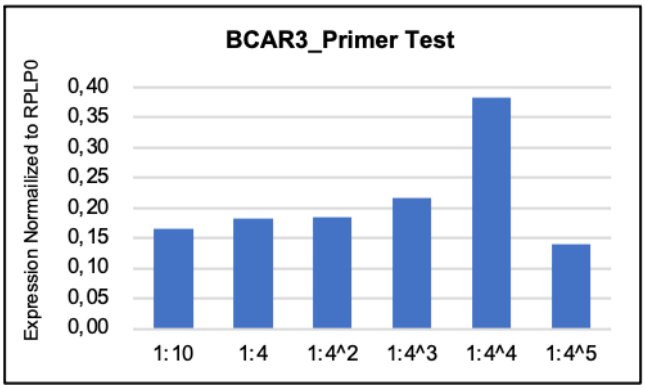

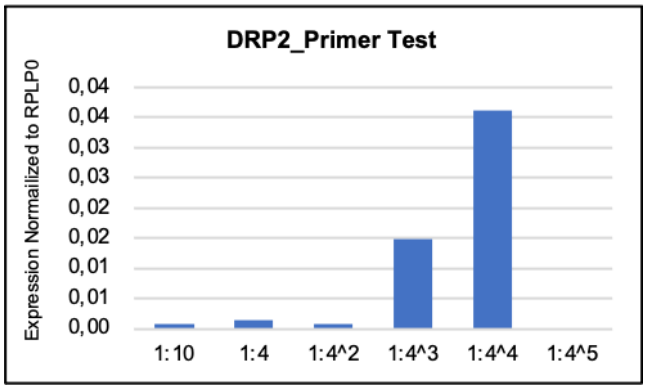

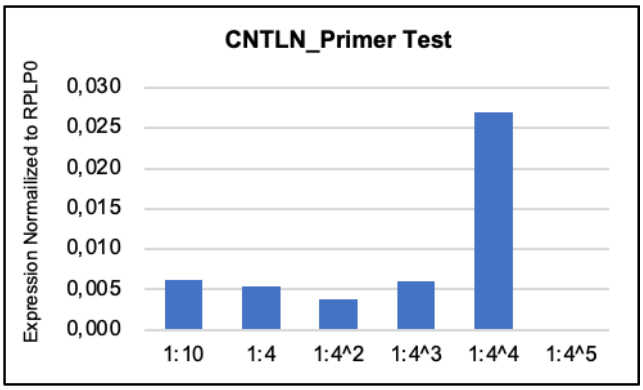

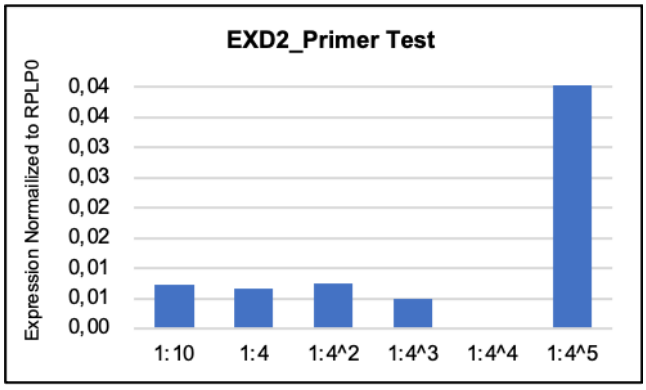

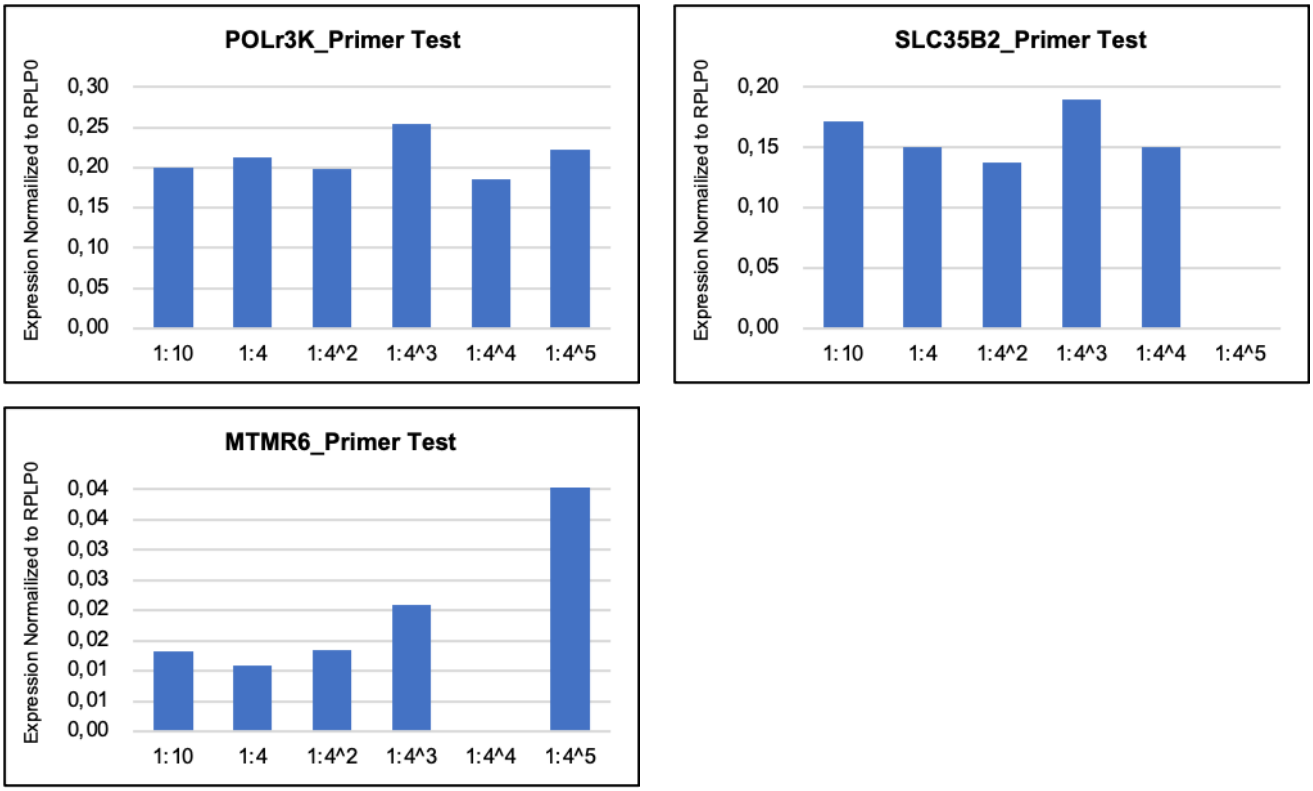

Figure 1. Primer test of candidate genes by qRT-PCR. A serially diluted cDNA pool (comprised of untreated cells of BON-1, S2-007, Panc-1, LON556, LON560, LON707) was analyzed by qRT- PCR to generate a standard curve for calculating reliability of primers. Results were normalized to the housekeeping gene RPLP0.

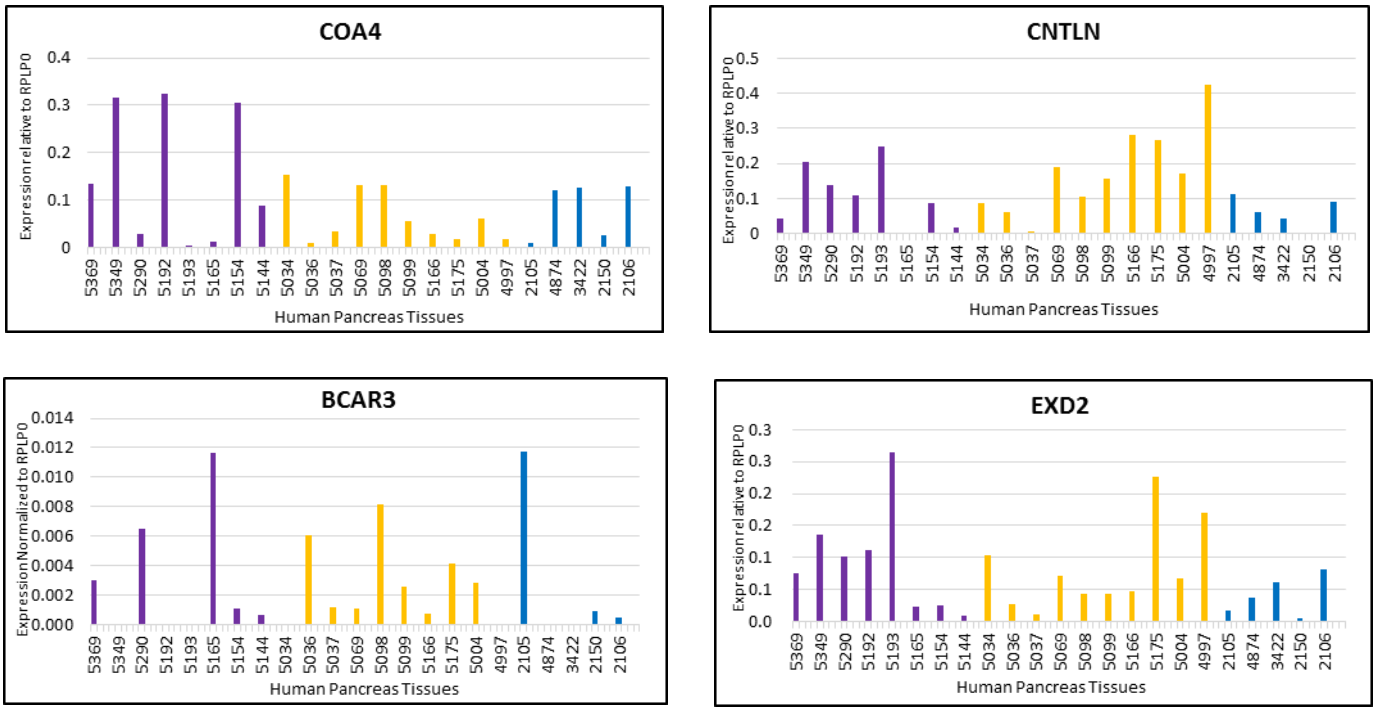

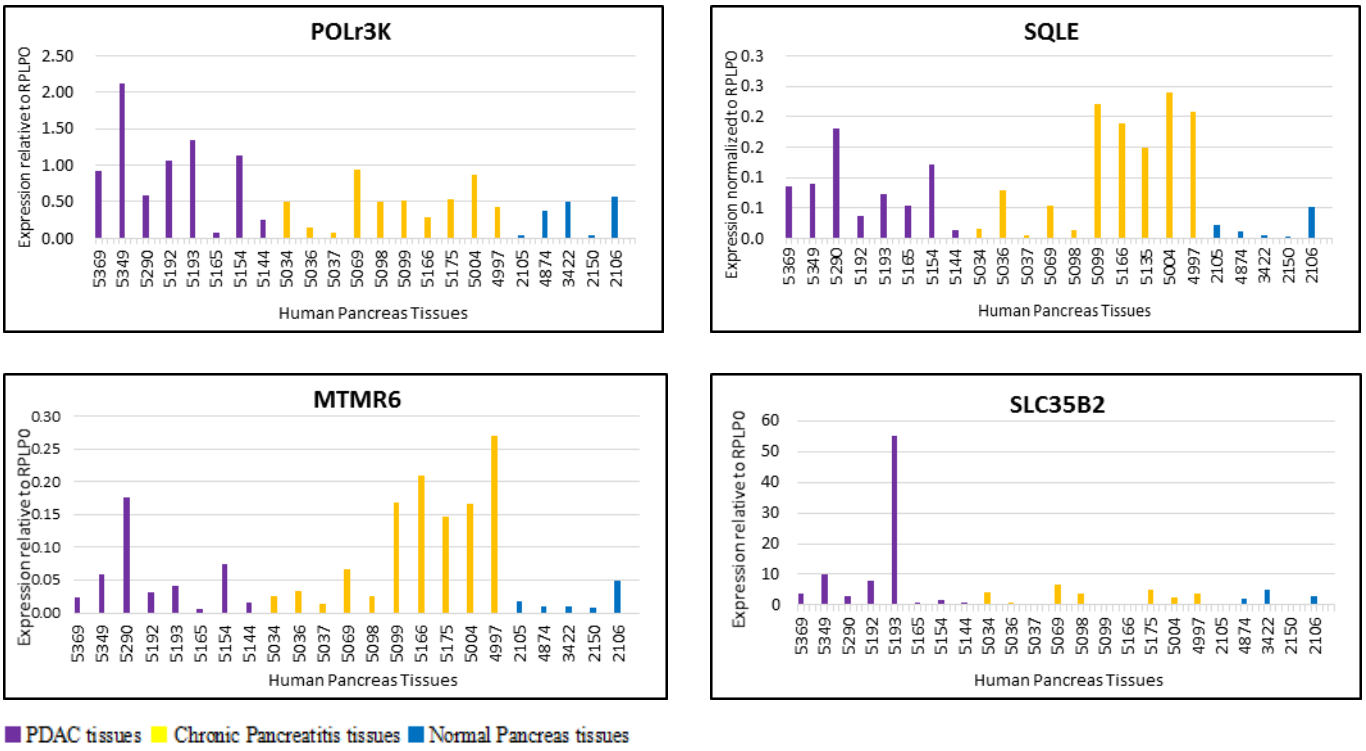

Figure 2. COA4 and POLr3K were differentially overexpressed among human PDAC specimens. qRT-PCR was performed on human pancreatic tissues (PDACs, chronic pancreatitis and normal pancreatic ducts) to measure expression level of candidate genes. Results were normalized to the housekeeping gene RPLP0.

A

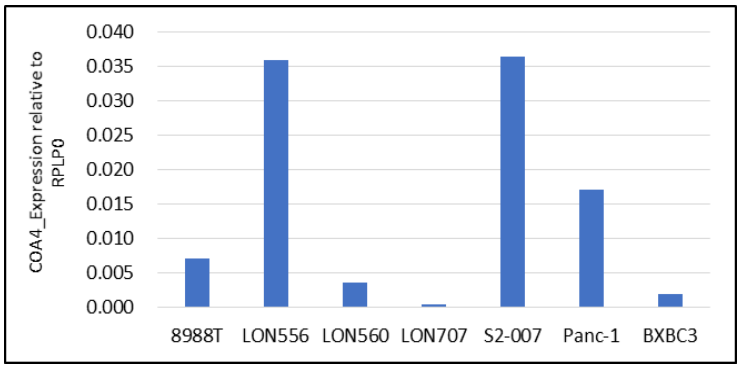

B

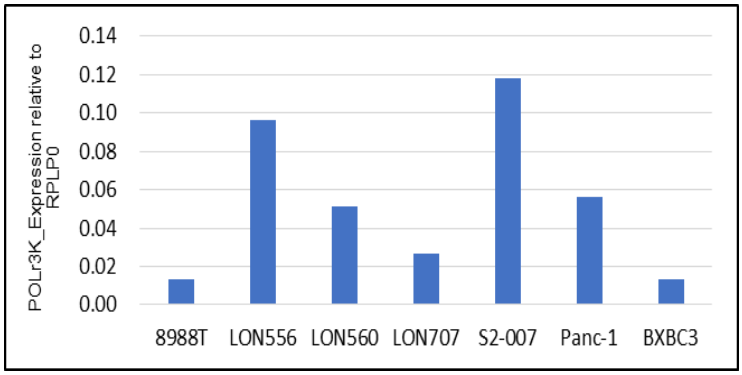

Figure 3. qRT-PCR demonstrated strong expression of COA4 (A) and POLr3K (B) in pancreatic cancer cell lines. Relative expression calculation was by ΔC_t method and was normalized to expression of the housekeeping gene RPLP0.

3.2 Loss function of COA4 impaired cell proliferation

3 independent siRNAs were transiently transfected into the COA4 high expressing cell lines S2-007, Panc-1 and LON556. 48h post-transfection, the effectiveness of the independent siRNAs was assessed by real-time PCR (**Figure 4A**). COA4 protein expression was also reduced upon target mRNA degradation (**Figure 4B**). In cell viability assays, silencing of COA4 in 3 cancer cell lines led to noticeable reduction of viable cells after 72 hours which was measured by MTT colorimetric assays (**Figure 5A**). In parallel to MTT, BrdU assays which detected DNA replication activity were performed to measure cell proliferation, demonstrating that proliferative activity of all 3 cell lines was attenuated upon COA4 inhibition (**Figure 5B**). Western-Blot analyses revealed no enhanced PARP cleavage signal in siRNA-treated cells (**Figure 5C**). Taken together, these results suggested that growth inhibition was based on cell proliferation inhibition rather than induction of apoptosis upon COA4 inhibition.

A

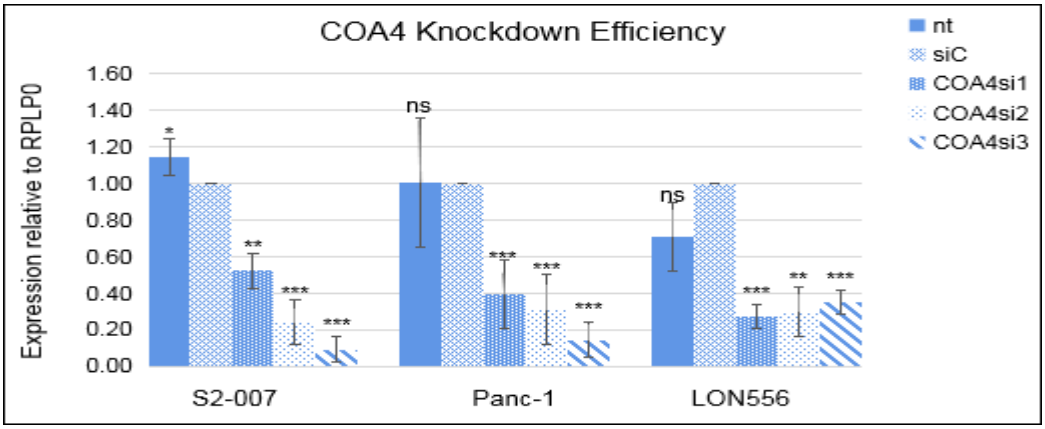

B

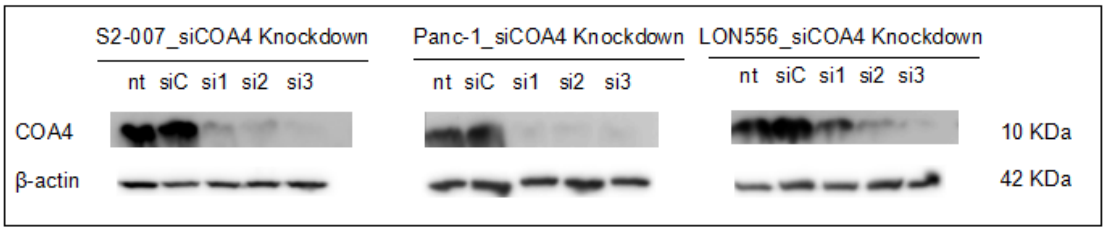

Figure 4. Independent COA4-specific siRNAs led to significant knockdown on mRNA and protein level in 3 pancreatic cancer cell lines.

A). Total RNA was harvested 48h post-transfection, efficiency of three specific COA4 siRNA was measured by rt-PCR. (* =P＜0.05, ** =P＜0.01, *** =P＜0.001 (Student t-Test)). B) Western-Blot analysis was applied to test COA4 protein expression after 48h of siRNA transfection. β-actin was used as loading control. (nt =non-treated sample, siC=non silencing siRNA, si1-3 = respective COA4 siRNA)

A

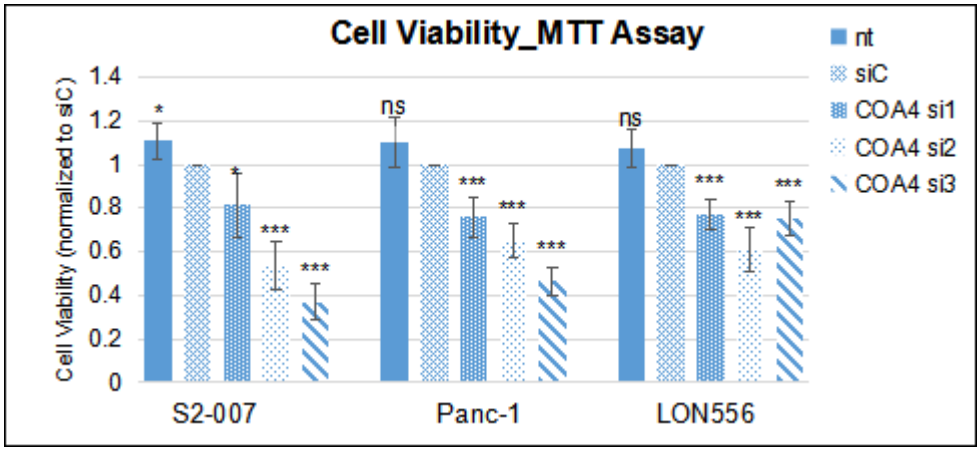

B

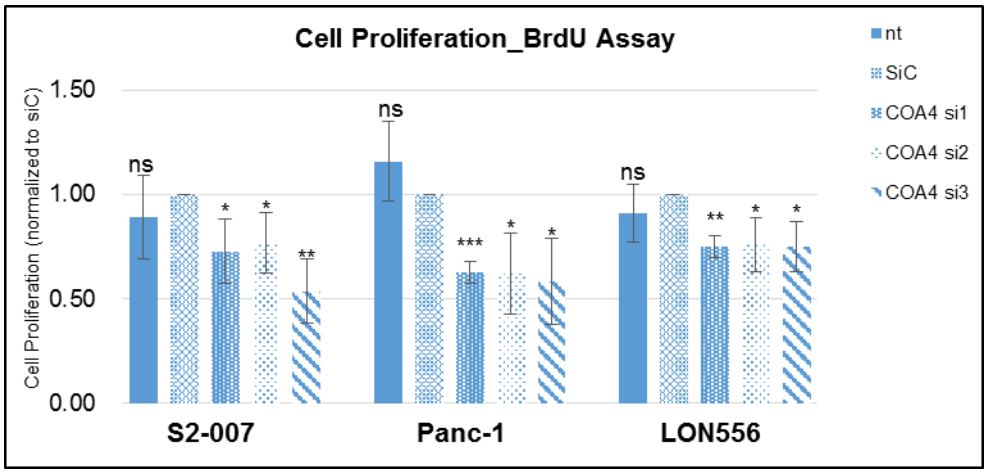

C

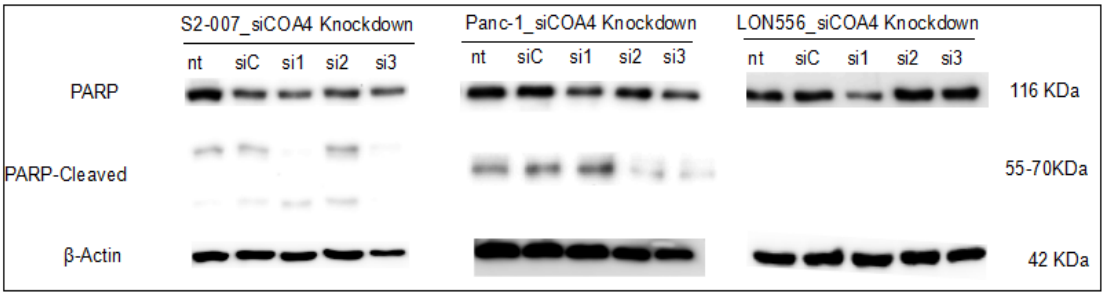

Figure 5. COA4 mediated reduction in cell proliferation rather than apoptosis in PDAC. A) Viable cells following RNAi was measured by MTT after 72h of siRNA transfection. Results were normalized to control-treated samples (siC). B) BrdU incorporation assays demonstrated significantly reduced proliferative activity after COA4 knockdown. Results were normalized to control-treated samples (siC). (nt=non-treated sample, siC=non silencing siRNA, si1-3 = respective COA4 siRNA) (* =P＜0.05, ** =P＜0.01, *** =P＜0.001 (Student t-Test)). C) 48h after siRNA transfection, Western-Blot analysis of PARP did not indicate any obvious or increased apoptosis signal on COA4 inhibited samples.

3.3 Effects of COA4 inhibition on cell cycle progression

The central cell cycle regulators Cyclin D1 and p21 were quantified by Western-Blot analyses. p21 was significantly upregulated following COA4 silencing, while Cyclin D1 was significantly downregulated upon COA4 mRNA degradation (**Figure 6A**), suggesting that COA4 might have a role in regulating cell cycle progression. To further analyze this, flow cytometry measurements were conducted as described in section 2.2.14.1. Results obtained in the absence of Nocodazole treatment did not reveal obviously general changes in cell cycle distribution, although an apparent G1-arrest in si1-treated Panc-1 cells and an apparent G2-arrest in si3-treated S2-007 cells was observed. Additional treatment with Nocodazole, which arrests cells at G2-M phase, however, clearly demonstrated an overall attenuated cell cycle progression in Panc-1 and S2-007 cells as evidenced by a marked reduction of cells that had reached the G2 phase after the 9h incubation period (**Figure 6B&C**). Results were less pronounced in LON556 cells, presumably because enrichment of cells in G2 was rather low even in control cells (untreated and siC-treated). Therefore, these results supported the notion that COA4 had a role in cell cycle progression in PDAC cells.

A

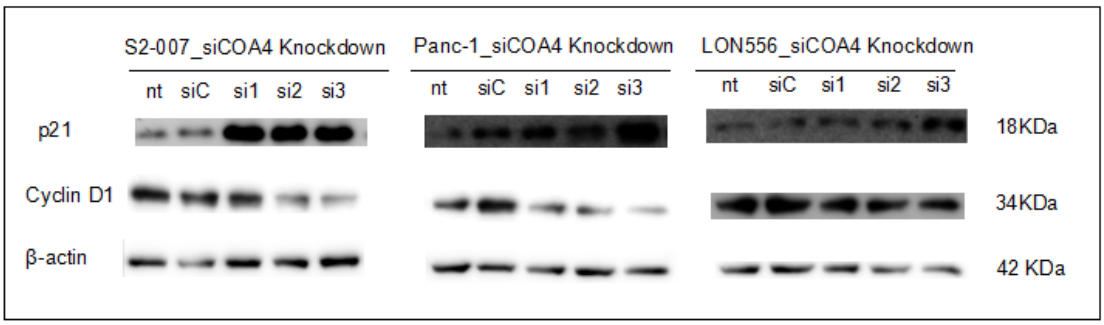
S2-007_siCOA4 Knockdown
Panc-1_siCOA4 Knockdown
LON556_siCOA4 Knockdown
nt siC si1 si2 si3
p21
Cyclin D1
β-actin
18KDa
34KDa
42 KDa

B

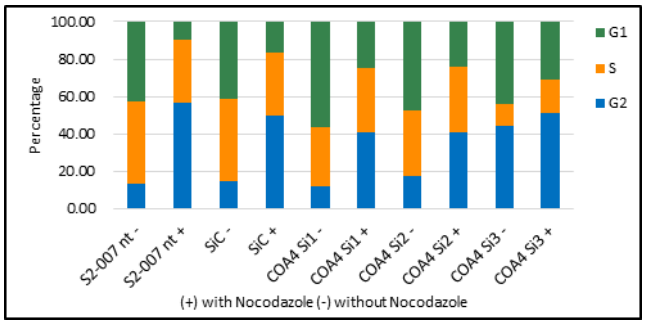
Percentage
100.00
80.00
60.00
40.00
20.00
0.00
G1
S
G2
S2-007 nt -
S2-007 nt +
SiC -
SiC +
COA4 Si1 -
COA4 Si1 +
COA4 Si2 -
COA4 Si2 +
COA4 Si3 -
COA4 Si3 +
(+) with Nocodazole (-) without Nocodazole

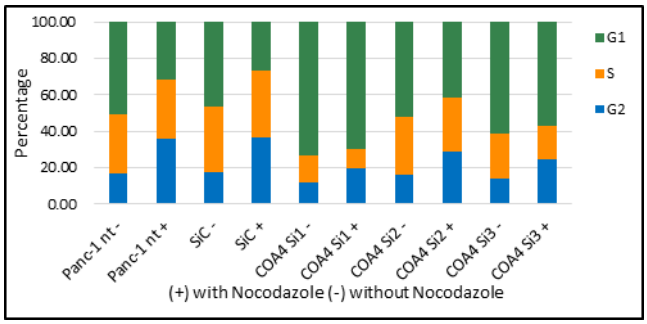
Percentage
100.00
80.00
60.00
40.00
20.00
0.00
G1
S
G2
Panc-1 nt -
Panc-1 nt +
SiC -
SiC +
COA4 Si1 -
COA4 Si1 +
COA4 Si2 -
COA4 Si2 +
COA4 Si3 -
COA4 Si3 +
(+) with Nocodazole (-) without Nocodazole

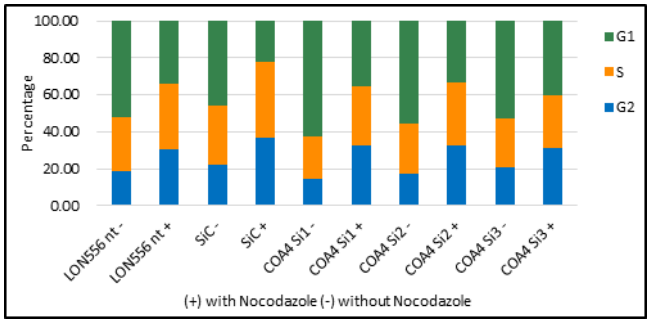
Percentage
100.00
80.00
60.00
40.00
20.00
0.00
G1
S
G2
LON556 nt -
LON556 nt +
SiC -
SiC +
COA4 Si1 -
COA4 Si1 +
COA4 Si2 -
COA4 Si2 +
COA4 Si3 -
COA4 Si3 +
(+) with Nocodazole (-) without Nocodazole

C

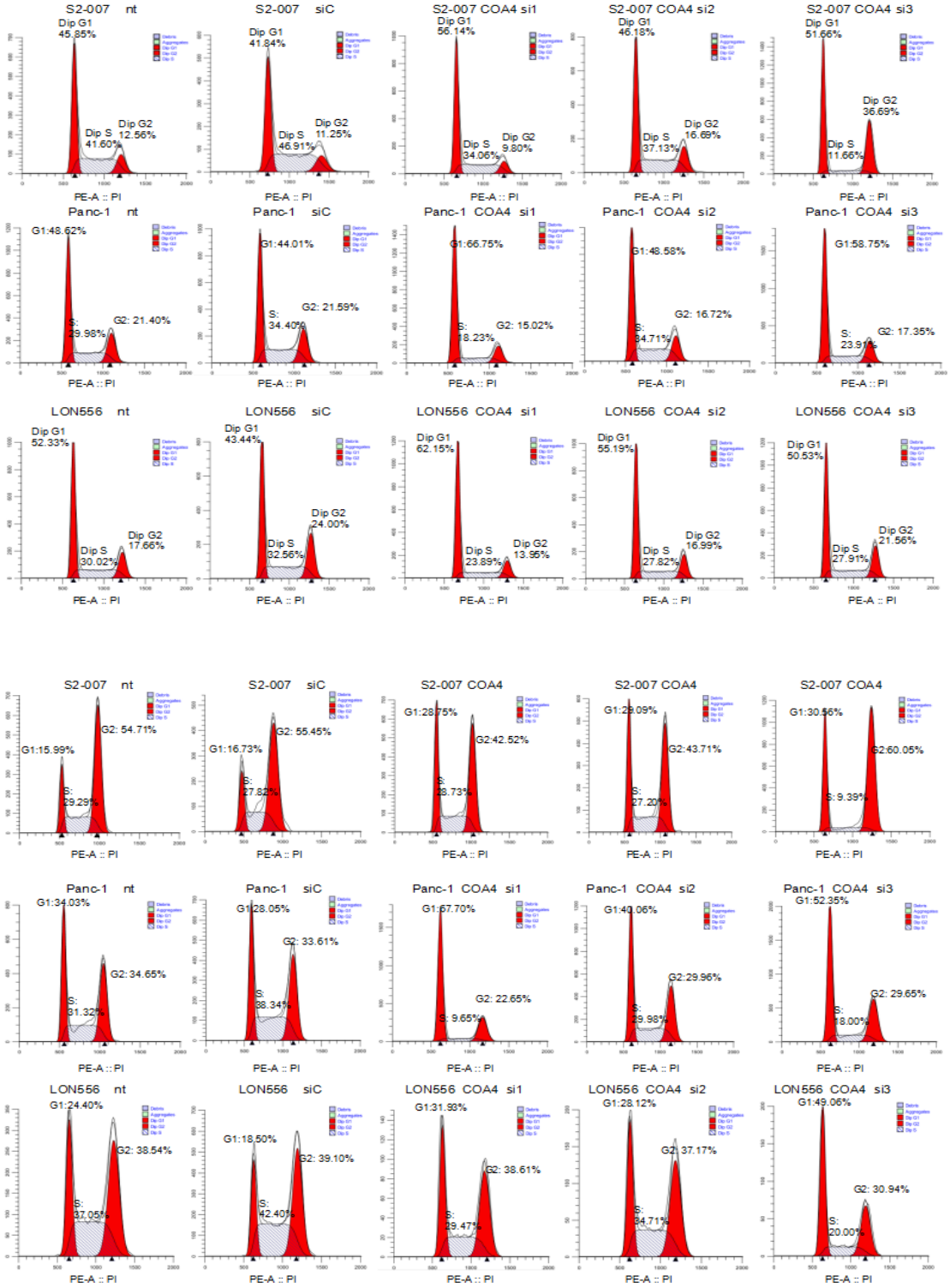

Figure 6. COA4 regulated cell cycle progression. A) Western-Blot of cell cycle regulators Cyclin D1 and p21 at 48 h post-transfection of COA4 siRNAs (nt=non-treated sample, siC=non silencing siRNA, si1-3 = respective COA4 siRNA). B) PI stained - cell cycle analysis on COA4 knockdown pancreatic cancer cells. 72h after siRNA transfection, cells were left untreated or incubated with 0.1 µg/ml Nocodazole for 9h, cells were harvested, stained with 20 µg/ml PI solution, and cell cycle distribution was measured by flow cytometry. Values were the

mean of 3 independent experiments. Cell cycle distribution upon COA4 knockdown was analyzed by Modfit LT. C) Representative individual results of cell cycle analyses without Nocodazole interference (upper panels) and with Nocodazole interference (lower panels) after 72 hours of COA4 siRNA transfection.

3.4 COA4 knockdown reduced cell anoikis resistance, and COA4 also affected cell migration

To further investigate cell anchorage-independent growth upon COA4 depletion, poly-HEMA was used to support semi-solid culture conditions (section 2.2.12). As demonstrated by CellTiter-Glo assays (48h post-transfection), the capacity for anchorage-independent growth was distinctly reduced in the absence of COA4 expression (**Figure 7A**). Moreover, cell migration which relates to cancer cell invasion and metastasis was assessed by time-lapse microscopy (section 2.2.13), demonstrating significant decrease of migratory activity upon COA4 inhibition in S2-007 (**Figure 7B**).

A

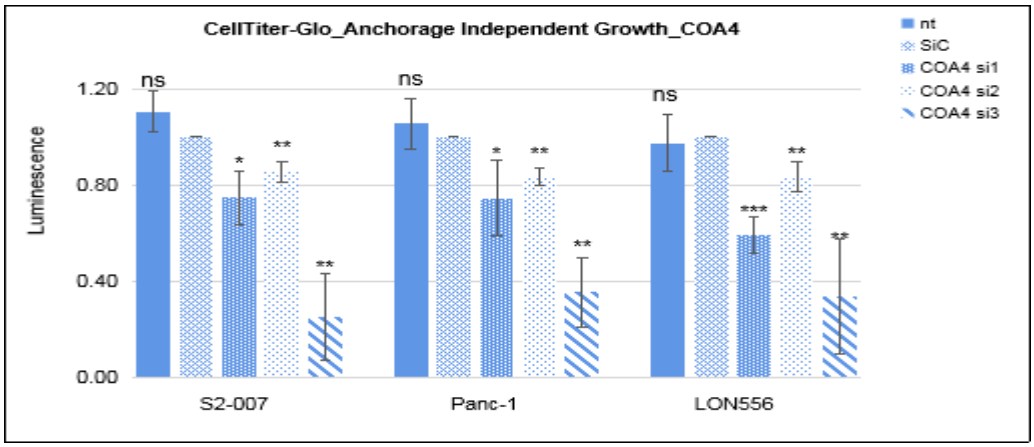

B

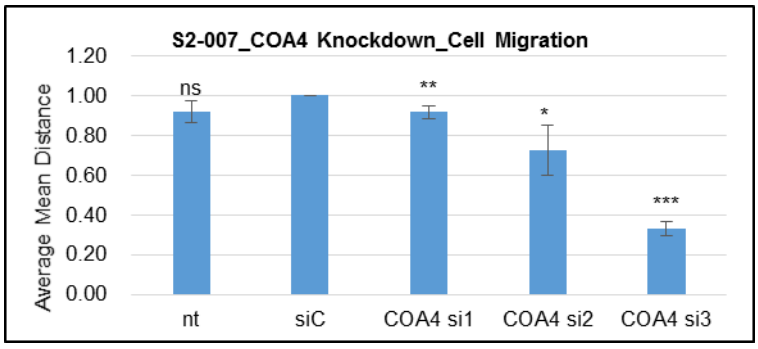

Figure 7. Impaired COA4 influenced cell anchorage independent growth and cell migration. A) The capacity for anchorage-independent growth was reduced in the absence of COA4 expression. Cells were reseeded on 20mg/ml Poly-HEMA coating plate after 48 h of siRNA transfection. Cells were incubated for 7 days, and viability assessed by CellTiter-Glo assay. B) Silenced COA4 decreased cell migration activity. Cells were reseeded on 10.1 mg/ml collagen coating plate after 48h of siRNA transfection and migratory activity (expressed as average mean distance of travel) measured by time-lapse microscopy.
Values were normalized to siC, and the mean ± SD of 3 independent experiments. * =P＜0.05, ** =P＜0.01, *** =P＜0.001 (Student t-Test).

3.5 Data analysis of RNA- Seq - Differentially expressed genes (DEGs) between control groups and COA4 siRNAs treatment groups

In this study, a list of 100 genes that significantly changed their expression levels upon knockdown of COA4 were identified in RNA-Seq analyses according to the criteria described in section 2.2.15 (full list of genes see appendix **supplementary Table 24**). To assist interpretation of these results, gene set enrichment analysis (GSEA) using the ClusterProfiler program was performed to search for significantly enriched pathways. The results showed 202 enriched gene ontology terms (GSEAGO) and 1 enriched GSEAKEGG potential pathway (metabolic pathway). Among the former, 24 biological process with 54 corresponding genes were selected out because they were specifically enriched in either the knockdown or the control condition (**Figure 8 A and B**). Subsequently, potential Protein-Protein-Interaction (PPI) networks were analyzed by the String algorithm (online software: https://string-db.org/), thus leading to the identification of a potential network of chemical and cytokine stimulus response involved genes PLAU, Thrombospondin 1 (THBS1) and Matrix Metalloproteinase 1 (MMP1) (**Figure 8 C**).

A

ID	Description	setSize	enrichmentScore	NES	p-value	rank	genenames
GO:0006811	ion transport	11	0.539325843	1.910038835	0.003756295	52	GLS2/PLLP/CHRNA7/KCNIP2/JPH1/SLC43A1/SLC25A30/NFKBIE/ATP1B2/THBS1/CRACR2B
GO:0003008	system process	11	0.476258066	1.686681949	0.022556291	31	CST4/HSD11B2/PRKCG/RTP4/CHRNA7/CST1/CCDC78/KCNIP2
GO:0008219	cell death	10	0.451447241	1.597408921	0.054532416	25	GLS2/CD24/PRODH/PRKCG/SOCS2/CHRNA7
GO:0042221	response to chemical	33	0.294878286	1.523070135	0.057723345	41	HIST1H3J/CST4/CD24/PRODH/HSD11B2/SOSTDC1/CISH/PRKCG/ESRP2/SOCS2/RTP4/CHRNA7/CST1/TRIM31/PLAU/KCNIP2/IFITM1/MMP1/NRTN/NFKBIE
GO:0065008	regulation of biological quality	22	0.305046608	1.386870666	0.114754098	33	RAB38/HIST1H3J/CST4/LARGE2/CD24/HSD11B2/PRKCG/SOCS2/CHRNA7/PLAU/KCNIP2/JPH1
GO:0006996	organelle organization	15	-0.334576597	-1.375353246	0.124165514	29	MAP1B/EREG/ARHGAP21/IFT27/SNAI2/BICD2/HDAC9/TUBA1A
GO:0022607	cellular component assembly	16	0.329574839	1.342541372	0.15647482	7	COA4/RAB38/LAMC2/HIST1H3J
GO:0044085	cellular component biogenesis	16	0.329574839	1.342541372	0.15647482	7	COA4/RAB38/LAMC2/HIST1H3J
GO:0042592	homeostatic process	10	0.382469889	1.302505734	0.172913043	12	RAB38/CST4/LARGE2/CD24
GO:1901566	organonitrogen compound biosynthetic process	13	0.326246494	1.225097525	0.210922787	10	RAB38/GLS2/GALNT18/LARGE2
GO:0044267	cellular protein metabolic process	33	0.230805946	1.192131331	0.235591769	27	RAB38/GALNT18/HIST1H3J/CST4/LARGE2/CD24/CISH/PRKCG/PPP1R14C/SOCS2/CHRNA7/CST1/TRIM31
GO:0071345	cellular response to cytokine stimulus	12	0.309471724	1.141603552	0.300154162	48	HIST1H3J/CD24/CISH/SOCS2/TRIM31/IFITM1/MMP1/CXCL2/THBS1
GO:0019538	protein metabolic process	34	0.215973228	1.127655401	0.311418685	27	RAB38/GALNT18/HIST1H3J/CST4/LARGE2/CD24/CISH/PRKCG/PPP1R14C/SOCS2/CHRNA7/CST1/TRIM31
GO:0006464	cellular protein modification process	24	0.240655541	1.123924197	0.329693246	27	RAB38/GALNT18/LARGE2/CD24/CISH/PRKCG/PPP1R14C/SOCS2/CHRNA7/TRIM31
GO:0036211	protein modification process	24	0.240655541	1.123924197	0.329693246	27	RAB38/GALNT18/LARGE2/CD24/CISH/PRKCG/PPP1R14C/SOCS2/CHRNA7/TRIM31
GO:0010033	response to organic substance	24	0.222686279	1.040003052	0.41712204	27	HIST1H3J/CD24/HSD11B2/SOSTDC1/CISH/PRKCG/ESRP2/SOCS2/CHRNA7/TRIM31
GO:0070887	cellular response to chemical stimulus	22	0.210162309	0.955486585	0.517304189	27	HIST1H3J/CD24/PRODH/SOSTDC1/CISH/ESRP2/SOCS2/CHRNA7/TRIM31
GO:0071705	nitrogen compound transport	10	0.263863084	0.898588856	0.565217391	12	RAB38/GLS2/CD24
GO:0050790	regulation of catalytic activity	17	0.211846313	0.888216626	0.571936057	26	CST4/CD24/CISH/PPP1R14C/SOCS2/CHRNA7/CST1
GO:0009888	tissue development	16	-0.204553344	-0.861068575	0.64573991	25	DUSP10/SNAI2/TNC/HDAC9/NTN4
GO:2000026	regulation of multicellular organismal development	14	0.220942201	0.851277965	0.656192237	25	HIST1H3J/CD24/SOSTDC1/DLX2/SOCS2/CHRNA7
GO:0071702	organic substance transport	12	0.215882913	0.796365811	0.7053407	3	RAB38/GLS2
GO:0006468	protein phosphorylation	11	0.213483146	0.756056841	0.757518797	81	CD24/PRKCG/CHRNA7/NRTN/THBS1/NOG/DUSP3/SBK3/ZNF675/EREG/DUSP10
GO:0048731	system development	27	-0.145167144	-0.731664478	0.759115646	33	ETS2/MAP1B/EREG/IFT27/DUSP10/SNAI2/ATXN1/TNC/HDAC9/NTN4

B

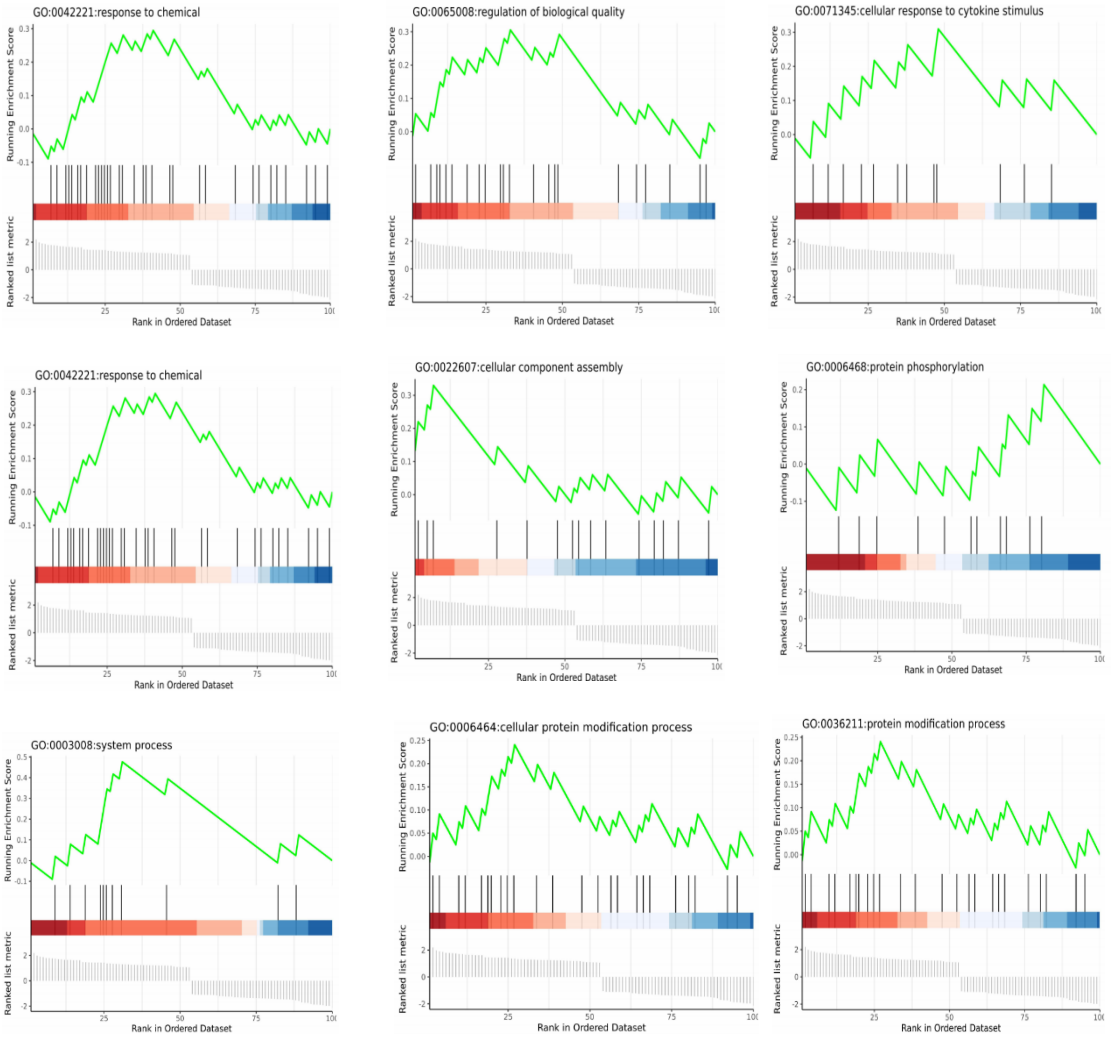

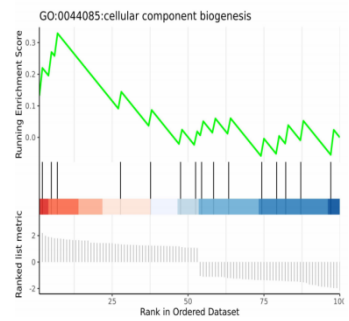
GO:0044085:cellular component biogenesis
Running Enrichment Score
Ranked list metric
Rank in Ordered Dataset

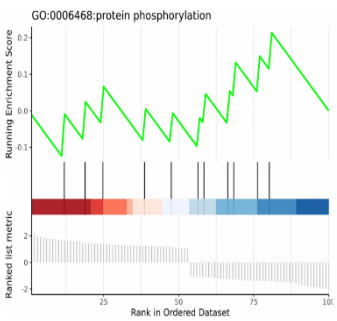
GO:0006468:protein phosphorylation
Running Enrichment Score
Ranked list metric
Rank in Ordered Dataset

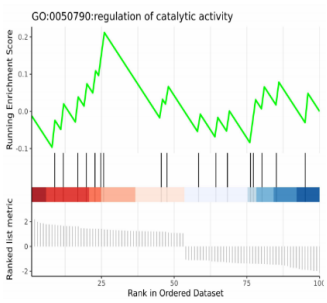
GO:0050790:regulation of catalytic activity
Running Enrichment Score
Ranked list metric
Rank in Ordered Dataset

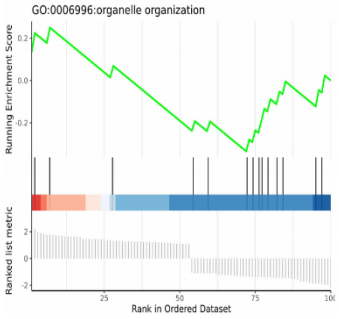
GO:0006996:organelle organization
Running Enrichment Score
Ranked list metric
Rank in Ordered Dataset

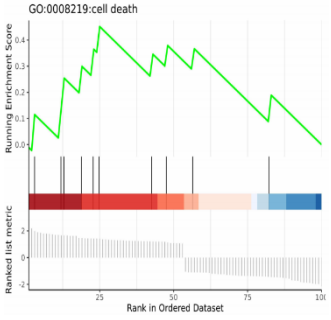
GO:0008219:cell death
Running Enrichment Score
Ranked list metric
Rank in Ordered Dataset

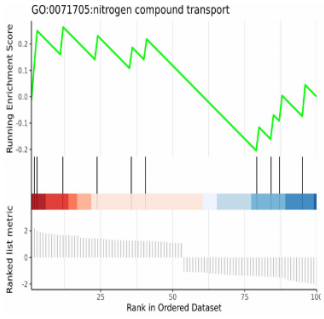
GO:0071705:nitrogen compound transport
Running Enrichment Score
Ranked list metric
Rank in Ordered Dataset


GO:0009888:tissue development
Running Enrichment Score
Ranked list metric
Rank in Ordered Dataset

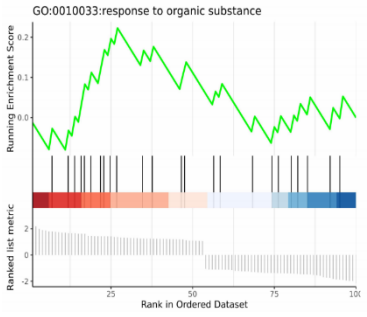
GO:0010033:response to organic substance
Running Enrichment Score
Ranked list metric
Rank in Ordered Dataset


GO:2000026:regulation of multicellular organismal developme
Running Enrichment Score
Ranked list metric
Rank in Ordered Dataset

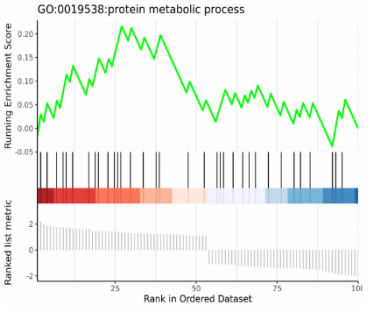
GO:0019538:protein metabolic process
Running Enrichment Score
Ranked list metric
Rank in Ordered Dataset

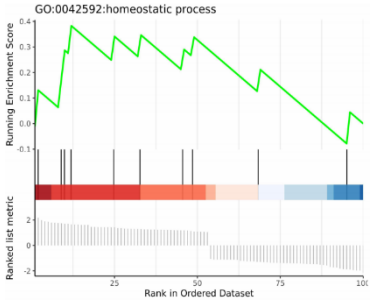
GO:0042592:homeostatic process
Running Enrichment Score
Ranked list metric
Rank in Ordered Dataset

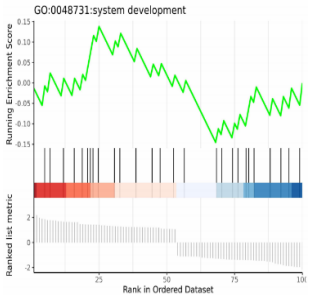
GO:0048731:system development
Running Enrichment Score
Ranked list metric
Rank in Ordered Dataset

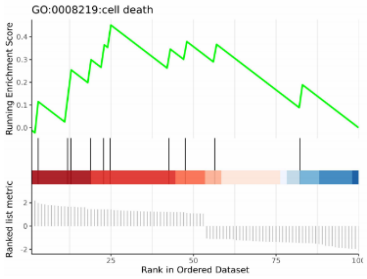
GO:0008219:cell death
Running Enrichment Score
Ranked list metric
Rank in Ordered Dataset

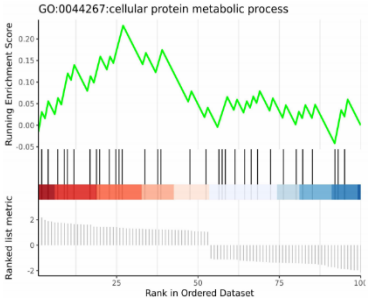
GO:0044267:cellular protein metabolic process
Running Enrichment Score
Ranked list metric
Rank in Ordered Dataset

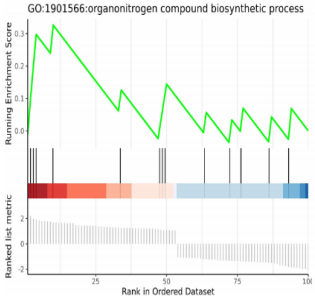
GO:1901566:organonitrogen compound biosynthetic process
Running Enrichment Score
Ranked list metric
Rank in Ordered Dataset

C

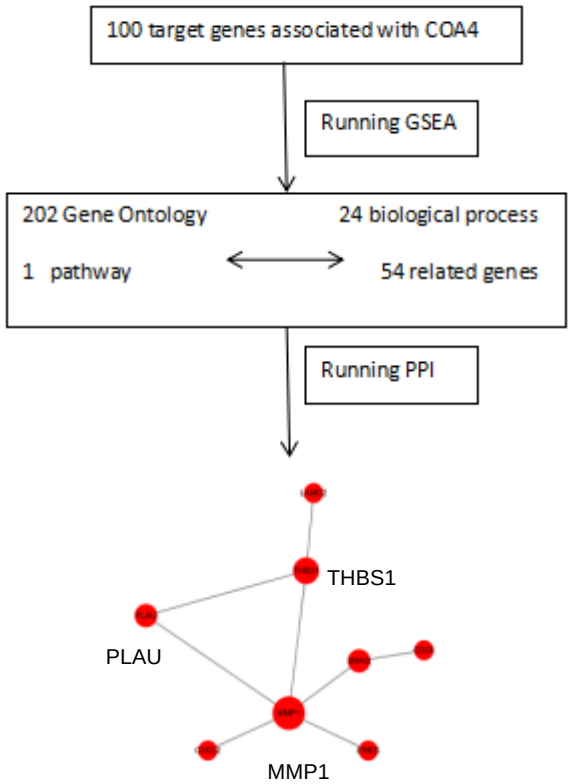

Figure 8. Workflow of RNA-Seq data analysis to find functional effector genes upon COA4 knockdown. A) List (excerpt) of GO terms (and associated genes) significantly enriched among differentially expressed genes. B) Results of gene set enrichment analyses (GSEA) for the different GO terms, demonstrating distribution of over- and under- expression of associated genes across the gene sets. C) Hypothetical protein interaction network as determined by String analysis.

3.6 Verification of DEGs by qRT-PCR - PLAU was downregulated following loss function of COA4

To verify that the putative DEGs were differentially expressed on COA4 siRNA treated samples and consistent with the RNA-Seq expression profile, real-time PCR was performed. However, there was no detectable THBS1 signal in S2-007 cells, and expression levels of MMP1 were extremely low in non-treated S2-007 cells. In contrast, PLAU was strongly and uniformly downregulated upon COA4 knockdown in all 3 PDAC cell lines, consistent with RNA-Seq results (**Figure 9**). Thus, PLAU was confirmed as a potential functional effector of COA4.

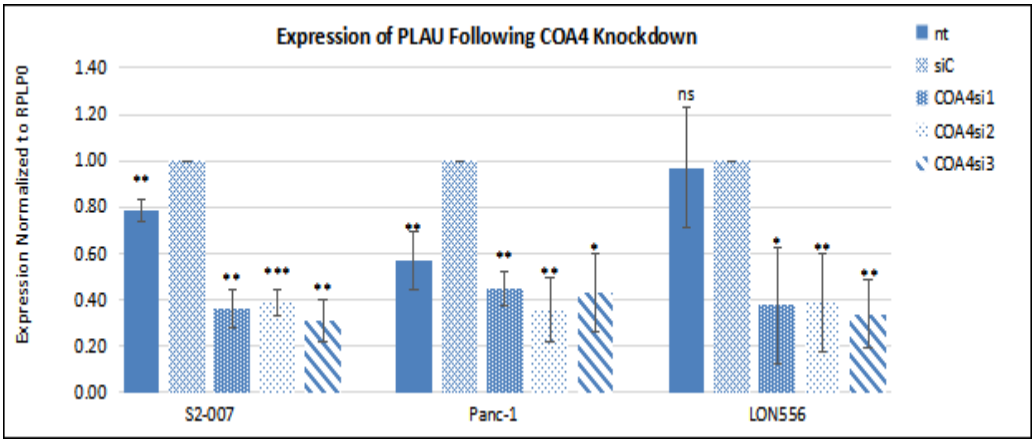

Figure 9. Expression of PLAU was attenuated following COA4 inhibition. 48h after COA4 siRNA transfection, real-time PCR analysis of PLAU expression was performed. Values were normalized to siControl treated sample. Analyses of each cell line were repeated at least 3 times to get Mean±SD. * =P＜0.05, ** =P＜0.01, *** =P＜0.001 (Student t-Test). (nt=non-treated sample, siC=non silencing siRNA, si1-3 = respective COA4 siRNA)

3.7 COA4 regulated cell migration and cell growth (3D cell culture) by targeting PLAU

To verify PLAU as a downstream effector of COA4, a replacement vector encoding an EGFP-tagged PLAU gene was constructed (section 2.1.11). At first, cell clones stably expressing the PLAU construct were established (see section 2.2.3), real-time PCR was applied to identify the plasmid efficiency. As the result showed (**Figure 10**), overexpression of PLAU indeed appeared on PLAU stably expressed cells regardless if they were treated or non-treated with COA4-specific siRNAs. However, unexpectedly there was significant downregulation of recombinant PLAU in response to COA4 siRNA, prompting the hypothesis that there might exist a positive-feed-back loop regulating the expression of endogenous PLAU in response to recombinant PLAU expression. To investigate this, two different PLAU primer pairs were used for qRT-PCR, one within the open reading frame (ORF), thus detecting both endogenous and recombinant PLAU, and one outside the ORF, detecting only endogenous PLAU. Analysis of three independent stably transfected clones confirmed that levels of endogenous PLAU were significantly elevated in transfected clones, supporting the notion of a positive PLAU feedback-loop.

Total PLAU levels in the stably transfected clones even in the presence of COA4 siRNAs still remained far above base levels in untransfected cells.

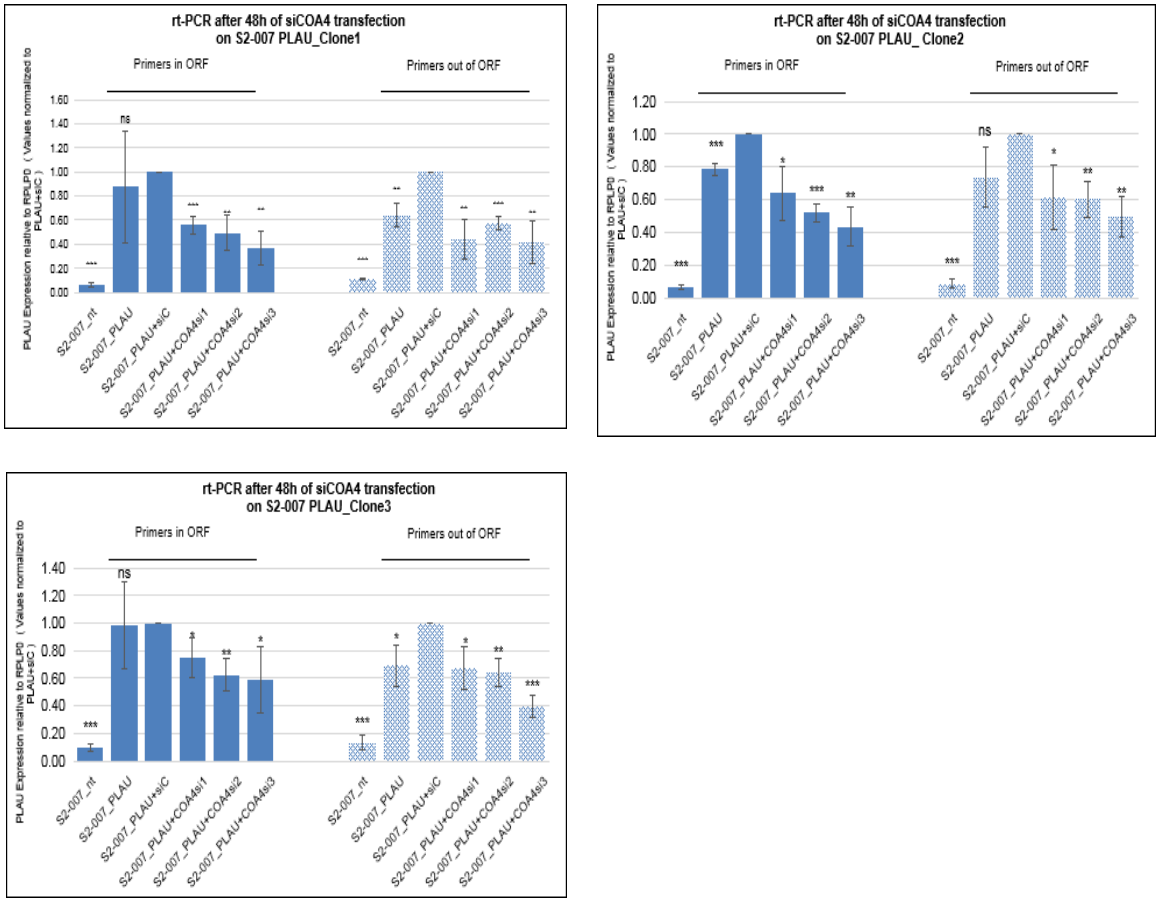

Figure 10. PLAU expression levels in stably transfected cell clones were analyzed by qRT-PCR. Using primer pairs located within the PLAU ORF (solid bars) as well as outside the ORF (hashed bars). Cells were either left untreated or transfected with COA4-specific- and control siRNAs and harvested after 48h of siRNA transfection. Values were normalized to siControl-treated samples. Each stably transfected clone was analyzed at least 3 times to get Mean±SD, * =P＜0.05, ** =P＜0.01, *** =P＜0.001 (Student t-Test).

Subsequently, MTT, CellTiter-Glo assays, and Time-Lapse-Microscopy were analyzed on the three independent PLAU-EGFP expressing clones. The rate of cell growth reduction in response to COA4-inhibition in PLAU overexpressing cells was not significantly changed in 2D cell culture as measured by MTT assay (**Figure 11A**). In contrast, cell growth reduction was partially prevented in 3D cell culture condition (**Figure 11B**), as measured by CellTiter-Glo assay. Furthermore, cell migration analysis by

time-lapse-microscopy assay revealed that overexpression of PLAU could completely rescue cell migration reduction upon COA4 siRNAs in S2-007 cells (**Figure 12**).

A

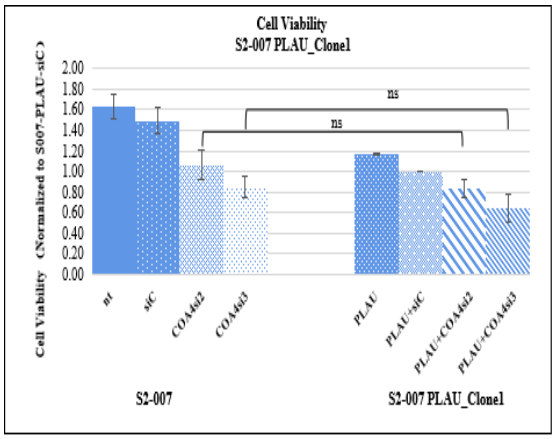

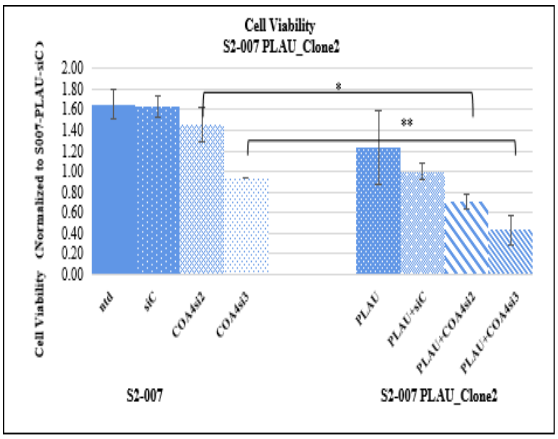

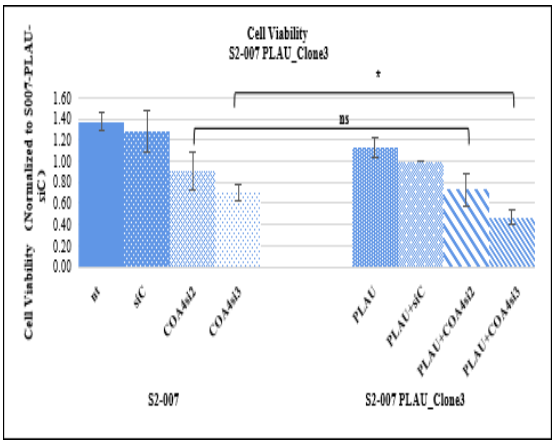

B

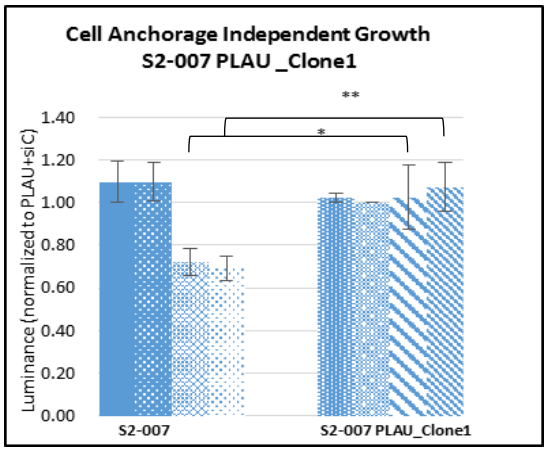

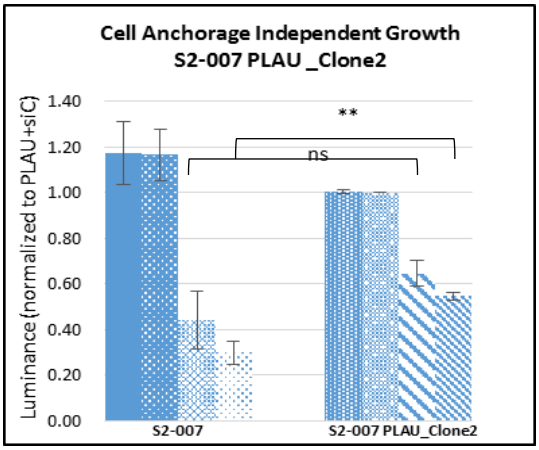

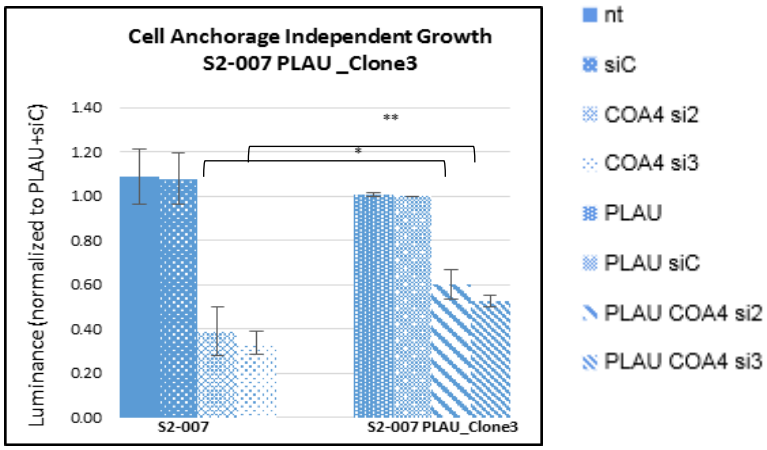

Figure 11. Cell viability and Cell-anchorage-independent growth assessed by A) MTT assay, B) CellTiter-Glo assay in COA4 siRNA transfected parental S2-007 cells (left panels) and PLAU DNA stable expressed clones respectively (right panels) 72 h after transfection. Since clones stemmed from different rounds of stable transfection, parental S2-007 cells were independently analyzed in parallel to the individual clones each time.
Each experiment was repeated at least 3 times to get Mean±SD, * =P＜0.05, ** =P＜0.01, *** =P＜0.001 (Student t-Test).

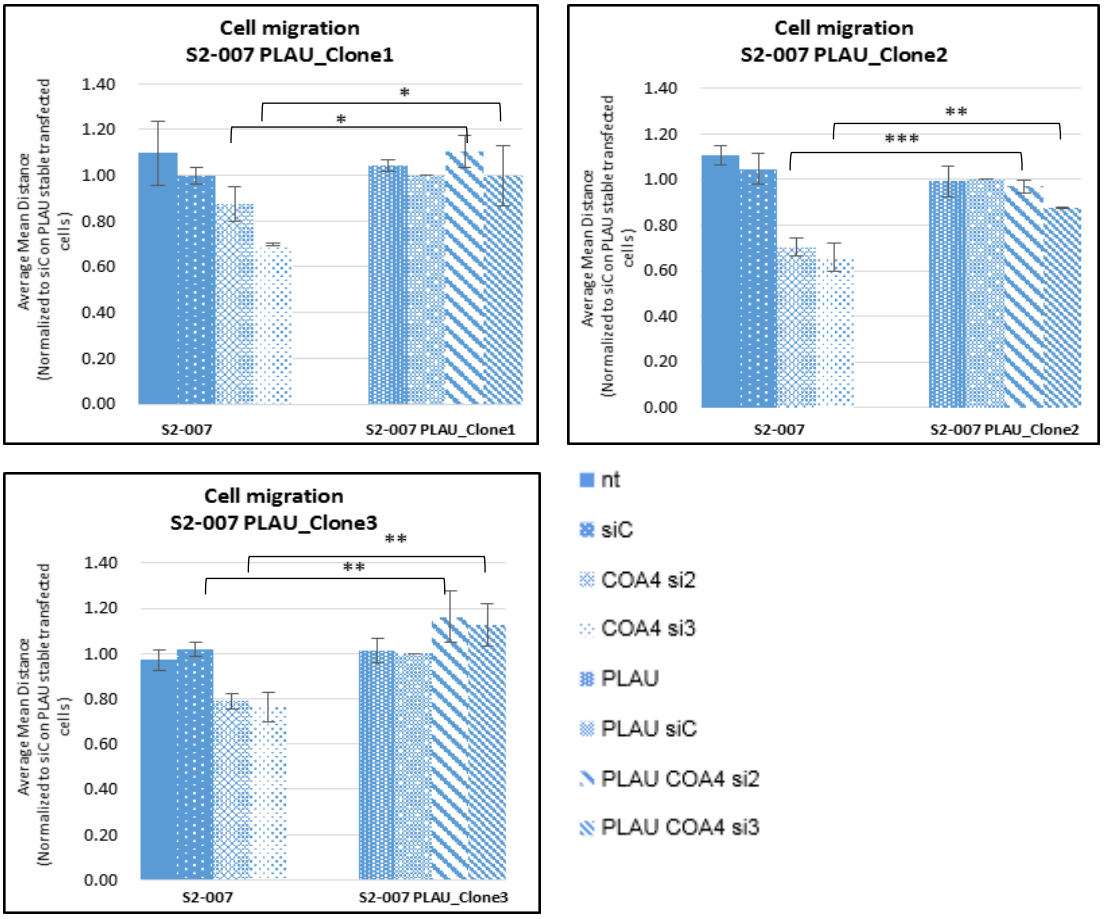

Figure 12. Induction of cell migration reduction through loss-of COA4 could be rescued in PLAU overexpressed cells. PLAU DNA stable expressed clones were treated with 17nM

non-silencing siRNA or COA4 siRNA (right panels). In parallell, COA4 siRNA transfected parental S2-007 cells (left panels) were used for comparison. Time-Lapse-Microscopy was performed after 72h of transfection.
Each experiment of each stable transfected clone was repeated at least 3 times to get Mean±SD, * =P＜0.05, ** =P＜0.01, *** =P＜0.001 (Student t-Test).

3.8 COA4 expression did not correlate with patient survival

To assess COA4 protein expression on patient tissue samples, a tissue microarray (TMA) comprising 58 human PDAC and adjunct control tissues were stained with an anti-COA4 antibody. The COA4 protein was moderately expressed in the cytoplasm of non-cancerous pancreatic cells (**Figure 13D**), in malignant tissues (n=58), COA4 was not consistently expressed in the cytoplasm, but showed different subcellular localizations (**Figure 13A to C**). There were 2 samples with negative stain and 9 tissues with strong nuclear stain. Interestingly, among invasive cancer samples, 12 samples showed obvious COA4 staining on the cell membrane which had significantly stronger COA4 levels (**Figure 13E**). Kaplan–Meier survival analysis demonstrated that the PDAC patients with high COA4 expression did not have different overall survival compared to patients with low COA4 levels. Additionally, overall survival was not different among cases with different subcellular localization of COA4 (**Figure 13F&G**).

A

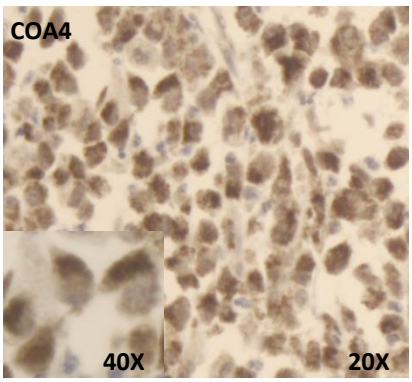

B

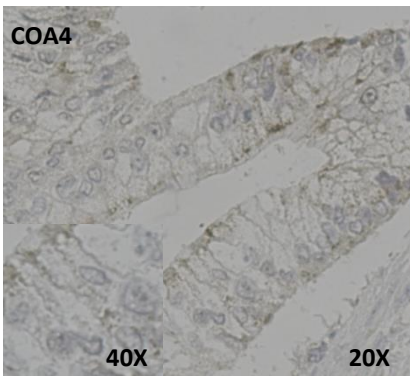

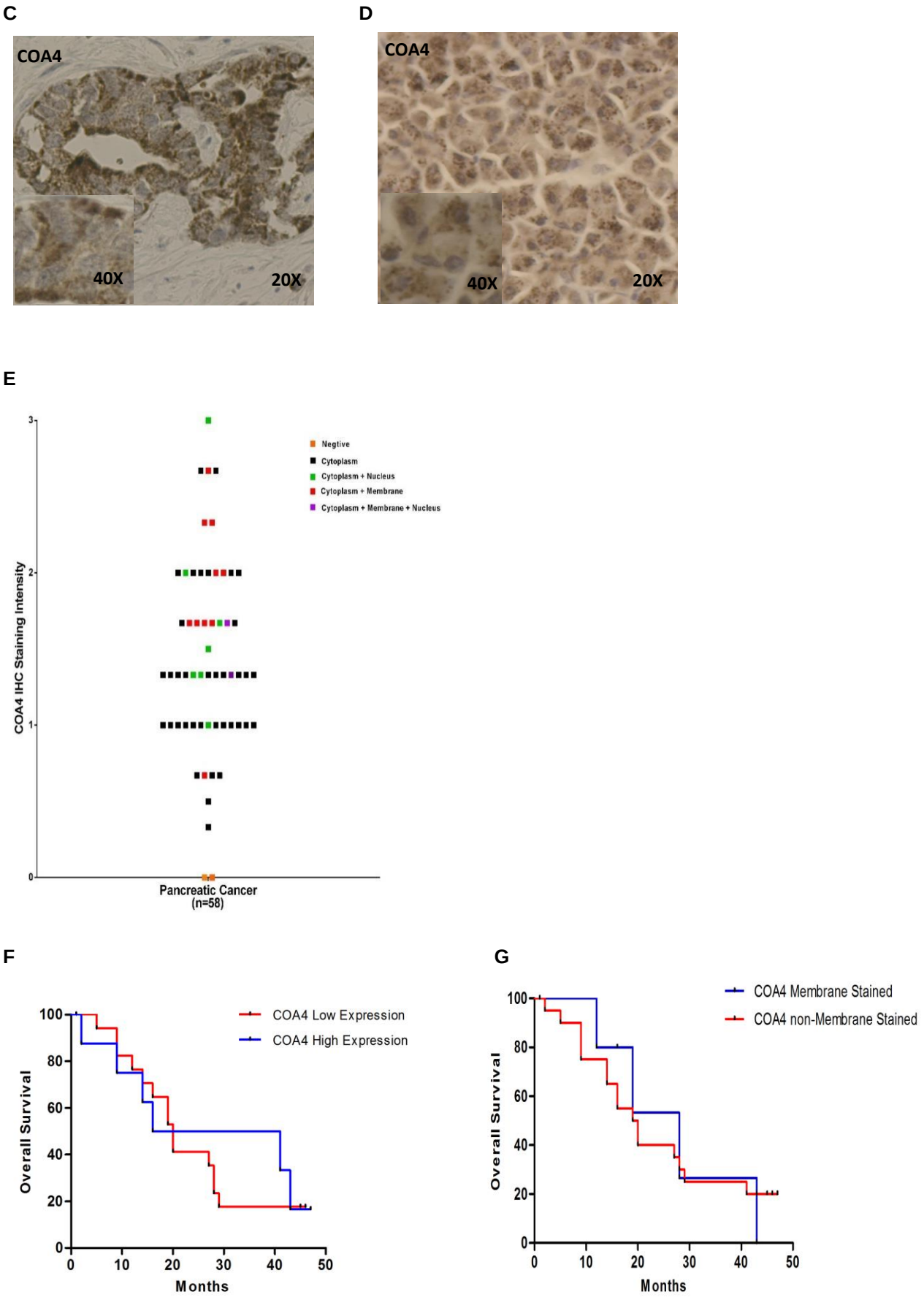

Figure 13. Representative images of TMA based IHC analysis of COA4 expression in

pancreatic cancer and normal pancreatic tissues. COA4 protein expression showed a significant difference in staining location. A) Strong nucleus and cytoplasm stain. B) Cytoplasm and cell membrane were clearly stained. C) Protein was stained on cytoplasm only. D) Normal tissue was always stained on cytoplasm. E) COA4 staining on membrane was correlated with stronger protein intensity. F) & G) Kaplan-Meier analyses of overall survival among cases with high vs. low COA4 staining intensity (F) and different subcellular staining patterns of COA4 (G).

3.9 Suppression of POLr3K induced cell growth reduction and necrosis

The impact of POLr3K knockdown on mRNA expression was evaluated by real-time PCR after 48h of siRNA transfection (**Figure 14A**). Inhibition of POLr3K resulted in sharp reduction of target mRNA which was at least 60% reduced compared to negative control, and each siRNA had comparable effectiveness. Western-Blot analyses showed that POLr3K was also significantly downregulated on the protein level upon siRNA transfection (**Figure 14B**). To investigate potential effects on cell growth, MTT and BrdU assays were performed to assess cell viability and cell proliferation, respectively. In all three cell lines, viability and proliferation rates of the tumor cells were significantly reduced in POLr3K siRNA transfected cells (**Figure 15A&B**). Western Blot assays for PARP cleavage presented no enhanced apoptosis signal on POLr3K inhibited cells (**Figure 15C**). Flow cytometry analyses of annexin V/PI dual stained cells (see section 2.2.14.2) likewise did not show elevated apoptosis rates, whereas the rate of cell necrosis was clearly elevated in POLr3K inhibited cells, most strongly in siRNA2 treated cells (**Figure 15D**).

A

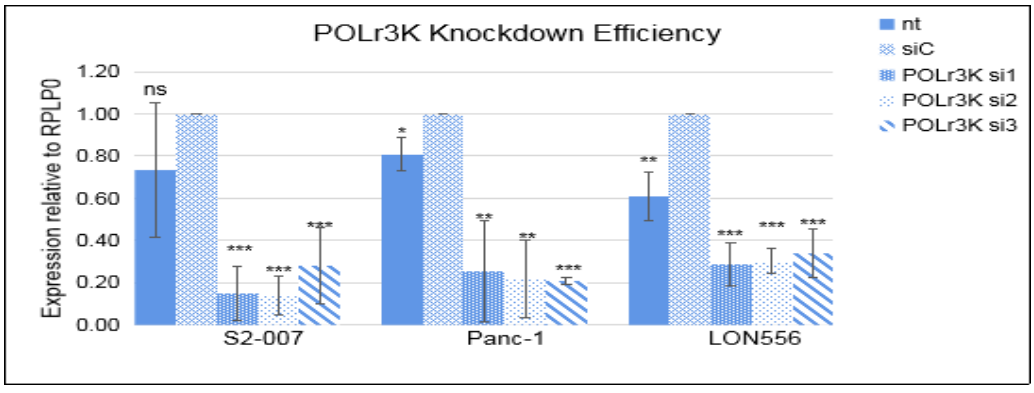

B

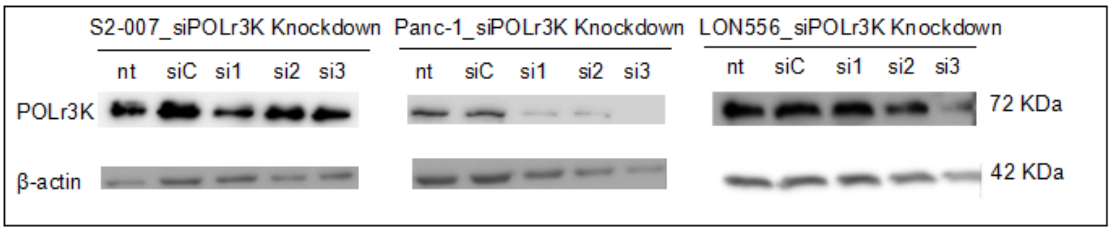

Figure 14. Knockdown of POLr3K mRNA on pancreatic cancer cell lines. A) Efficiency of POLr3K siRNA was assessed by rt-PCR. mRNA expression was normalized to RPLP0. Values were the mean ± SD of at least 3 independent experiments. * =P＜0.05, ** =P＜0.01, *** =P＜0.001 (Student t-Test). B) POLr3K protein expression on Western-Blot after 48 h of siRNA transfection. Sample loading was controlled by staining for β-actin.

A

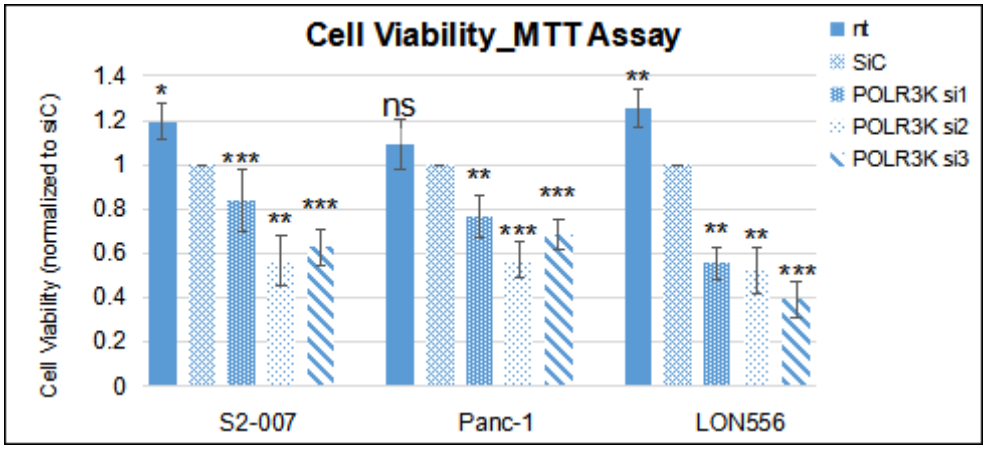

B

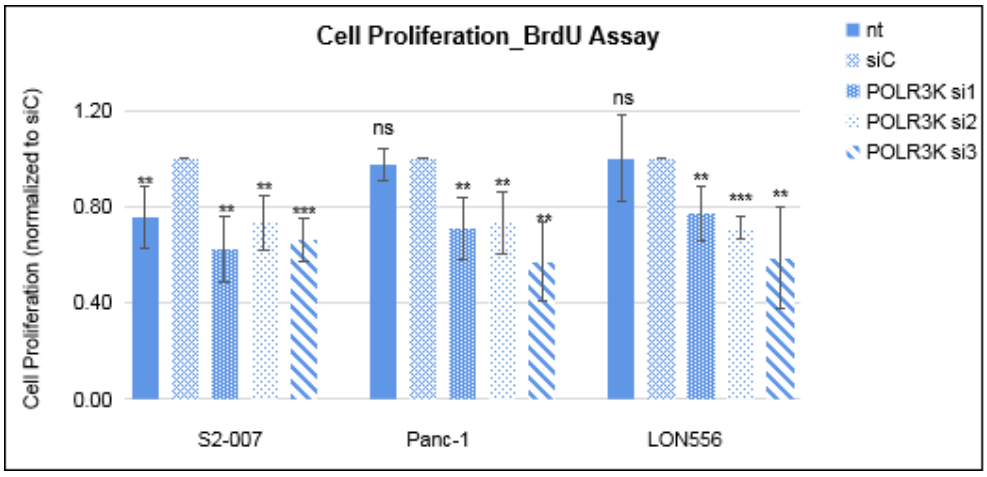

C

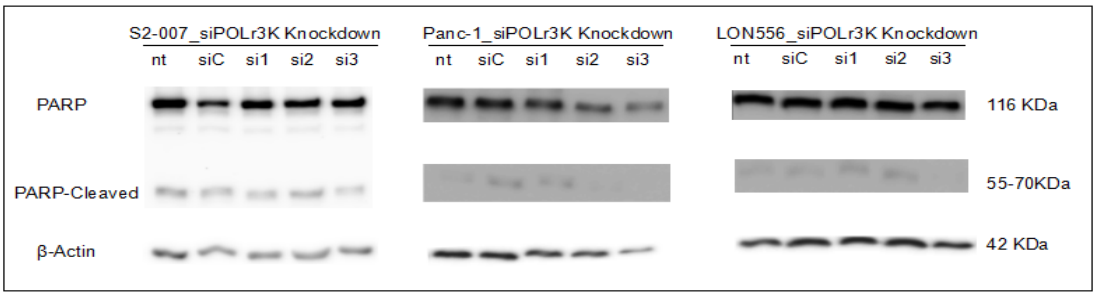

D

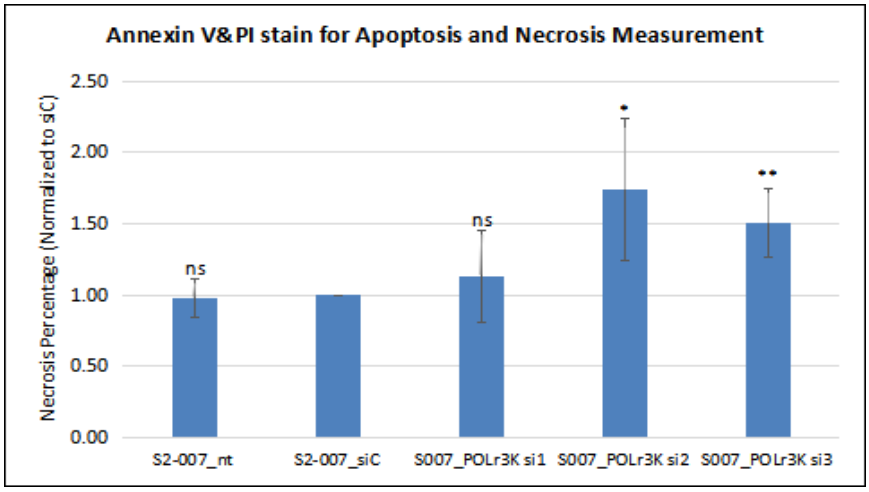

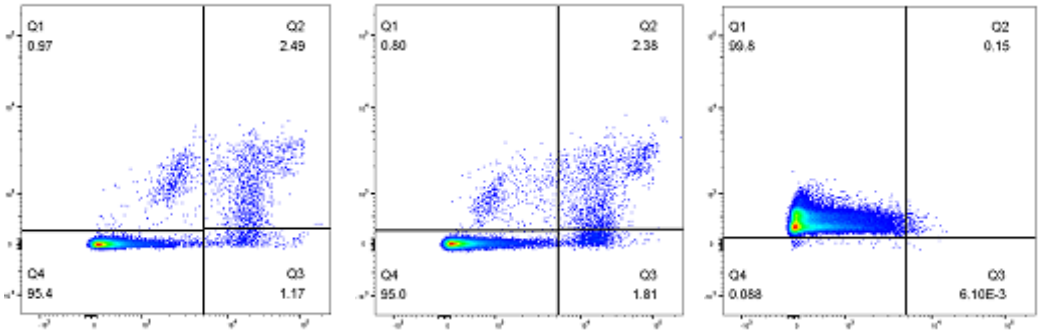

S2-007_nt

S2-007_siC

S2-007_nt with 0.5% Tritonx100

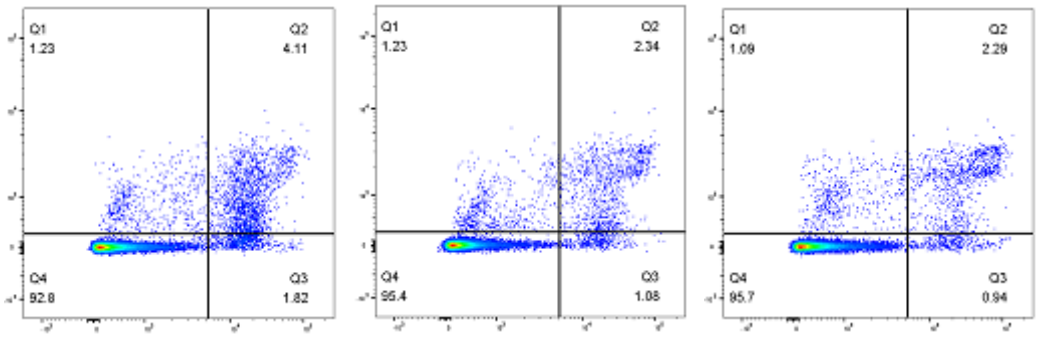

S2-007_POLr3K si1

S2-007_POLr3K si2

S2-007_POLr3K si3

Figure 15. Inhibition of POLr3K attenuated cell proliferation and elevated cell necrosis.
A) MTT assay was performed after 72h of siRNAs transient transfection, B) BrdU incorporation of DNA assay was done after 48h of siRNAs interference. C) 48h after siRNA transfection, apoptosis induction was monitored by Western-Blot-based detection of the PARP protein. PARP cleavage did not increase on POLr3K inhibited samples. D) 72h after POLr3K siRNA transfection, cell necrosis was assessed by Annexin V/PI dual stained flow cytometry. 0.5% Tritonx100 was used as positive control, Annexin V alone stained cells were used as negative control.
All values represented were mean ± SD of at least 3 independent experiments. For MTT, BrdU and necrosis measurements, values were normalized to siC. * =P＜0.05, ** =P＜0.01, *** =P＜0.001 (Student t-Test).

3.10 POLr3K had no impact on cell cycle progression

Western-Blot analyses demonstrated that inhibition of POLr3K led to upregulation of the tumor suppressor p21. Simultaneously, Cyclin D1 was uniformly downregulated upon POLr3K silencing (**Figure 16A**). Cell cycle analysis using flow cytometry revealed no obvious changes in cell cycle progression within 72 hours of POLr3K siRNAs transfection. Then, cells were subjected to 0.1 µg/ml Nocodazole for 9 hours' incubation, which arrested cells at the G2-M phase and prevented individual cells from re-entering into cell cycle. However, POLr3K siRNA transfection again did not significantly alter cell cycle progression although p21 and CyclinD1 expression were clearly altered (**Figure 16B&C**).

A

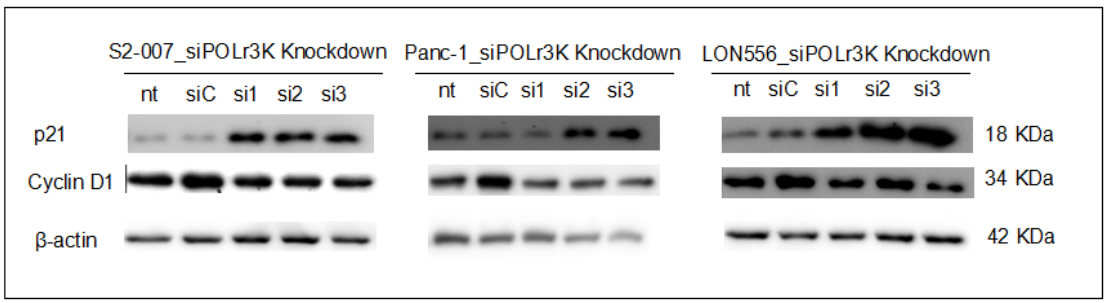

B

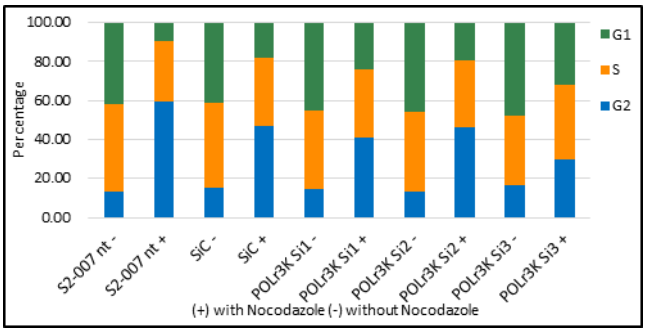
100.00
80.00
60.00
40.00
20.00
0.00
Percentage
G1
S
G2
S2-007 nt -
S2-007 nt +
SiC -
SiC +
POLr3K Si1 -
POLr3K Si1 +
POLr3K Si2 -
POLr3K Si2 +
POLr3K Si3 -
POLr3K Si3 +
(+) with Nocodazole (-) without Nocodazole

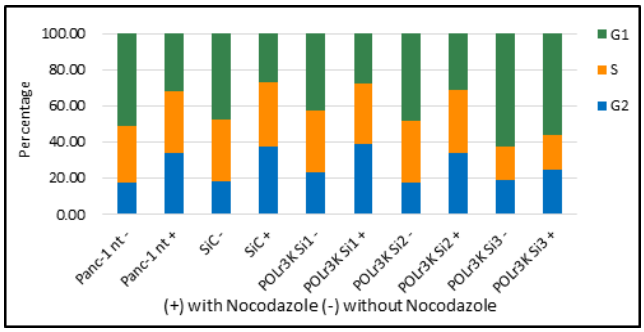
100.00
80.00
60.00
40.00
20.00
0.00
Percentage
G1
S
G2
Panc-1 nt -
Panc-1 nt +
SiC -
SiC +
POLr3K Si1 -
POLr3K Si1 +
POLr3K Si2 -
POLr3K Si2 +
POLr3K Si3 -
POLr3K Si3 +
(+) with Nocodazole (-) without Nocodazole

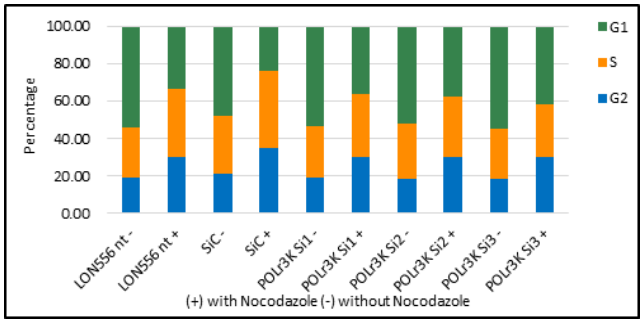
100.00
80.00
60.00
40.00
20.00
0.00
Percentage
G1
S
G2
LON556 nt -
LON556 nt +
SiC -
SiC +
POLr3K Si1 -
POLr3K Si1 +
POLr3K Si2 -
POLr3K Si2 +
POLr3K Si3 -
POLr3K Si3 +
(+) with Nocodazole (-) without Nocodazole

C

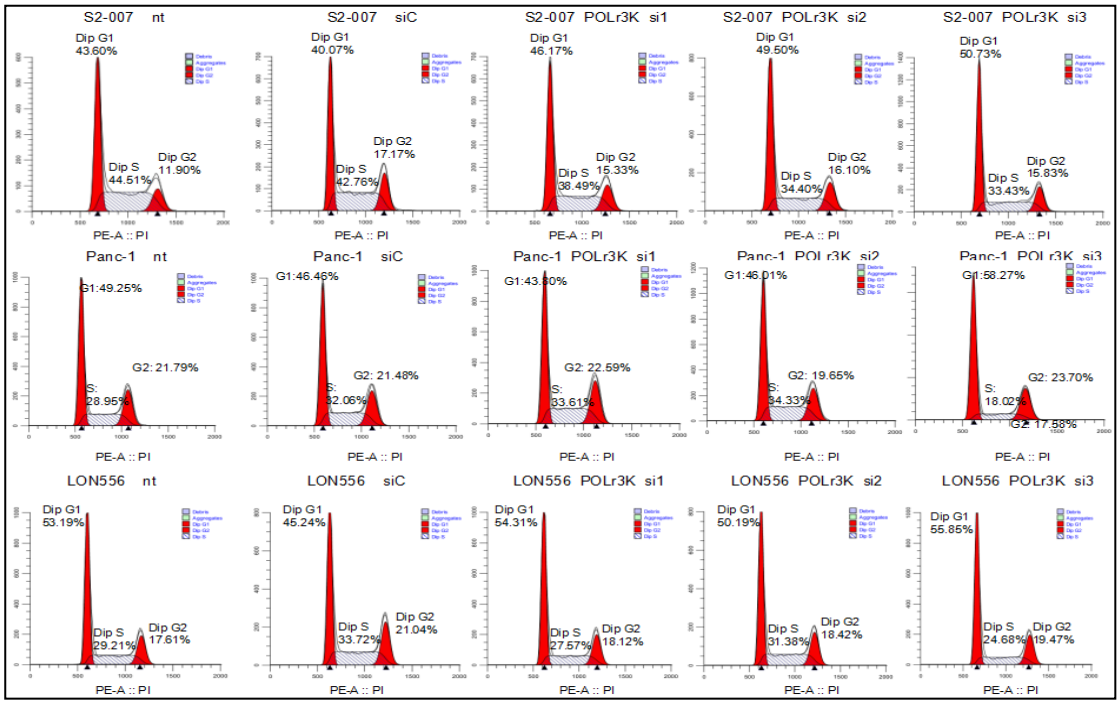
S2-007 nt
Dip G1 43.60%
Dip S 44.51%
Dip G2 11.90%
S2-007 siC
Dip G1 40.07%
Dip S 42.76%
Dip G2 17.17%
S2-007 POLr3K si1
Dip G1 46.17%
Dip S 38.49%
Dip G2 15.33%
S2-007 POLr3K si2
Dip G1 49.50%
Dip S 34.40%
Dip G2 16.10%
S2-007 POLr3K si3
Dip G1 50.73%
Dip S 33.43%
Dip G2 15.83%
Panc-1 nt
G1:49.25%
G2: 21.79%
S: 28.95%
Panc-1 siC
G1:46.46%
G2: 21.48%
S: 32.06%
Panc-1 POLr3K si1
G1:43.80%
G2: 22.59%
S: 33.61%
Panc-1 POLr3K si2
G1:46.01%
G2: 19.65%
S: 34.33%
Panc-1 POLr3K si3
G1:58.27%
G2: 23.70%
S: 18.02%
G2: 17.58%
LON556 nt
Dip G1 53.19%
Dip S 29.21%
Dip G2 17.61%
LON556 siC
Dip G1 45.24%
Dip S 33.72%
Dip G2 21.04%
LON556 POLr3K si1
Dip G1 54.31%
Dip S 27.57%
Dip G2 18.12%
LON556 POLr3K si2
Dip G1 50.19%
Dip S 31.38%
Dip G2 18.42%
LON556 POLr3K si3
Dip G1 55.85%
Dip S 24.68%
Dip G2 19.47%
PE-A :: PI

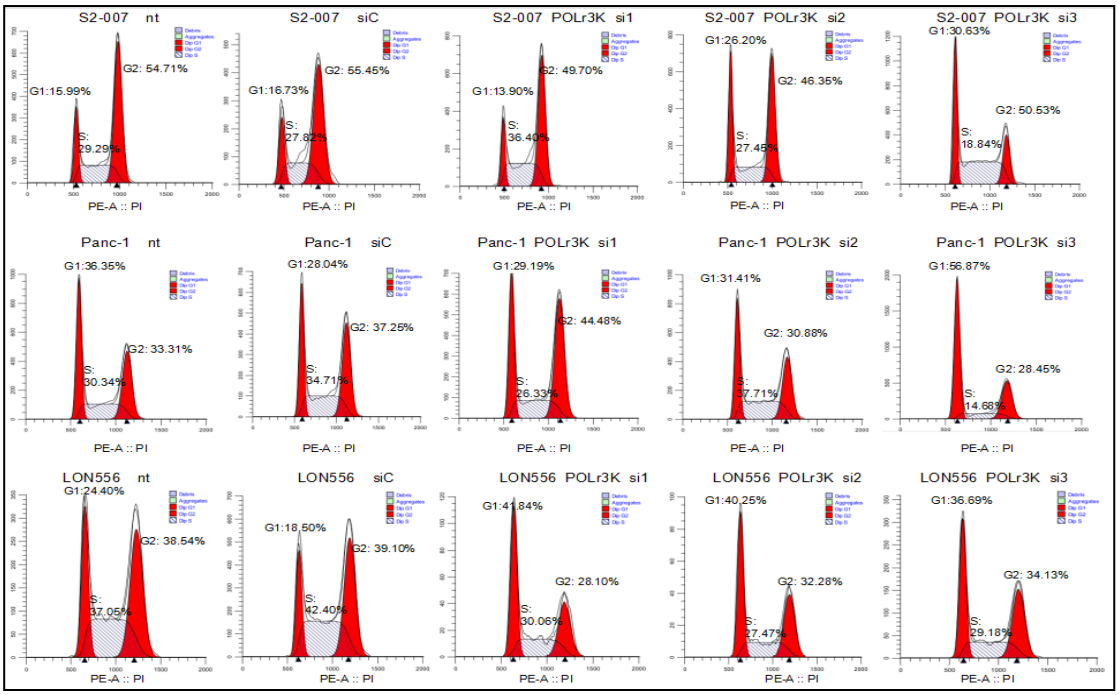

Figure 16. POLr3K inhibition had no overt effect on cell cycle. A) Cell cycle regulators Cyclin D1 and p21 were assessed by western-Blot after 48 h transfection of POLr3K siRNAs (nt=non-treated sample, siC=non silencing siRNA, si1-3 = respective POLr3K siRNA). B) PI stained - cell cycle analysis on POLr3K knockdown pancreatic cancer cells. 72h after siRNA transfection, cells were left untreated or incubated with 0.1 µg/ml Nocodazole for 9h, cells were harvested, stained with 20 µg/ml PI solution, and cell cycle distribution measured by flow cytometry. Values are the mean of 3 independent experiments. Cell cycle distribution upon POLr3K knockdown was analyzed by Modfit LT. C) Representative individual results of cell cycle analyses without Nocodazole interference (upper panels) and with Nocodazole interference (lower panels) after 72 hours of POLr3K siRNA transfection.

3.11 POLr3K regulated cell anchorage independent growth but not cell migration

In order to determine whether manipulating POLr3K expression could affect anchorage independent growth, CellTiter-Glo assays were performed with cells grown on Poly-HEMA-coated plates. POLr3K siRNA treated cells of all 3 cell lines showed significantly reduced anchorage independent growth compared to nonsilencing siRNA-treated or untreated cells (**Figure 17A**). On the other hand, time-lapse microscopy did not reveal any changes in migratory activity upon loss of function of POLr3K (**Figure 17B**).

A

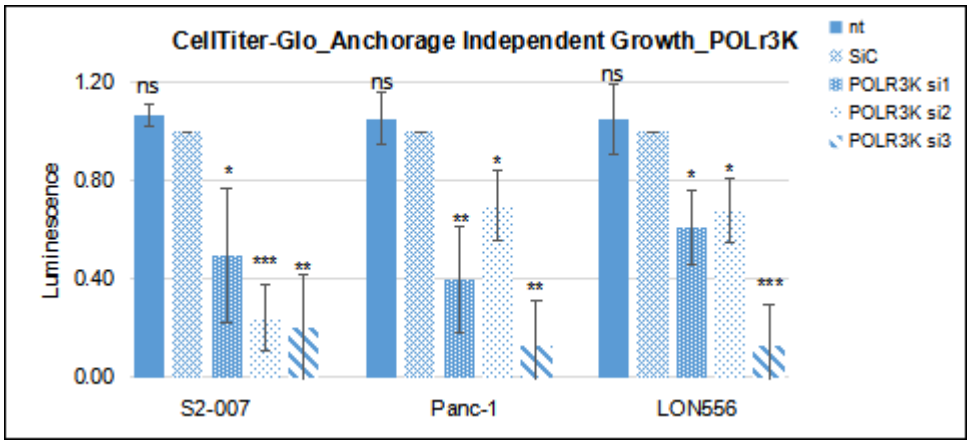

B

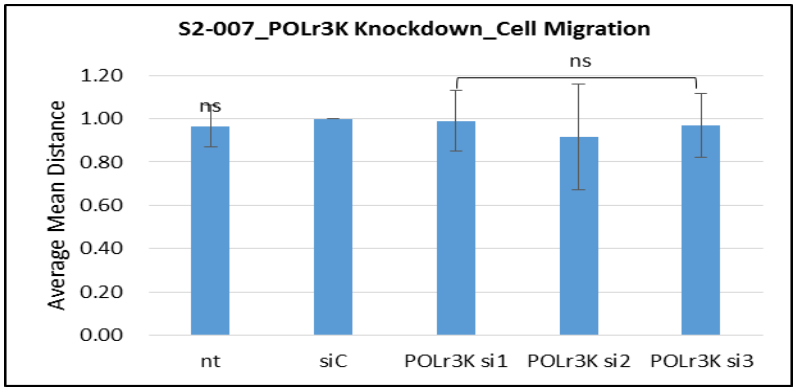

Figure 17. Reduction of POLr3K expression reduced cell anchorage dependent growth but not cell migration. A) Cell viability of spheroids was tested by CellTiter-Glo assay. After 48 h of siRNA transfection, cells were grown on Poly-HEMA coated 3D cell culture condition and incubated for 7 days to form spheroids. B) Silenced POLr3K did not affect cell migration activity. Cells were reseeded on 10.1 mg/ml collagen coating plate after 48h of siRNA transfection and migratory activity (expressed as average mean distance of travel) measured by time-lapse-microscopy. Values were the mean±SD of 3 independent experiments. * =P＜0.05, ** =P＜0.01, *** =P＜0.001 (Student t-Test).

3.12 POLr3K silencing led to miR-30d-5p repression

microRNA profiling was performed using TaqMan microRNA array cards to identify miRNAs which changed expression levels upon POLr3K knockdown in S2-007 cells (see section 2.2.17). Relative expression was calculated by the ΔCt method; the mean Ct value of all miRNA probes on each array was used for normalization. miR-135a-5p (miR135a), miR-30d-5p (miR30d), and miR-24-2-5p (miR24-2) were identified as potentially downregulated by

POLr3K inhibition, while miR-1291 (miR1291) appeared to be upregulated (**Table 23**).

Table 23. Analyzed data of Candidate microRNAs

NO.	miRNA Name	Ct value siC_Crt ①	Ct value siC_Crt ②	si2 Crt	si3 Crt	Rel Expression of siC ①	Rel Expression of siC②	Rel Expression of si2	Rel Expression of si3
Array A_79	miR-135a-000460	24.80	24.80	29.04	30.50	0.216	0.192	0.029	0.014
Array B_5	miR-30d-000420	22.41	20.77	22.22	24.67	1.003	1.490	0.864	0.318
Array B_340	miR-1291-002838	29.00	26.21	24.33	26.86	0.010	0.034	0.200	0.070
Array B_280	miR-24-2#-002441	27.53	24.78	27.39	28.53	0.029	0.092	0.024	0.022

* TaqMan array analyses of miRNA expression after POLr3K knockdown. Two independent samples treated with control siRNA (siC) as well as one sample each treated with POLr3K si2 and si3, respectively, were analyzed. The table shows raw Ct values as well as rel. expression values (normalized to mean Ct values of all miRNA targets on each array).

3.13 Verification of miRNA candidates on S2-007 cell line by real-time PCR

Potential microRNAs of interest were validated by real-time PCR (section 2.2.6 & 2.2.18). After reverse transcription of RNA from POLr3K siRNA-treated and negative control siRNA treated S2-007 cells with a stem-loop primer pool of the target microRNAs, real-time PCR was performed to elucidate whether expression of candidate microRNAs was consistent with the TaqMan array results. As result shown in **Figure 18**, miR-30d was confirmed to be significantly downregulated in response to POLr3K silencing, while results for the other three candidate miRNAs could not be verified. Therefore, miR30d was selected for further experiments.

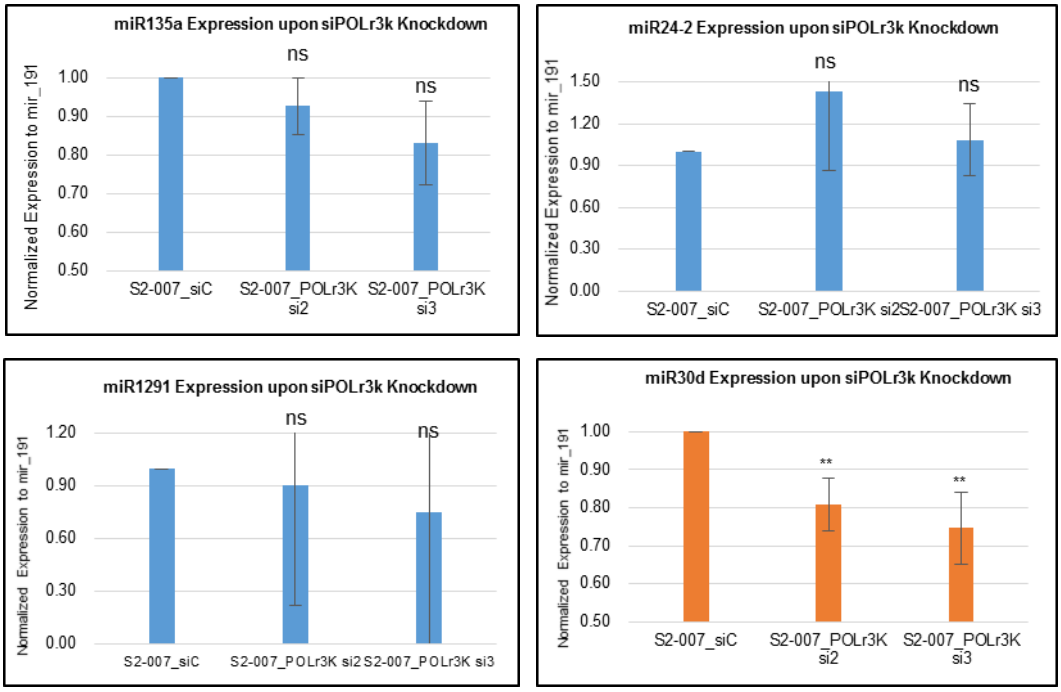

Figure 18. microRNAs of interest were verified by real-time PCR. Cells were treated with non-silencing control siRNA (siC) or POLr3K-specific siRNA 2 or 3, respectively. Expression levels were normalized to the "housekeeping"-miRNA miR-191-5p (miR191). Expression of miR-30d was consistent with TaqMan array results. Values were normalized to siC, and the mean ± SD of 3 independent experiments. * =P＜0.05, ** =P＜0.01, *** =P＜0.001 (Student t-Test).

3.14 POLr3K regulated 3D cell growth via miR-30d-5p

3.14.1 miR-30d-5p did not affect POLr3K mediated cell growth in 2D cell culture conditions

Using POLr3K-specific siRNA2 as representative siRNA, POLr3K mRNA expression was efficiently reduced by POLr3K siRNA transfection also under conditions of co-transfection with miR30d RNAmimics or control mimics in S2-007 cells (**Figure 19A**). Effects on cell viability were assessed by MTT assays. Transfection of miR mimics produced cell stress for both mR30d as well as control mimics (**Figure 19B**). Viability was not further reduced by co-transfection with POLr3K-specific siRNAs, and there was no systematic difference in viability with any combination of RNAmimics and gene-specific or control siRNAs.

A

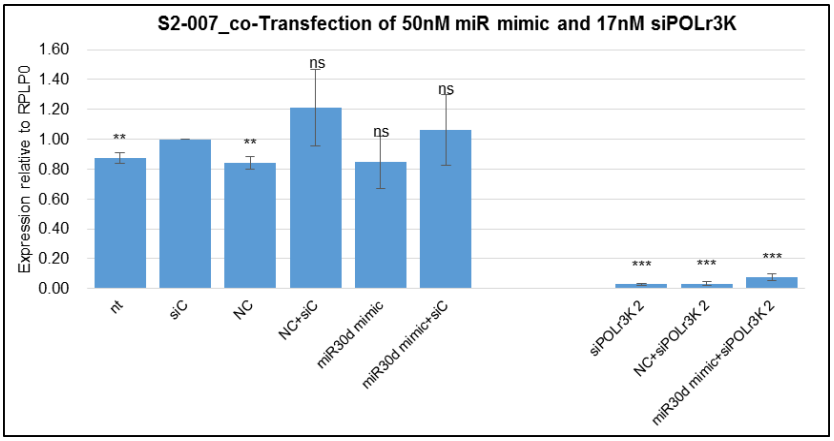

B

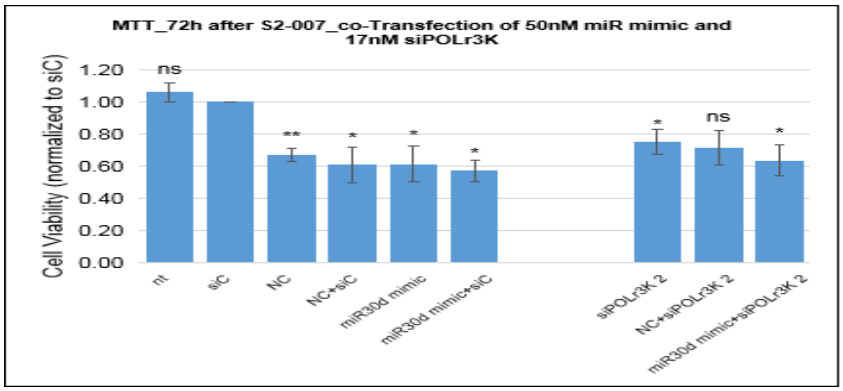

Figure 19. Overexpression of miR30d did not rescue POLr3K inhibition-induced attenuation of cell growth under 2D cell culture conditions. A) 48h after co-transfection of 50nM miR mimic and 17nM siPOLr3K siRNA2, real-time PCR was performed to assess expression level of POLr3K. B) 72h after co-Transfection of 50nM miR mimic and 17nM siPOLr3K-specific siRNA2, MTT assay were performed to evaluate cell viability. Values were normalized to siControl treated samples. Both experiments were repeated at least 3 times to get Mean±SD. siC=control siRNA; NC=non-coding control RNAmimic. * =P＜0.05, ** =P＜0.01, *** =P＜0.001 (Student t-Test).

3.14.2 POLr3K regulated cell growth in 3D cell culture via miR-30d-5p

CellTiter-Glo assays were performed to assess whether miR30d influenced cell growth upon POLr3K alteration. In contrast to the results of the 2D cell culture experiments, transfection of RNAmimics alone did not markedly impair anchorage-independent cell growth. Moreover, cell growth inhibition by POLr3K-specific siRNA 2 was efficiently rescued by co-transfection of miR30d-mimic, strongly implying that impairment of anchorage-independent growth in response to POLr3K silencing is mediated via downregulation of

miR30d (**Figure 20**).

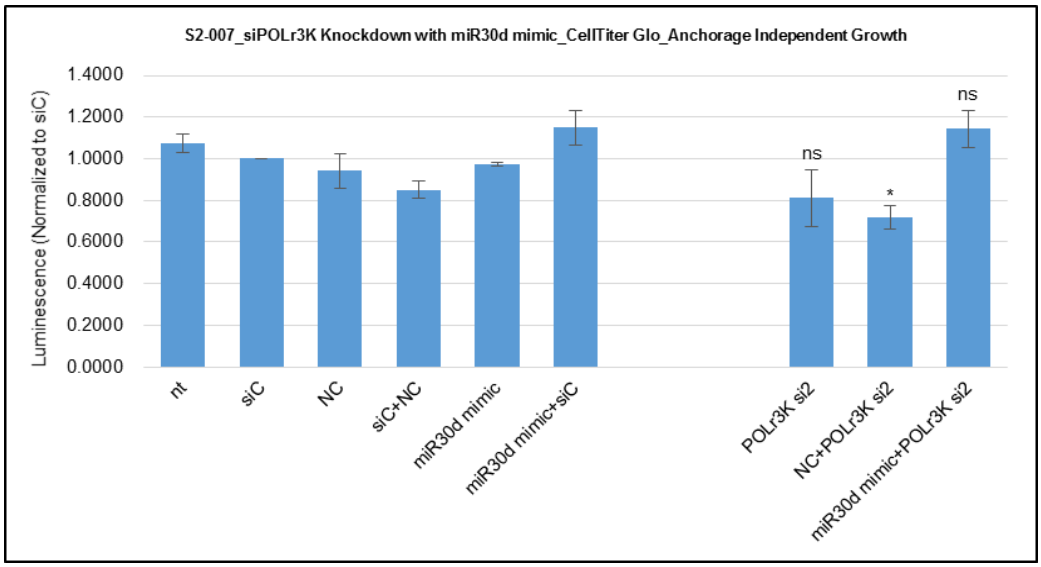

Figure 20. miR30d could prevent POLr3K impacted cell growth change in 3D cell culture. After 48h of miR 30d mimic and POLr3K siRNA2 co-transfection, the capacity for anchorage-independent growth was measured by CellTiter-Glo assay. Values were normalized to siControl treated sample. Experiments were repeated at least 3 times to get Mean±SD. * =P＜0.05, ** =P＜0.01, *** =P＜0.001 (Student t-Test). siC=control siRNA; NC=non-coding control RNAmimic.

3.15 POLr3K expression was not correlated with patient survival

To assess POLr3K protein expression on patient tissue samples, TMA analysis was performed as described above. By immunohistochemistry staining, POLR3K was detected moderately to highly express in malignant specimens. It was mainly localized in the nucleus in 24 individual specimens, while cytoplasm was the main subcellular location of POLr3K in 34 of the samples (**Figure 21A, B & D**). In adjacent normal tissue, POLr3K protein was consistently localized in the cytoplasm (**Figure 21C**). POLr3K expression levels were not significantly correlated with overall survival of PDAC patients who received resection. Kaplan–Meier survival analysis likewise did not reveal any differences in survival that correlated with different POLr3K subcellular localization (**Figure 21E to F**).

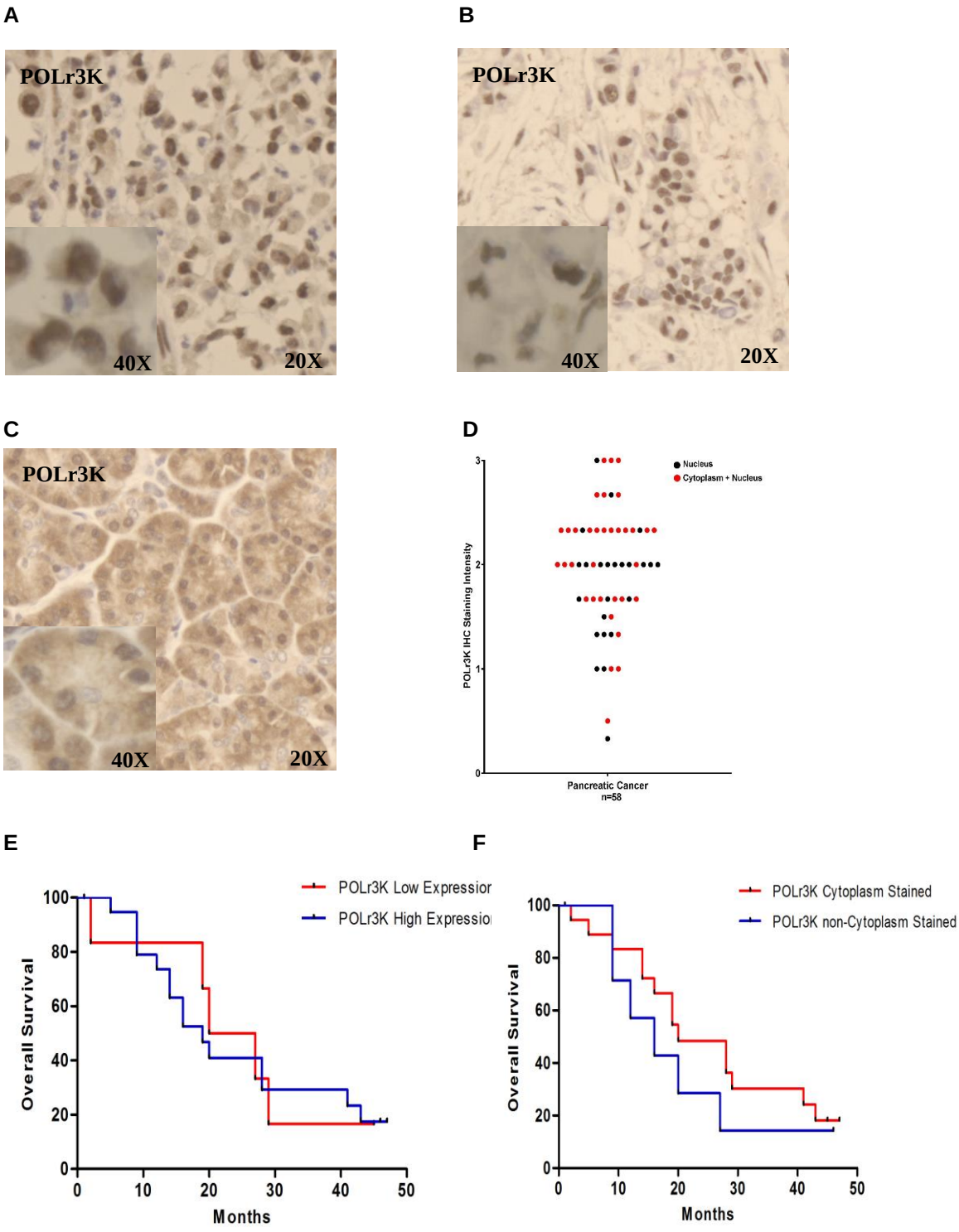

Figure 21. Representative images of tissue microarray based IHC analysis of POLr3K expression in normal pancreas and pancreatic cancer tissues. POLr3K was variably expressed among malignant tissues. A) & B) In tumor tissue, POLr3K is significantly stained in nucleus, some samples are simultaneous with slight to moderate cytoplasm staining. C) In non-cancer tissues, POLr3K is moderately to highly stained in cytoplasm. D) POLr3K protein intensity was higher in cytoplasm stained pancreatic malignant tissues. E) and F) Kaplan-Meier analyses of overall survival among cases with high vs. low POLr3K staining intensity (E) and different subcellular staining patterns of POLr3K (F).

4. Discussion

4.1 COA4 promotes PDAC cell proliferation

This project validated that COA4 was strongly overexpressed in the majority of human pancreatic cancers compared to healthy or chronically inflamed pancreatic tissues.

COA4 is part of twin CX9C family of proteins involved in COX assembly or stability [39]. COX, in turn, regulates mitochondrial respiration and is related to metabolic mechanisms and cellular processes in many kinds of cancers, which makes COA4 an interesting protein to study [87]. However, the role of COX varies in different cellular contexts. Defects in the assembly of COX can sensitize cells by elevating hydrogen peroxide and blocking cell proliferation. Overexpression of cytosolic catalase could rescue cell growth inhibition in COA4 deficient cells, suggesting that the increased hydrogen peroxide level in the cytosol is crucial for growth arrest [79]. On the other hand, defects of COA4 influence intracellular redox-dependent signaling pathways and decrease mitochondria-derived oxidative stress [42], as demonstrated in mitochondria of yeast. Other examples of context-dependent differential roles of COX include the fact that COX assembly factor 1 (COA1) is overexpressed in colon rectal cancer, where knockdown of COA1 could reduce cell proliferation and induce cell apoptosis by PI3K/AKT signaling pathway [125]. Inversely, overexpression of cytochrome c oxidase subunit 7A1 in human lung cancer cells leads to inhibition of cell proliferation and increase in cell death via apoptosis [76]. In our own study, siRNAs targeting COA4 reduced cell proliferation, while Western Blot analyses of PARP cleavage as well as flow cytometry did not exhibit increased apoptosis in COA4 inhibited cells. Moreover, upon siRNA treatment in three PDAC cell lines, cyclin D1 levels decreased and p21 levels increased, suggesting that cell growth reduction was due to anti-proliferation rather than increased cell death.

Previous research demonstrated that the effect of cell apoptosis in hepatoma cells produced by the chemotherapeutic drug N-(4-hydroxyphenyl) retinamide (4HPR) is due to oxidative mitochondrial damage, specifically through downregulation of cytochrome c oxidase subunit III (CO III) transcript levels and thus decreased activity of COX complex IV [60]. 4HPR treatment led to growth inhibition by producing a G1 arrest in a p53-dependent manner. Although we did observe downregulation of Cyclin D1 and upregulation of p21 upon COA4 knockdown, which would be consistent with a G1 arrest, flow cytometry analysis did not consistently show G1 phase arrest in all COA4 silenced samples of all three PDAC cell lines. It remains unclear if cell growth inhibition upon COA4 silencing was mediated through an alternative p21 dependent signaling pathway.

4.2 RNA Seq and DEGs validation - The capacity of COA4 to regulate cell migration by targeting PLAU

Cancer cell migration and invasion are required for metastasis which are core factors for cancer lethality. Disruption of COX function could alter cell migration behavior [103]. We applied a collagen coating 3D cell culture method to closely resemble the tumor microenvironment for cell-cell and cell-matrix interactions. Time-lapse-microscopy demonstrated that dynamic cell migration of PDAC cells was attenuated upon COA4 silencing. Previously, a study by Chen et al. [20] measured cell migratory behavior of cytochrome c oxidase subunit Va (COX Va) inhibited non-small cell lung carcinoma by Boyden chamber assays and found that cells had decreased migratory activity following COX Va knockdown. The authors also parallelly conducted transwell invasion assays, noting reduced invasive capacity after COX Va knockdown. Similarly, Chu and colleagues investigated the gene COX5B, which is a nuclear-encoded subunit in COX complexes and highly expressed in hepatic carcinoma [25]. In transwell migration assays with hepatoma cell lines, they observed significantly

attenuated cell migration in COX5B silenced cells. Moreover, the oncogene U2AF homology motif kinase1 (UHMK1) was identified as downstream effector of COXB5, and the COXB5-UHMK1 axis was revealed to modulate cell migration. In our study, based on RNA-Seq on negative control siRNA- and COA4 siRNA- treated cells, we validated PLAU was a differentially expressed gene upon COA4 silencing to regulate cell migration. Overexpressed PLAU relieved cell migratory suppression by COA4 inhibition, which could be replicated on different independent PLAU DNA stably overexpressing cell clones.

PLAU (urokinase) encodes a serine protease and is associated with cell migration in pancreatic cancer [122]. There are multiple studies which indicate urokinase involved in cell migration regulation. Liu and colleagues detected PLAU as a therapeutic target of pancreatic cancer through a protein fractionation and filter-aided sample preparation (FASP) strategy (MLEFF) [66]. PLAU related siRNA was applied to induce PLAU knockdown in the human pancreatic cancer cell line PC-1.0, showing that growth and migration were both inhibited following PLAU silencing. Carlin et al. observed that PLAU could influence cell migration through altered phosphorylation states [16]. Moreover, in a study by Xue et al., PLAU induced promotion of cell migration was mediated through the ERK/p38 signaling pathway via a positive feedback loop [124]. Consistent with Xue et al., cell migration reduction upon COA4 silencing was successfully rescued on PLAU stably overexpressed cells, and PLAU indeed mediated a positive feedback loop stimulating its own expression. Xue et al. also observed that disruption of the positive feedback loop of PLAU by phosphorylated ERK or PLAU siRNA could reduce cell growth. Additional evidence comes from research in head and neck squamous cell carcinoma (HNSCC), where cell growth rate was reduced when PLAU siRNA was transfected [19].

PLAU has also been implicated in the Wnt signaling pathway which is mutated in some cancer types [55] [71]. Evidence indicates that Wnt/β-catenin

transcriptional activity is upregulated in some PDAC patients, and that cell growth and migration are stimulated by Wnt ligand signaling [4]. Moreover, synergistic effects with other oncogenes were described in pancreatic cancer development. For example, Wnt/β-catenin signaling pathway is activated via upregulation of the oncogene Cyr61 [94]. According to the RNA-seq results in our study, Wnt4 was downregulated following COA4 knockdown, and it was predicted to interact with NKD1 and NOTUM on protein level. However, expression levels of Wnt4 appeared to be low in qRT-PCR validation experiments, so that a connection between COA4, PLAU and Wnt signaling could not be finally assessed and need to be further evaluated in future studies.

4.3 POLr3K regulated cell growth and cell cycle, and may exist as protein complex or protein isoforms

POLr3K is overexpressed in human PDAC and enriched in PDAC cell lines. To investigate the function of POLr3K, siRNA induced POLr3K knockdown was applied. Successful POLr3K knockdown on the protein level was confirmed by Western-Blot; however, the POLr3K-specific band was detected at 70 to 100 Kda size, while the predicted molecular weight of POLr3K is expected to be 12.3 Kda. There are several potential causes for this phenomenon. Pol III is a 17 subunits complex [92]. It is thus possible that the holoenzyme is stable enough to not be dissociated under standard SDS-electrophoresis conditions. Similar effects have been described for the conserved subunit RPB5 which is common to all RNA polymerases [29], where studies indicated a larger apparent molecular weight than predicted for the singular RPB5 subunit.

POLr3K is paralogous to subunits found in Pol I and Pol II, some structure and function of it would be homologs to Pol I or Pol II, so it is not specific to RNA polymerase III [33]. In mammals, transcription by Pol III is related to the cellular growth rate. When Pol III is targeting the Pol III-specific transcription factor

TFIIIB, TFIIIB directly binds positive regulators, such as ERK and c-Myc to promote cell growth. Meanwhile, growth induction also leads to RB hyperphosphorylation, which decreases the RB repression effect to TFIIIB [129]. In our study, POLr3K was found to be overexpressed in invasive human pancreatic cancer tissue and to be regulating cell growth through influencing the cell cycle regulators cyclin D1 and p21. Regulation of cell growth by Pol III has been described in many studies. Yee et al. demonstrated that Pol III is required for exocrine pancreatic epithelial proliferation during morphogenesis in zebrafish and human pancreatic adenocarcinoma cells [128]. In their study, soft agar colony formation was used to mimic 3D cell culture conditions and anchorage independent growth was measured by CellTiter-Glo. However, the inhibitor of pol III, ML-60218, alone was not sufficient to reduce proliferation in Panc-1 and BxPC3 cells. Instead, co-treatment with histone deacetylase- and Pol III inhibitors was required for efficient attenuation of tumor cell growth. Regulation of various target genes by Pol III is mediated by several transcription factors, which vary according to different types of Pol III promoter structures [40]. It is thus possible that the effect of Pol III inhibition by ML-60218 is different than the effect induced by silencing of specific subunits like POLr3K. This may also explain why in the study by Yee et al., HDAC and Pol III inhibition induced apoptosis in addition p21-mediated cell cycle inhibition, while in our study POLr3K silencing did not induce apoptosis. Interestingly, there was a clearly elevated rate of necrosis observed in POLr3K silenced cells, indicating that a potential pathway to induce cell necrosis is activated upon POLr3K downregulation. tRNAs which are transcribed by Pol III are crucial for protein translation. Graczyk et al. established that in mouse macrophages, treatment with lipopolysaccharides (LPS) induces upregulation of tRNA genes [41]. In addition, NFkB-mediated transcription of TNFα was also increased, inducing necrotic cell death in M1 macrophage. A study by Cao et al. [15] suggested that transcription and processing of small RNAs could influence neuronal necrosis through identifying high level of tRNA-derived

fragments (tRFs) and piwi-interacting RNA (piRNAs) species in glutamate-induced neuronal necrosis. The exact mechanism of POLr3K knockdown-induced cell necrosis in PDAC cells remains to be established.

4.4 miR-30d-5p mediated POLr3K-stimulated cell growth

microRNAs are the focus of intense research and have been shown to be involved in processes including metabolism, cell proliferation, apoptosis, neuronal cell fate of many diseases [6] by binding and modulating the translation of specific mRNAs. Pol II is thought to be primarily responsible for microRNA gene transcription [64], but Pol III is also associated with human miRNA gene transcription [10]. In our study, miR30d was detected to be positively regulated by POLr3K. Subsequent gain-of-function experiments by miR30d mimic transfection demonstrated that POLr3K regulated cell growth was mediated by miR30d in S2-007 pancreatic cancer cells. miR30d is localized on chromosomal region 8q24 and miR30d expression is deregulated in various cancer types [132]. miR30d is overexpressed in hepatocellular carcinoma (HCC) and involved in regulating cell invasion and metastasis by targeting Galphai2 [127]. Kumar et al. detected inhibition of miR30d could elevate cellular apoptosis in myeloma [58]. Conversely, in a study by Yu et al., working on renal carcinoma, higher expression of miR30d was associated with better overall survival [132]. Yu et al. also observed that overexpression of miR-30d downregulated cyclin E2 and induced G1 cell cycle arrest as well as decreased S-phase distribution. The role of miR30d thus appears to be context-dependent. Our own results demonstrated a tumor-promoting role of miR30d in pancreatic cancer, but whether the miR30d-POLr3K axis directly regulates cell cycle progression is unclear.

In our TaqMan array assays, additional putative miR candidates downstream of POLr3K (miR-135a-5p, miR-24-2-5p and miR-1291) were identified, but qRT-PCR analyses using our own designed stem-loop primers failed to

confirm expression in S2-007 cells. This may have been a technical problem, so that qRT-PCR with commercially designed assays should be performed. Previous studies have shown that miR135a is a PDAC suppressor which inhibits cell proliferation and induces G1 arrest in Panc-1 and ASPC-1 pancreatic cancer cells [26]. Tu et al. showed that miR1291 could dramatically reduce cell growth in Panc-1 cells [111]. While miR24-2 has also been identified as deregulated in pancreatic cancer, no information is available about its function [63]. Nevertheless, all three candidates may still be interesting to further evaluate as potential downstream mediators of POLr3K function in pancreatic cancer

4.5 Difference of tumor cell culture between 2D and 3D conditions

COA4 siRNA induced cell growth reduction is not prevented through overexpression of PLAU in 2D monolayer cultures, but partially reversed under poly-HEMA-mediated 3D culture conditions. Similarly, MTT assays performed with miR30d-mimic-expressing cells in 2D culture failed to demonstrate rescue of cell viability upon POLr3K inhibition (on the contrary, RNA mimic transfection even produced cellular stress). But in 3D cell culture, cell growth attenuation upon POLr3K silencing was efficiently rescued by miR30d overexpression.

One reason for this could be that cell culture conditions affect cell viability in general. In our study, MTT assays with COA4 knockdown and control cells indicated that viability of untreated tumor cells in 2D was higher than 3D culture, whereas relative response to COA4 siRNA1 and siRNA3 in 2D monolayer was stronger than in 3D culture. Some studies indicate that cells in 3D environment produce specific physiological and biomechanical signals that affect cell migration, adhesion, proliferation, and gene expression [89]. Specific cellular processes, such as differentiation and morphogenesis have been shown to occur more easily in a 3D environment than in a 2D environment [17]. Chen et al. [22] demonstrated that Poly-HEMA-supported microfluidic spheres

of breast cancer cells had higher photodynamic therapy resistance than 2D cells. Identically, Breslin et al.'s work [11] also applied Poly-HEMA to induce formation of tumor spheres from breast cancer cells, demonstrating that they were more resistant to neratinib and docetaxel than monolayer cells. In contrast to drug resistance, cell viability and proliferation rates were significantly decreased in 3D compared to cells in 2D monolayer, which might be due to relative space of cell growth, and deficient delivery of oxygen and nutrition to the centers of larger spheres. Meanwhile, 3D cell culture was shown to support cell-cell and cell-matrix physiological interactions that increase cell viability in various cell types [1] [65] [2]. Data also indicates that cells in spheroids have increased ability to block penetration of toxic reagents [110].

4.6 Localization of COA4 and POLr3K in primary PDAC tissues

Tissue microarray based IHC staining provided evidence that COA4 and POLr3K were stably and moderately expressed in the cytoplasm of normal pancreas cells. In malignant cells, although COA4 and POLr3K were predominantly localized in cytoplasm, COA4 in some cases also localized to the nucleus and cytomembrane, and POLr3K could be found at the nucleus too. Interestingly, tumor specimens with positive COA4 staining on the cell membrane possessed stronger COA4 protein intensity overall. Similarly, tissue with POLr3K dual stain in nucleus and cytoplasm had higher overall POLr3K protein intensity.

Subcellular localization is important for predicting protein function and surveillance of drug metabolism [56]. A prominent example is the transcription factor FOXP3, which is synthesized in the cytoplasm and then transported to the nucleus to play a transcriptional regulatory role. It is mainly localized in the nucleus in lymphocytes, whereas in breast cancer cells, FOXP3 is primarily expressed in the cytoplasm, but in some specimens in both cytoplasm and nucleus, and rarely in nucleus only [109]. For the variation of localization,

mutations, deletions, post-translational modifications have been made responsible, and splicing isomers of FOXP3 can cause FOXP3 to be unable to transit to the nucleus [47]. As a result, when FOXP3 does not localize to the nucleus, it loses its tumor suppressor effect and instead induces tumor formation [136].

To date, no study has analyzed the impact of different subcellular localizations of POLr3K or Pol III on the function of the enzyme. However, the Pol II subunit 5 (RPB5) interacting protein RMP has been described to change its subcellular location depending on the activity of the DNA methyltransferase 1-associating protein (DMAP1), which supports the translocation of RMP into the nucleus [28]. In our own study, Kaplan-Meier analysis did not reveal any significant association of either overall staining intensities or subcellular staining patterns of COA4 and POLr3K with patient survival. However, it has to be said that the sample size of this study was limited, so that confounding effects of factors such as TNM stage, different therapy regimens, dietary habits etc. could not be adequately addressed. It is thus not excluded that expression and/or localization of COA4 or POLr3K could emerge as prognostic factors in PDAC.

4.7 Conclusion and perspective

This study validated that COA4 and POLr3K were overexpressed in human pancreatic cancers compared to normal pancreas and chronic pancreatitis. Both target genes were demonstrated to promote PDAC development by cyclin D1/p21 mediated modulation of cell proliferation and stimulation of cell migration (only COA4) activity. Moreover, the gene PLAU was shown to be a downstream effector of COA4 which mediated cell migration in response to COA4 activity. In addition, miR30d-5p was verified as a downstream mediator of pro-tumorigenic effects of POLr3K expression. Although COA4 and POLr3K were not correlated with patient survival in our cohort of PDAC patients, correlation of subcellular localization with the overall degree of protein

expression was observed. Therefore, COA4 and POLr3K could potentially serve as novel diagnostic and therapeutic targets in pancreatic cancer. In future studies, biofunction and mechanisms of action of the two candidates, as well as their downstream mediators PLAU and miR30d should be further investigated to:

1. Assess whether overexpression of COA4 impacts tumor associated macrophages and their role in PDAC progression.
2. Detect potential respiration changes upon COA4 depletion, e.g. by Seahorse analyses, measuring oxygen consumption rates in the presence of mitochondria inhibitors at different time points.
3. Study whether expression of COA4 confers resistance to gemcitabine in tumor cells.
4. Further analyze mechanism of POLr3K induced tumor necrosis.
5. Analyze expression levels of miR30d in different tumor stages compared to normal pancreatic tissues.
6. Analyze larger cohorts of patients for COA4 and POLr3K expression to be able to control Kaplan-Meier survival analysis for other univariates, for example TNM stage, chemoradiotherapy condition, medical history of pancreas etc.
7. Further analyze the mechanisms and functional effects of different subcellular localizations of COA4 and POLr3K in pancreatic cancer cells.

5. Summary

Pancreatic cancer is a leading cause of cancer deaths in both men and women, and approximately 90% of all pancreatic malignancies are pancreatic ductal adenocarcinoma (PDAC). Therapeutic efficacy and long-term prognosis of treatment are strongly depended on time of diagnosis and stage of tumor, but overall patient prognosis remains dismal. Thus, it is imperative to further study the underlying biology of PDAC. Previous large-scale expression profiling analyses performed by the group identified, among others, Cytochrome C Oxidase Assembly Factor 4 Homolog (COA4) and RNA Polymerase III Subunit K (POLr3K) as significantly overexpressed among PDAC tissues. My work aimed to detect the molecular function of these two candidate genes in PDAC. RNAi-mediated knockdown approaches against the candidate genes revealed that cell growth inhibition caused by COA4 and POLr3K was due to inhibition of proliferation rather than induction of cell apoptosis. Moreover, knockdown of target genes interfered with anchorage independent growth (both targets) as well as cell migration (only COA4). Expression of the cell cycle related proteins p21 and Cyclin D1 were significantly changed upon siRNA transfection in both cases. Cell cycle analyses by flow cytometry suggested that inhibition of COA4, but not POLr3K, could attenuate cell cycle progression. To further investigate functional effectors of COA4 and POLr3K, RNA-Seq and TaqMan human microRNA array analyses were performed respectively. Gene enrichment analysis and subsequent functional analyses demonstrated that Plasminogen Activator (PLAU) was differentially expressed gene upon COA4 inhibition and was a central mediator of the inhibitory effects of COA4 silencing on cell migratory potential. miR-30d-5p (miR30d) was identified as significantly repressed upon POLr3K inhibition, and rescue experiments using microRNA mimics indicated that miR30d served to regulate cell growth downstream of POLr3K. Tissue microarray (TMA) based immunohistochemistry analyses did not indicate a direct and strong association of COA4 or POLr3K expression

with patient survival. Nonetheless, COA4 and POLr3K appeared to be potential novel therapeutic targets in PDAC and may turn out to be clinically useful prognostic markers as well as.

6. Zusammenfassung

Bauchspeicheldrüsenkrebs ist sowohl bei Männern als auch bei Frauen die häufigste Krebstodesursache, und etwa 90 % aller bösartigen Erkrankungen der Bauchspeicheldrüse sind Adenokarzinome des Pankreasganges (PDAC). Die therapeutische Wirksamkeit und die Langzeitprognose der Behandlung hängen stark vom Zeitpunkt der Diagnose und dem Tumorstadium ab, doch die Gesamtprognose der Patienten ist nach wie vor schlecht. Daher ist es unerlässlich, die zugrundeliegende Biologie des PDAC weiter zu untersuchen. Frühere Hochdurchsatz-Expressionsprofilanalysen, die von der Gruppe durchgeführt wurden, ergaben unter anderem, dass Cytochrom C Oxidase Assembly Factor 4 Homolog (COA4) und RNA Polymerase III Subunit K (POLr3K) in PDAC-Geweben deutlich überexprimiert sind. Ziel meiner Arbeit war es, die molekulare Funktion dieser beiden Kandidatengene bei PDAC zu ermitteln. RNAi-vermittelte Knockdown-Ansätze gegen die Kandidatengene zeigten, dass die durch COA4 und POLr3K verursachte Hemmung des Zellwachstums eher auf die Hemmung der Proliferation als auf die Induktion der Zellapoptose zurückzuführen ist. Darüber hinaus beeinträchtigte die Ausschaltung der Zielgene sowohl das substratunabhängige Wachstum (beide Zielgene) als auch die Zellmigration (nur COA4). Die Expression der Zellzyklusregulatoren p21 und Cyclin D1 wurde in beiden Fällen durch die siRNA-Transfektion signifikant verändert. Zellzyklusanalysen mittels Durchflusszytometrie deuteten darauf hin, dass die Hemmung von COA4, aber nicht von POLr3K, die Zellzyklusprogression verlangsamen konnte. Um die funktionellen Effektoren von COA4 und POLr3K weiter zu untersuchen, wurden RNA-Seq- bzw. TaqMan-Analysen mit humanen microRNA-Arrays durchgeführt. Die Analyse der Genexpression und die anschließenden funktionellen Analysen zeigten, dass der Plasminogen-Aktivator (PLAU) bei der Hemmung von COA4 differenziell exprimiert wurde und ein zentraler Vermittler der hemmenden Wirkung der COA4-Inhibition auf das

Migrationspotenzial der Zellen war. miR-30d-5p (miR30d) wurde bei der Hemmung von POLr3K als signifikant unterdrückt identifiziert, und Rescue-Experimente mit mikroRNA-Mimics deuteten darauf hin, dass miR30d das Zellwachstum stromabwärts von POLr3K mit regulierte. Auf Gewebe-Mikroarrays (TMA) basierende immunhistochemische Analysen ergaben keinen direkten Zusammenhang zwischen der COA4- oder POLr3K-Expression und dem Überleben der Patienten. Nichtsdestotrotz scheinen COA4 und POLr3K potenzielle neue therapeutische Ziele bei PDAC zu sein und könnten sich auch als klinisch nützliche Prognosemarker erweisen.

7. References

1. 3D Cell Culture vs. Traditional 2D Cell Culture Explained. Available at: https://www.mimetas.com/en/blogs/345/3d-cell-culture-vs.-traditional-2d-cell-culture-explained.html.
2. 5 Reasons Cancer Researchers Adopt 3D Cell Culture: A Review of Recent Literature. Available at: https://www.sigmaaldrich.com/DE/de/technical-documents/technical-article/cell-culture-and-cell-culture-analysis/3d-cell-culture/5-reasons-cancer-researchers-adopt-3d-cell-culture-white-paper#Conclusions.
3. Acker, J.; Conesa, C.; Lefebvre, O., Yeast RNA polymerase III transcription factors and effectors. *Biochim Biophys Acta* 2013, *1829* 283-95.
4. Aguilera, K. Y.; Dawson, D. W., WNT Ligand Dependencies in Pancreatic Cancer. *Front Cell Dev Biol* 2021, *9* 671022.
5. Anirban Maitra, R. H. H., Pancreatic cancer. *Annual Review of pathology* 2008, 157-188.
6. Ardekani, A. M.; Naeini, M. M., The Role of MicroRNAs in Human Diseases. *Avicenna J Med Biotechnol* 2010, *2* 161-79.
7. Ayloo, S.; Molinari, M., Pancreatic manifestations in von Hippel-Lindau disease: A case report. *Int J Surg Case Rep* 2016, *21* 70-2.
8. Bode, M.; Longen, S.; Morgan, B.; Peleh, V.; Dick, T. P.; Bihlmaier, K.; Herrmann, J. M., Inaccurately assembled cytochrome c oxidase can lead to oxidative stress-induced growth arrest. *Antioxid Redox Signal* 2013, *18* 1597-612.
9. Boerner, J. L.; Demory, M. L.; Silva, C.; Parsons, S. J., Phosphorylation of Y845 on the epidermal growth factor receptor mediates binding to the mitochondrial protein cytochrome c oxidase subunit II. *Mol Cell Biol* 2004, *24* 7059-71.
10. Borchert, G. M.; Lanier, W.; Davidson, B. L., RNA polymerase III transcribes human microRNAs. *Nat Struct Mol Biol* 2006, *13* 1097-101.

11. Breslin, S.; O'Driscoll, L., The relevance of using 3D cell cultures, in addition to 2D monolayer cultures, when evaluating breast cancer drug sensitivity and resistance. *Oncotarget* 2016, *7* 45745-45756.
12. Buchholz, M.; Braun, M.; Heidenblut, A.; Kestler, H. A.; Kloppel, G.; Schmiegel, W.; Hahn, S. A.; Luttges, J.; Gress, T. M., Transcriptome analysis of microdissected pancreatic intraepithelial neoplastic lesions. *Oncogene* 2005, *24* 6626-36.
13. C S Changchine , C. Y. Y., K Y Tzen, Serum carcinoembryonic antigen (CEA) and carbohydrate antigen (CA 19-9) values in patients with pancreatic cancer or pancreatitis. *Changgeng Yi Xue Za Zhi* 1991, *14(1)*.
14. Cantero, D.; Friess, H.; Deflorin, J.; Zimmermann, A.; Brundler, M. A.; Riesle, E.; Korc, M.; Buchler, M. W., Enhanced expression of urokinase plasminogen activator and its receptor in pancreatic carcinoma. *Br J Cancer* 1997, *75* 388-95.
15. Cao, Y.; Liu, K.; Xiong, Y.; Zhao, C.; Liu, L., Increased expression of fragmented tRNA promoted neuronal necrosis. *Cell Death Dis* 2021, *12* 823.
16. Carlin, S. M.; Resink, T. J.; Tamm, M.; Roth, M., Urokinase signal transduction and its role in cell migration. *FASEB J* 2005, *19* 195-202.
17. Chang, T. T.; Hughes-Fulford, M., Monolayer and spheroid culture of human liver hepatocellular carcinoma cell line cells demonstrate distinct global gene expression patterns and functional phenotypes. *Tissue Eng Part A* 2009, *15* 559-67.
18. Chen, D.; Guo, W.; Qiu, Z.; Wang, Q.; Li, Y.; Liang, L.; Liu, L.; Huang, S.; Zhao, Y.; He, X., MicroRNA-30d-5p inhibits tumour cell proliferation and motility by directly targeting CCNE2 in non-small cell lung cancer. *Cancer Lett* 2015, *362* 208-17.
19. Chen, G.; Sun, J.; Xie, M.; Yu, S.; Tang, Q.; Chen, L., PLAU Promotes Cell Proliferation and Epithelial-Mesenchymal Transition in Head and Neck Squamous Cell Carcinoma. *Front Genet* 2021, *12* 651882.

20. Chen, W. L.; Kuo, K. T.; Chou, T. Y.; Chen, C. L.; Wang, C. H.; Wei, Y. H.; Wang, L. S., The role of cytochrome c oxidase subunit Va in non-small cell lung carcinoma cells: association with migration, invasion and prediction of distant metastasis. *BMC Cancer* 2012, *12* 273.
21. Chen, W.; Heierhorst, J.; Brosius, J.; Tiedge, H., Expression of Neural BCI RNA: Induction in Murine Tumours *European Journal of Cancer.* 1997, *33* 5.
22. Chen, Y. C.; Lou, X.; Zhang, Z.; Ingram, P.; Yoon, E., High-Throughput Cancer Cell Sphere Formation for Characterizing the Efficacy of Photo Dynamic Therapy in 3D Cell Cultures. *Sci Rep* 2015, *5* 12175.
23. Chiao, P. J.; Ling, J., Kras, Pten, NF-kappaB, and inflammation: dangerous liaisons. *Cancer Discov* 2011, *1* 103-5.
24. Chu, L. C.; Goggins, M. G.; Fishman, E. K., Diagnosis and Detection of Pancreatic Cancer. *The Cancer Journal* 2017, *23* 10.
25. Chu, Y. D.; Lin, W. R.; Lin, Y. H.; Kuo, W. H.; Tseng, C. J.; Lim, S. N.; Huang, Y. L.; Huang, S. C.; Wu, T. J.; Lin, K. H.; Yeh, C. T., COX5B-Mediated Bioenergetic Alteration Regulates Tumor Growth and Migration by Modulating AMPK-UHMK1-ERK Cascade in Hepatoma. *Cancers (Basel)* 2020, *12*.
26. Dang, Z.; Xu, W. H.; Lu, P.; Wu, N.; Liu, J.; Ruan, B.; Zhou, L.; Song, W. J.; Dou, K. F., MicroRNA-135a inhibits cell proliferation by targeting Bmi1 in pancreatic ductal adenocarcinoma. *Int J Biol Sci* 2014, *10* 733-45.
27. Daniel Ansari 1 , B. T., Bodil Andersson 1 , Fredrik Holmquist 2 , Christian Sturesson 1 , Caroline Williamsson 1 , Agata Sasor 3 , David Borg 4 , Monika Bauden 1 , Roland Andersson 1, Pancreatic cancer: yesterday, today and tomorrow. *Future oncology* 2016, *12*.
28. Delgermaa, L.; Hayashi, N.; Dorjsuren, D.; Nomura, T.; Thuy le, T. T.; Murakami, S., Subcellular localization of RPB5-mediating protein and its putative functional partner. *Mol Cell Biol* 2004, *24* 8556-66.
29. Devaux, S.; Kelly, S.; Lecordier, L.; Wickstead, B.; Perez-Morga, D.; Pays,

E.; Vanhamme, L.; Gull, K., Diversification of function by different isoforms of conventionally shared RNA polymerase subunits. *Mol Biol Cell* 2007, *18* 1293-301.

30. Distler, M.; Aust, D.; Weitz, J.; Pilarsky, C.; Grutzmann, R., Precursor lesions for sporadic pancreatic cancer: PanIN, IPMN, and MCN. *Biomed Res Int* 2014, *2014* 474905.
31. Dorboz, I.; Dumay-Odelot, H.; Boussaid, K.; Bouyacoub, Y.; Barreau, P.; Samaan, S.; Jmel, H.; Eymard-Pierre, E.; Cances, C.; Bar, C.; Poulat, A. L.; Rousselle, C.; Renaldo, F.; Elmaleh-Berges, M.; Teichmann, M.; Boespflug-Tanguy, O., Mutation in POLR3K causes hypomyelinating leukodystrophy and abnormal ribosomal RNA regulation. *Neurol Genet* 2018, *4* e289.
32. Dragovich, T., What is the role of carbohydrate antigen 19-9 testing in the evaluation of pancreatic cancer? 2020.
33. Dumay-Odelot, H.; Durrieu-Gaillard, S.; Da Silva, D.; Roeder, R. G.; Teichmann, M., Cell growth- and differentiation-dependent regulation of RNA polymerase III transcription. *Cell Cycle* 2010, *9* 3687-99.
34. Eser, S.; Schnieke, A.; Schneider, G.; Saur, D., Oncogenic KRAS signalling in pancreatic cancer. *Br J Cancer* 2014, *111* 817-22.
35. Ferlay, J.; Steliarova-Foucher, E.; Lortet-Tieulent, J.; Rosso, S.; Coebergh, J. W.; Comber, H.; Forman, D.; Bray, F., Cancer incidence and mortality patterns in Europe: estimates for 40 countries in 2012. *Eur J Cancer* 2013, *49* 1374-403.
36. Fiedorczuk, K.; Sazanov, L. A., Mammalian Mitochondrial Complex I Structure and Disease-Causing Mutations. *Trends Cell Biol* 2018, *28* 835-867.
37. Fischer, M.; Horn, S.; Belkacemi, A.; Kojer, K.; Petrungaro, C.; Habich, M.; Ali, M.; Kuttner, V.; Bien, M.; Kauff, F.; Dengjel, J.; Herrmann, J. M.; Riemer, J., Protein import and oxidative folding in the mitochondrial intermembrane space of intact mammalian cells. *Mol Biol Cell* 2013, *24* 2160-70.

38. Ghiorzo, P., Genetic predisposition to pancreatic cancer. *World J Gastroenterol* 2014, *20* 10778-89.
39. Gladyck, S.; Aras, S.; Huttemann, M.; Grossman, L. I., Regulation of COX Assembly and Function by Twin CX9C Proteins-Implications for Human Disease. *Cells* 2021, *10*.
40. Goodfellow, S. J.; White, R. J., Regulation of RNA polymerase III transcription during mammalian cell growth. *Cell Cycle* 2007, *6* 2323-6.
41. Graczyk, D.; White, R. J.; Ryan, K. M., Involvement of RNA Polymerase III in Immune Responses. *Mol Cell Biol* 2015, *35* 1848-59.
42. Greetham, D.; Kritsiligkou, P.; Watkins, R. H.; Carter, Z.; Parkin, J.; Grant, C. M., Oxidation of the yeast mitochondrial thioredoxin promotes cell death. *Antioxid Redox Signal* 2013, *18* 376-85.
43. Guidlines, N., <pancreatic cancer NCCN guidlines.pdf>.
44. Halkova, T.; Cuperkova, R.; Minarik, M.; Benesova, L., MicroRNAs in Pancreatic Cancer: Involvement in Carcinogenesis and Potential Use for Diagnosis and Prognosis. *Gastroenterol Res Pract* 2015, *2015* 892903.
45. Hammond, S. M.; Bernstein, E.; Beach, D.; Hannon, G. J., An RNA-directed nuclease mediates post-transcriptional gene silencing in Drosophila cells. *Nature* 2000, *404* 293-6.
46. Han, M.; Wang, Y.; Guo, G.; Li, L.; Dou, D.; Ge, X.; Lv, P.; Wang, F.; Gu, Y., microRNA-30d mediated breast cancer invasion, migration, and EMT by targeting KLF11 and activating STAT3 pathway. *J Cell Biochem* 2018, *119* 8138-8145.
47. Hancock, W. W.; Ozkaynak, E., Three distinct domains contribute to nuclear transport of murine Foxp3. *PLoS One* 2009, *4* e7890.
48. Hingorani, S. R.; Wang, L.; Multani, A. S.; Combs, C.; Deramaudt, T. B.; Hruban, R. H.; Rustgi, A. K.; Chang, S.; Tuveson, D. A., Trp53R172H and KrasG12D cooperate to promote chromosomal instability and widely metastatic pancreatic ductal adenocarcinoma in mice. *Cancer Cell* 2005, *7* 469-83.

49. Hoffman, M., Pancreatic Cancer Diagnosis and Early Detection. *WebMed* 2019.
50. https://www.krebsdaten.de/Krebs/EN/Content/Cancer_sites/Pancreatic_cancer/pancreatic_cancer_node.html, R. K. I., Pancreatic Cancer data from Robert Koch Insititute. 2021.
51. Hu, Y.; Ou, Y.; Wu, K.; Chen, Y.; Sun, W., miR-143 inhibits the metastasis of pancreatic cancer and an associated signaling pathway. *Tumour Biol* 2012, *33* 1863-70.
52. Huang, J.; Lok, V.; Ngai, C. H.; Zhang, L.; Yuan, J.; Lao, X. Q.; Ng, K.; Chong, C.; Zheng, Z. J.; Wong, M. C. S., Worldwide Burden of, Risk Factors for, and Trends in Pancreatic Cancer. *Gastroenterology* 2021, *160* 744-754.
53. J. L. Humphris, D. K. C., 1,2,3 A. L. Johns,1 C. J. Scarlett,1,4 M. Pajic,1 M. D. Jones,1 E. K. Colvin,1 A. Nagrial,1 V. T. Chin,1 L. A. Chantrill,1 J. S. Samra,5 A. J. Gill,6,7 J. G. Kench,1,7,8 N. D. Merrett,2,9 A. Das,2 E. A. Musgrove,1,10 R. L. Sutherland,1,10 and A. V. Biankin, The prognostic and predictive value of serum CA19.9 in pancreatic cancer. *Annals of Oncology* 2012.
54. Jiao, L. R.; Frampton, A. E.; Jacob, J.; Pellegrino, L.; Krell, J.; Giamas, G.; Tsim, N.; Vlavianos, P.; Cohen, P.; Ahmad, R.; Keller, A.; Habib, N. A.; Stebbing, J.; Castellano, L., MicroRNAs targeting oncogenes are down-regulated in pancreatic malignant transformation from benign tumors. *PLoS One* 2012, *7* e32068.
55. Jo, M.; Eastman, B. M.; Webb, D. L.; Stoletov, K.; Klemke, R.; Gonias, S. L., Cell signaling by urokinase-type plasminogen activator receptor induces stem cell-like properties in breast cancer cells. *Cancer Res* 2010, *70* 8948-58.
56. Kaleel, M.; Zheng, Y.; Chen, J.; Feng, X.; Simpson, J. C.; Pollastri, G.; Mooney, C., SCLpred-EMS: subcellular localization prediction of endomembrane system and secretory pathway proteins by Deep N-to-1

Convolutional Neural Networks. *Bioinformatics* 2020, *36* 3343-3349.

57. Kanda, M.; Matthaei, H.; Wu, J.; Hong, S. M.; Yu, J.; Borges, M.; Hruban, R. H.; Maitra, A.; Kinzler, K.; Vogelstein, B.; Goggins, M., Presence of somatic mutations in most early-stage pancreatic intraepithelial neoplasia. *Gastroenterology* 2012, *142* 730-733 e9.
58. Kumar, M.; Lu, Z.; Takwi, A. A.; Chen, W.; Callander, N. S.; Ramos, K. S.; Young, K. H.; Li, Y., Negative regulation of the tumor suppressor p53 gene by microRNAs. *Oncogene* 2011, *30* 843-53.
59. Kurata S, K. K. a. S. B., Nucleolar size in parallel with ribosomal RNA synthesis at diapause termination in the eggs of Bombyx mori. *Chromosoma* 1978.
60. Kyung-Ran You , J. W., Soo-Taek Lee, Dae-Ghon Kim, Cytochrome c oxidase subunit III: a molecular marker for N-(4-hydroxyphenyl)retinamise-induced oxidative stress in hepatoma cells. *the Journal of Biological Chemistry* 2002, *277* 8.
61. Labrinus van Manen , J. V. G., Hein Putter , Alexander L Vahrmeijer , Rutger-Jan Swijnenburg , Bert A Bonsing , J Sven D Mieog, Elevated CEA and CA19-9 serum levels independently predict advanced pancreatic cancer at diagnosis. *Biomarkers* 2020, *25, 2020* 186-193.
62. Lake, N. J.; Compton, A. G.; Rahman, S.; Thorburn, D. R., Leigh syndrome: One disorder, more than 75 monogenic causes. *Ann Neurol* 2016, *79* 190-203.
63. Lee, E. J.; Gusev, Y.; Jiang, J.; Nuovo, G. J.; Lerner, M. R.; Frankel, W. L.; Morgan, D. L.; Postier, R. G.; Brackett, D. J.; Schmittgen, T. D., Expression profiling identifies microRNA signature in pancreatic cancer. *Int J Cancer* 2007, *120* 1046-54.
64. Lee, Y.; Kim, M.; Han, J.; Yeom, K. H.; Lee, S.; Baek, S. H.; Kim, V. N., MicroRNA genes are transcribed by RNA polymerase II. *EMBO J* 2004, *23* 4051-60.
65. Lin, R. Z.; Chang, H. Y., Recent advances in three-dimensional

multicellular spheroid culture for biomedical research. *Biotechnol J* 2008, *3* 1172-84.

66. Liu, P.; Weng, Y.; Sui, Z.; Wu, Y.; Meng, X.; Wu, M.; Jin, H.; Tan, X.; Zhang, L.; Zhang, Y., Quantitative secretomic analysis of pancreatic cancer cells in serum-containing conditioned medium. *Sci Rep* 2016, *6* 37606.
67. Lowenfels, A. B.; Maisonneuve, P.; Cavallini, G.; Ammann, R. W.; Lankisch, P. G.; Andersen, J. R.; Dimagno, E. P.; Andren-Sandberg, A.; Domellof, L., Pancreatitis and the risk of pancreatic cancer. International Pancreatitis Study Group. *N Engl J Med* 1993, *328* 1433-7.
68. Lowenfels, A. B.; Maisonneuve, P.; DiMagno, E. P.; Elitsur, Y.; Gates, L. K., Jr.; Perrault, J.; Whitcomb, D. C., Hereditary pancreatitis and the risk of pancreatic cancer. International Hereditary Pancreatitis Study Group. *J Natl Cancer Inst* 1997, *89* 442-6.
69. Lucas, A. L.; Frado, L. E.; Hwang, C.; Kumar, S.; Khanna, L. G.; Levinson, E. J.; Chabot, J. A.; Chung, W. K.; Frucht, H., BRCA1 and BRCA2 germline mutations are frequently demonstrated in both high-risk pancreatic cancer screening and pancreatic cancer cohorts. *Cancer* 2014, *120* 1960-7.
70. M, K. W. Â. n. P., Serum level of Urokinase Plasminogen Activator (uPA) Correlates with the Survival of Patients with Pancreatic Ductal Adenocarcinoma (PDAC). *Pancreatic Disorders and Therapy* 2015.
71. Ma, Z. G.; Lv, X. D.; Zhan, L. L.; Chen, L.; Zou, Q. Y.; Xiang, J. Q.; Qin, J. L.; Zhang, W. W.; Zeng, Z. J.; Jin, H.; Jiang, H. X.; Lv, X. P., Human urokinase-type plasminogen activator gene-modified bone marrow-derived mesenchymal stem cells attenuate liver fibrosis in rats by down-regulating the Wnt signaling pathway. *World J Gastroenterol* 2016, *22* 2092-103.
72. Malczewska, A.; Kidd, M.; Matar, S.; Kos-Kudla, B.; Modlin, I. M., A Comprehensive Assessment of the Role of miRNAs as Biomarkers in Gastroenteropancreatic Neuroendocrine Tumors. *Neuroendocrinology* 2018, *107* 73-90.
73. Mao, Y.; Shen, J.; Lu, Y.; Lin, K.; Wang, H.; Li, Y.; Chang, P.; Walker, M. G.;

Li, D., RNA sequencing analyses reveal novel differentially expressed genes and pathways in pancreatic cancer. *Oncotarget* 2017, *8* 42537-42547.

74. McGuigan, A.; Kelly, P.; Turkington, R. C.; Jones, C.; Coleman, H. G.; McCain, R. S., Pancreatic cancer: A review of clinical diagnosis, epidemiology, treatment and outcomes. *World J Gastroenterol* 2018, *24* 4846-4861.
75. Minamoto, T.; Mai, M.; Ronai, Z., K-ras mutation: early detection in molecular diagnosis and risk assessment of colorectal, pancreas, and lung cancers--a review. *Cancer Detect Prev* 2000, *24* 1-12.
76. Mishra, N.; Timilsina, U.; Ghimire, D.; Dubey, R. C.; Gaur, R., Downregulation of cytochrome c oxidase subunit 7A1 expression is important in enhancing cell proliferation in adenocarcinoma cells. *Biochem Biophys Res Commun* 2017, *482* 713-719.
77. Mitochondrial DNA-associated Leigh syndrome. Available at: https://rarediseases.info.nih.gov/diseases/3671/mitochondrial-dna-associated-leigh-syndrome.
78. Moore, M. J.; Goldstein, D.; Hamm, J.; Figer, A.; Hecht, J. R.; Gallinger, S.; Au, H. J.; Murawa, P.; Walde, D.; Wolff, R. A.; Campos, D.; Lim, R.; Ding, K.; Clark, G.; Voskoglou-Nomikos, T.; Ptasynski, M.; Parulekar, W.; National Cancer Institute of Canada Clinical Trials, G., Erlotinib plus gemcitabine compared with gemcitabine alone in patients with advanced pancreatic cancer: a phase III trial of the National Cancer Institute of Canada Clinical Trials Group. *J Clin Oncol* 2007, *25* 1960-6.
79. Moslemi, A. R.; Darin, N.; Tulinius, M.; Oldfors, A.; Holme, E., Two new mutations in the MTATP6 gene associated with Leigh syndrome. *Neuropediatrics* 2005, *36* 314-8.
80. Mourelatos, Z.; Dostie, J.; Paushkin, S.; Sharma, A.; Charroux, B.; Abel, L.; Rappsilber, J.; Mann, M.; Dreyfuss, G., miRNPs: a novel class of ribonucleoproteins containing numerous microRNAs. *Genes Dev* 2002, *16*

720-8.

81. Navas, C.; Hernandez-Porras, I.; Schuhmacher, A. J.; Sibilia, M.; Guerra, C.; Barbacid, M., EGF receptor signaling is essential for k-ras oncogene-driven pancreatic ductal adenocarcinoma. *Cancer Cell* 2012, *22* 318-30.
82. O'Brien, J.; Hayder, H.; Zayed, Y.; Peng, C., Overview of MicroRNA Biogenesis, Mechanisms of Actions, and Circulation. *Front Endocrinol (Lausanne)* 2018, *9* 402.
83. Oliva, C. R.; Markert, T.; Ross, L. J.; White, E. L.; Rasmussen, L.; Zhang, W.; Everts, M.; Moellering, D. R.; Bailey, S. M.; Suto, M. J.; Griguer, C. E., Identification of Small Molecule Inhibitors of Human Cytochrome c Oxidase That Target Chemoresistant Glioma Cells. *J Biol Chem* 2016, *291* 24188-24199.
84. Ormanns, S.; Haas, M.; Remold, A.; Kruger, S.; Holdenrieder, S.; Kirchner, T.; Heinemann, V.; Boeck, S., The Impact of SMAD4 Loss on Outcome in Patients with Advanced Pancreatic Cancer Treated with Systemic Chemotherapy. *Int J Mol Sci* 2017, *18*.
85. Oshima, M.; Okano, K.; Muraki, S.; Haba, R.; Maeba, T.; Suzuki, Y.; Yachida, S., Immunohistochemically detected expression of 3 major genes (CDKN2A/p16, TP53, and SMAD4/DPC4) strongly predicts survival in patients with resectable pancreatic cancer. *Ann Surg* 2013, *258* 336-46.
86. Park, J.-K. D. L., Eun Joo PhD*; Esau, Christine PhD†; Schmittgen, Thomas D. PhD, <Antisense_Inhibition_of_microRNA_21_or__221.28.pdf>. *Journal of Neuroendocrine Tumors and Pancreatic Diseases and Sciences* 2009, *38* 10.
87. Payne, C. M.; Holubec, H.; Bernstein, C.; Bernstein, H.; Dvorak, K.; Green, S. B.; Wilson, M.; Dall'Agnol, M.; Dvorakova, B.; Warneke, J.; Garewal, H., Crypt-restricted loss and decreased protein expression of cytochrome C oxidase subunit I as potential hypothesis-driven biomarkers of colon cancer

risk. *Cancer Epidemiol Biomarkers Prev* 2005, *14* 2066-75.

88. POLR3-Related Leukodystrophy. Available at: https://medlineplus.gov/genetics/condition/pol-iii-related-leukodystrophy/.
89. Qutub, A. A.; Popel, A. S., Elongation, proliferation & migration differentiate endothelial cell phenotypes and determine capillary sprouting. *BMC Syst Biol* 2009, *3* 13.
90. Radiation therapy for pancreatic cancer. Available at: https://www.cancer.org/cancer/pancreatic-cancer/treating/radiation-therapy.html.
91. Rak, M.; Benit, P.; Chretien, D.; Bouchereau, J.; Schiff, M.; El-Khoury, R.; Tzagoloff, A.; Rustin, P., Mitochondrial cytochrome c oxidase deficiency. *Clin Sci (Lond)* 2016, *130* 393-407.
92. Ramsay, E. P.; Abascal-Palacios, G.; Daiss, J. L.; King, H.; Gouge, J.; Pilsl, M.; Beuron, F.; Morris, E.; Gunkel, P.; Engel, C.; Vannini, A., Structure of human RNA polymerase III. *Nat Commun* 2020, *11* 6409.
93. Roeder, R. G.; Rutter, W. J., Multiple forms of DNA-dependent RNA polymerase in eukaryotic organisms. *Nature* 1969, *224* 234-7.
94. Sano, M.; Driscoll, D. R.; DeJesus-Monge, W. E.; Quattrochi, B.; Appleman, V. A.; Ou, J.; Zhu, L. J.; Yoshida, N.; Yamazaki, S.; Takayama, T.; Sugitani, M.; Nemoto, N.; Klimstra, D. S.; Lewis, B. C., Activation of WNT/beta-Catenin Signaling Enhances Pancreatic Cancer Development and the Malignant Potential Via Up-regulation of Cyr61. *Neoplasia* 2016, *18* 785-794.
95. Schramm, L.; Hernandez, N., Recruitment of RNA polymerase III to its target promoters. *Genes Dev* 2002, *16* 2593-620.
96. Schwartz, L. B.; Sklar, V. E.; Jaehning, J. A.; Weinmann, R.; Roeder, R. G., Isolation and partial characterization of the multiple forms of deoxyribonucleic acid-dependent ribonucleic acid polymerase in the mouse myeloma, MOPC 315. *J Biol Chem* 1974, *249* 5889-97.
97. Sentenac, A.; Riva, M., Odd RNA polymerases or the A(B)C of eukaryotic

transcription. *Biochim Biophys Acta* 2013, *1829* 251-7.

98. Shen, G. Q.; Aleassa, E. M.; Walsh, R. M.; Morris-Stiff, G., Next-Generation Sequencing in Pancreatic Cancer. *Pancreas* 2019, *48* 739-748.

99. Shen, R.; Wang, Q.; Cheng, S.; Liu, T.; Jiang, H.; Zhu, J.; Wu, Y.; Wang, L., The biological features of PanIN initiated from oncogenic Kras mutation in genetically engineered mouse models. *Cancer Lett* 2013, *339* 135-43.

100. Society, A. C., <cancer-facts-and-figures-2021.pdf>.

101. Soto, I. C.; Fontanesi, F.; Liu, J.; Barrientos, A., Biogenesis and assembly of eukaryotic cytochrome c oxidase catalytic core. *Biochim Biophys Acta* 2012, *1817* 883-97.

102. Sperti, C.; Moletta, L.; Merigliano, S., Multimodality treatment of recurrent pancreatic cancer: Mith or reality? *World J Gastrointest Oncol* 2015, *7* 375-82.

103. Srinivasan, S.; Guha, M.; Dong, D. W.; Whelan, K. A.; Ruthel, G.; Uchikado, Y.; Natsugoe, S.; Nakagawa, H.; Avadhani, N. G., Disruption of cytochrome c oxidase function induces the Warburg effect and metabolic reprogramming. *Oncogene* 2016, *35* 1585-95.

104. Telang, S.; Nelson, K. K.; Siow, D. L.; Yalcin, A.; Thornburg, J. M.; Imbert-Fernandez, Y.; Klarer, A. C.; Farghaly, H.; Clem, B. F.; Eaton, J. W.; Chesney, J., Cytochrome c oxidase is activated by the oncoprotein Ras and is required for A549 lung adenocarcinoma growth. *Mol Cancer* 2012, *11* 60.

105. Test for pancreatic cancer. Available at: https://www.cancer.org/cancer/pancreatic-cancer/detection-diagnosis-staging/how-diagnosed.html.

106. Tinder, T. L.; Subramani, D. B.; Basu, G. D.; Bradley, J. M.; Schettini, J.; Million, A.; Skaar, T.; Mukherjee, P., MUC1 enhances tumor progression and contributes toward immunosuppression in a mouse model of spontaneous pancreatic adenocarcinoma. *J Immunol* 2008, *181* 3116-25.

107. Todd W. Bauer, W. L., Fan Fan, Ernest R. Camp, Anthony Yang, Ray J. Somcio, Corazon D. Bucana, Jennifer Callahan, Graham C. Parry, Douglas B. Evans, Douglas D. Boyd, Andrew P. Mazar and Lee M. Ellis, Targeting of Urokinase Plasminogen Activator Receptor in Human Pancreatic Carcinoma Cells Inhibits c-Met– and Insulin-like Growth Factor-I Receptor–Mediated Migration and Invasion and Orthotopic Tumor Growth in Mice. *Cancer Research* 2005, *65*.

108. Tong, H.; Fan, Z.; Liu, B.; Lu, T., The benefits of modified FOLFIRINOX for advanced pancreatic cancer and its induced adverse events: a systematic review and meta-analysis. *Sci Rep* 2018, *8* 8666.

109. Triulzi, T.; Tagliabue, E.; Balsari, A.; Casalini, P., FOXP3 expression in tumor cells and implications for cancer progression. *J Cell Physiol* 2013, *228* 30-5.

110. Tseng, H.; Gage, J. A.; Shen, T.; Haisler, W. L.; Neeley, S. K.; Shiao, S.; Chen, J.; Desai, P. K.; Liao, A.; Hebel, C.; Raphael, R. M.; Becker, J. L.; Souza, G. R., A spheroid toxicity assay using magnetic 3D bioprinting and real-time mobile device-based imaging. *Sci Rep* 2015, *5* 13987.

111. Tu, M. J.; Pan, Y. Z.; Qiu, J. X.; Kim, E. J.; Yu, A. M., MicroRNA-1291 targets the FOXA2-AGR2 pathway to suppress pancreatic cancer cell proliferation and tumorigenesis. *Oncotarget* 2016, *7* 45547-45561.

112. Turowski, T. W.; Tollervey, D., Transcription by RNA polymerase III: insights into mechanism and regulation. *Biochem Soc Trans* 2016, *44* 1367-1375.

113. Types of pancreatic cancer. Available at: https://www.pancan.org/facing-pancreatic-cancer/about-pancreatic-cancer/types-of-pancreatic-cancer/.

114. Ulla Klaiber, T. H., and John P. Neoptolemos, Adjuvant treatment for pancreatic cancer. *Transl Gastroenterol Hepatol* 2019.

115. Umashankar K Ballehaninna, R. S. C., Serum CA 19-9 as a Biomarker for Pancreatic Cancer-A Comprehensive Review. *Indian J Surg Oncol* 2011,

88-100.

116. Vannini, A.; Cramer, P., Conservation between the RNA polymerase I, II, and III transcription initiation machineries. *Mol Cell* 2012, *45* 439-46.

117. Vincenza Granata 1 , R. F., Orlando Catalano 1 , Sergio Venanzio Setola 1 , Elisabetta de Lutio di Castelguidone 1 , Mauro Piccirillo 2 , Raffaele Palaia 2 , Roberto Grassi 3 , Francesco Granata 4 , Francesco Izzo 2 , Antonella Petrillo 1, Multidetector computer tomography in the pancreatic adenocarcinoma assessment: an update. *Infect Agent Cancer* 2016.

118. Wang, S.; Zheng, Y.; Yang, F.; Zhu, L.; Zhu, X. Q.; Wang, Z. F.; Wu, X. L.; Zhou, C. H.; Yan, J. Y.; Hu, B. Y.; Kong, B.; Fu, D. L.; Bruns, C.; Zhao, Y.; Qin, L. X.; Dong, Q. Z., The molecular biology of pancreatic adenocarcinoma: translational challenges and clinical perspectives. *Signal Transduct Target Ther* 2021, *6* 249.

119. Watson, S. A.; McStay, G. P., Functions of Cytochrome c oxidase Assembly Factors. *Int J Mol Sci* 2020, *21*.

120. Werner, J.; Combs, S. E.; Springfeld, C.; Hartwig, W.; Hackert, T.; Buchler, M. W., Advanced-stage pancreatic cancer: therapy options. *Nat Rev Clin Oncol* 2013, *10* 323-33.

121. White, R. J., RNA polymerase III transcription and cancer. *Oncogene* 2004, *23* 3208-16.

122. Wu, J.; Li, Z.; Zeng, K.; Wu, K.; Xu, D.; Zhou, J.; Xu, L., Key genes associated with pancreatic cancer and their association with outcomes: A bioinformatics analysis. *Mol Med Rep* 2019, *20* 1343-1352.

123. Xu, X.; Zong, K.; Wang, X.; Dou, D.; Lv, P.; Zhang, Z.; Li, H., miR-30d suppresses proliferation and invasiveness of pancreatic cancer by targeting the SOX4/PI3K-AKT axis and predicts poor outcome. *Cell Death Dis* 2021, *12* 350.

124. Xue, A.; Xue, M.; Jackson, C.; Smith, R. C., Suppression of urokinase plasminogen activator receptor inhibits proliferation and migration of

pancreatic adenocarcinoma cells via regulation of ERK/p38 signaling. *Int J Biochem Cell Biol* 2009, *41* 1731-8.

125. Xue, Y.; Li, P. D.; Tang, X. M.; Yan, Z. H.; Xia, S. S.; Tian, H. P.; Liu, Z. L.; Zhou, T.; Tang, X. G.; Zhang, G. J., Cytochrome C Oxidase Assembly Factor 1 Homolog Predicts Poor Prognosis and Promotes Cell Proliferation in Colorectal Cancer by Regulating PI3K/AKT Signaling. *Onco Targets Ther* 2020, *13* 11505-11516.

126. Yan, L.; Qiu, J.; Yao, J., Downregulation of microRNA-30d promotes cell proliferation and invasion by targeting LRH-1 in colorectal carcinoma. *Int J Mol Med* 2017, *39* 1371-1380.

127. Yao, J.; Liang, L.; Huang, S.; Ding, J.; Tan, N.; Zhao, Y.; Yan, M.; Ge, C.; Zhang, Z.; Chen, T.; Wan, D.; Yao, M.; Li, J.; Gu, J.; He, X., MicroRNA-30d promotes tumor invasion and metastasis by targeting Galphai2 in hepatocellular carcinoma. *Hepatology* 2010, *51* 846-56.

128. Yee, N. S.; Gong, W.; Huang, Y.; Lorent, K.; Dolan, A. C.; Maraia, R. J.; Pack, M., Mutation of RNA Pol III subunit rpc2/polr3b Leads to Deficiency of Subunit Rpc11 and disrupts zebrafish digestive development. *PLoS Biol* 2007, *5* e312.

129. Yee, N. S.; Zhou, W.; Chun, S. G.; Liang, I. C.; Yee, R. K., Targeting developmental regulators of zebrafish exocrine pancreas as a therapeutic approach in human pancreatic cancer. *Biol Open* 2012, *1* 295-307.

130. Yeganeh, M.; Hernandez, N., RNA polymerase III transcription as a disease factor. *Genes Dev* 2020, *34* 865-882.

131. Yonezawa, S.; Higashi, M.; Yamada, N.; Goto, M., Precursor lesions of pancreatic cancer. *Gut Liver* 2008, *2* 137-54.

132. Yu, H.; Lin, X.; Wang, F.; Zhang, B.; Wang, W.; Shi, H.; Zou, B.; Zhao, J., Proliferation inhibition and the underlying molecular mechanisms of microRNA-30d in renal carcinoma cells. *Oncol Lett* 2014, *7* 799-804.

133. Zhang, B.; Pan, X.; Cobb, G. P.; Anderson, T. A., microRNAs as oncogenes and tumor suppressors. *Developmental Biology* 2007, *302*

1-12.

134. Zhang, Y.; Yang, W. Q.; Zhu, H.; Qian, Y. Y.; Zhou, L.; Ren, Y. J.; Ren, X. C.; Zhang, L.; Liu, X. P.; Liu, C. G.; Ming, Z. J.; Li, B.; Chen, B.; Wang, J. R.; Liu, Y. B.; Yang, J. M., Regulation of autophagy by miR-30d impacts sensitivity of anaplastic thyroid carcinoma to cisplatin. *Biochem Pharmacol* 2014, *87* 562-70.

135. Zhao, C.; Zhang, J.; Zhang, S.; Yu, D.; Chen, Y.; Liu, Q.; Shi, M.; Ni, C.; Zhu, M., Diagnostic and biological significance of microRNA-192 in pancreatic ductal adenocarcinoma. *Oncol Rep* 2013, *30* 276-84.

136. Zuo, T.; Wang, L.; Morrison, C.; Chang, X.; Zhang, H.; Li, W.; Liu, Y.; Wang, Y.; Liu, X.; Chan, M. W.; Liu, J. Q.; Love, R.; Liu, C. G.; Godfrey, V.; Shen, R.; Huang, T. H.; Yang, T.; Park, B. K.; Wang, C. Y.; Zheng, P.; Liu, Y., FOXP3 is an X-linked breast cancer suppressor gene and an important repressor of the HER-2/ErbB2 oncogene. *Cell* 2007, *129* 1275-86.

8. Appendix

8.1 Supplementary Table

Table 24. List of genes with significant expression alteration upon COA4 knockdown.

* Foldchange means FPKM value of control siRNA treated group / FPKM value of COA4 siRNA treated group.

SymbolID	Foldchange
COA4	9.96
RAB38	4.57
GLS2	3.96
GALNT18	3.74
LAMC2	3.63
DDN	3.47
HIST1H3J	3.45
CYP4X1	3.40
CST4	3.35
LARGE2	3.25
TAS2R20	3.24
CD24	3.15
PRODH	3.14
HSD11B2	3.13
PLLP	3.08
SOSTDC1	3.08
CISH	3.07
ICAM5	2.75
PRKCG	2.75
PPP1R14C	2.71
DLX2	2.70
ESRP2	2.70
SOCS2	2.69
RTP4	2.69
CHRNA7	2.68
CST1	2.58
TRIM31	2.58
CCDC78	2.51
ACYP1	2.50
PLAU	2.47
KCNIP2	2.45
SH2D1B	2.45

JPH1	2.44
ZDHHC23	2.39
IFITM1	2.39
SLC43A1	2.37
NUDT10	2.37
MMP1	2.36
NRTN	2.36
SLC25A30	2.34
NFKBIE	2.34
KHK	2.32
TNS4	2.30
HGD	2.29
ETV7	2.29
ATP1B2	2.28
CXCL2	2.27
THBS1	2.18
ELOVL6	2.13
DEGS2	2.13
SPIN4	2.11
CRACR2B	2.10
AMER1	2.07
43528	0.48
ZBTB4	0.48
KIF3C	0.46
SKIDA1	0.46
NOG	0.46
MSRB3	0.46
DUSP3	0.46
BFSP1	0.46
FNBP1	0.46
ZSWIM9	0.45
ZSCAN30	0.43
CDA	0.43
PHACTR2	0.42
AGMO	0.42
SBK3	0.42
ZNF845	0.41
ZNF675	0.41
LYPD5	0.40
ETS2	0.40
ZSCAN29	0.39
HABP4	0.39
OGFR	0.39

MAP1B	0.39
ZNF721	0.38
EREG	0.38
ARHGAP21	0.38
ZNF227	0.38
IFT27	0.38
DUSP10	0.37
TM4SF1	0.37
SNAI2	0.37
ZNF267	0.36
BICD2	0.36
TFPI	0.36
SPTLC3	0.35
PANX2	0.35
ATXN1	0.34
ZBTB7C	0.31
TMEM121B	0.30
STON1	0.30
TNC	0.28
RBMS3	0.27
HOXD4	0.27
HDAC9	0.27
ZNF616	0.26
TUBA1A	0.26
PCDHGB7	0.25
NTN4	0.23

8.2 Verzeichnis der akademischen Lehrer

Meine akademischen Lehrenden waren die folgenden Damen und Herren:
In Shiyan, China:
Zhaohong Deng, Chunxian Du, Xiju He, Xiang Jiang, Yujuan Li, Ming Sang, Jun Tian, Qiang Tong, Qiang Wang, Ronghua Wei, Jie Wu, Ling Xu, Hong Yang

In HongKong, China:
Joseph J.Y. SUNG, Francis K.L. CHAN, Henry L.Y. CHAN, Stephen L. CHAN, Winnie C.W. CHU, Philip W.Y. CHIU, B.S. LAI, Enders K.W. NG, Siew C. NG, Simon S.N. NG, Raymond S.Y. TANG, Anthony Y.B. TEOH, Grace L.H. WONG, Vincent W.S. WONG, Justin C.Y. WU

In Marburg, Deutschland:
Christian Bauer, Malte Buchholz, Thomas M. Gress, Corinna Keber, Rolf Müller

8.3 Acknowledgement

First of all, I express my sincere gratitude to my supervisor Prof. Dr. Malte Buchholz, for his instructive guide and extremely meticulous explanation of basic biology knowledge point. I deeply appreciate of this opportunity to complete my doctorate thesis in his group.

During the period, I always felt heart-warming help and concern from all members of the group. I am particularly grateful to Mr. Harald Schmidt, he is the enlightener of my scientific research, and a lot of optimal suggestions from him promote my efficiency. Each technology I applied was guided by friendly colleagues who were very professional at that filed, great thanks to all of them.

I also thank my parents and friends for their tremendous encouragement during the four years, especially at epidemic time, I cherish family affection and friendship, even though far apart thousands of miles and time difference. Moreover, I am very fortunate to own courage and persistence to complete study at Marburg, it is an excellent start of my future life.

Finally, I express my deep gratefulness again to all above, I could not achieve this without your help and care. The experience in Prof. Buchholz group, in university of Marburg would be strength in my future life.